TECHNICAL OPERATIONS RESEARCH

TECHNICAL REPORT ECOM-01309-1

DEVELOPMENT OF AN IMPROVED LAND-SURFACE FALLOUT MODEL

Interim Report

Contract No. DA 28-043-AMC-01309(E)

by

H.G. Norment, T.W. Schwenke, and I. Kohlberg

Report No. TO-B 65-99
Technical Operations Research
Burlington, Massachusetts
January 1966

U.S. Army Electronics Command
Fort Monmouth, New Jersey

techops

- 1473

NOTICES

Disclaimers

The findings in this report are not to be construed as an official Department of the Army position, unless so designated by other authorized documents.

The citation of trade names and names of manufacturers in this report is not to be construed as official Government indorsement or approval of commercial products or services referenced herein.

Disposition

Destroy this report when it is no longer needed. Do not return it to the originator.

TECHNICAL REPORT ECOM-01309-1

JANUARY 1966

TECHNICAL OPERATIONS RESEARCH

DEVELOPMENT OF AN IMPROVED LAND-SURFACE FALLOUT MODEL

Interim Report

1 April 1965 to 31 October 1965

Report No. 1

Contract No. DA 28-043-AMC-01309(E)

DA Project No. 1VO-14501-B-53A-01

DASA Subtask: NWER 10.058

Prepared by

H.G. Norment, T.W. Schwenke, and I. Kohlberg

Report No. TO-B 65-99

Technical Operations Research

Burlington, Massachusetts

For

U.S. Army Electronics Command
Fort Monmouth, New Jersey

Burlington, Massachusetts

TABLE OF CONTENTS

TABLE OF CONTENTS (Cont'd.)

TABLE OF CONTENTS (Cont'd.)

LIST OF ILLUSTRATIONS

LIST OF ILLUSTRATIONS (Cont'd.)

LIST OF TABLES

BLANK PAGE

PURPOSE

OVERALL OBJECTIVES

The purpose of the overall program, of which the project described here is the major constituent, is to develop an improved land-surface fallout model, the Department of Defense Fallout Prediction System, that is being designed to serve as the basis for the next generation of fallout prediction models. The improved predictor will account for the effects of nuclear cloud rise and growth dynamics and the transport of debris through a three-dimensional time variant atmosphere. The model will be programmed for digital computer computation in a flexible, highly modular fashion and will be coded in a macro-symbolic language (FORTRAN) that basically is independent of any particular computer system.

The overall model is intended to be a research system which, in accurately predicting fallout, can be used to test the sensitivity of a fallout pattern to the many parameters (nuclear, thermal, atmospheric) which enter into the development of a fallout pattern. The range of yields considered is from 0.01 kT to 100 MT and heights of burst from one fireball radius above ground to a scaled depth of 20 ft below ground.

The research effort on the DOD Fallout Prediction System has been divided into the following major tasks:

1. Specification of a set of critical initial conditions in the fireball
2. A dynamic description of the nuclear cloud rise and growth
3. Assignment of radiological properties to the fallout material
4. Simulation of the transport and settling of fallout through the atmosphere
5. Programming and coding of the analytical results and simulations for digital computer computation.

The project reported here is concerned with tasks 2, 4, and 5. Task 1 is being done by Technical Operations Research under contract to the Nuclear Defense Laboratory (Contract DA-18-035-AMC-346(A)); task 3, by the Naval Radiological Defense

Laboratory. Most of the project subtasks are unfinished at the time of this writing, so that only occasionally is it possible to present completed discussions. For the most part, this report presents the status of the various subtasks at the half-way point in the effort.

CLOUD RISE DYNAMICS

Nearly all of the currently available fallout predictors begin with a fully formed and stabilized cloud. Since there has been very little basis for the construction of these stabilized clouds, except visual observations of nuclear test shot cloud profiles, the assignments of distributions of particles and activity to them introduces artificialities that result in severely limited prediction capabilities. To give the DOD System increased range of applicability with regard to yield and height of burst and to introduce realistic means for generating nuclear clouds for use in further research, a dynamic cloud rise and growth submodel will be an integral part of the prediction model.

The cloud rise submodel will account for the thermodynamics of adiabatic expansion and entrainment by an analysis similar to that of Huebsch,[1] and for the effects of organized vortex circulation by a model similar to that described by Norment.[2,3] Effects of vortex circulation on both the cloud rise dynamics and on distributions of particles will be included. This submodel will yield a distribution of particles in space in the vicinity of ground zero. These data will be smoothed and expanded to an essentially continuous distribution in space, and the cloud will be sectioned three-dimensionally into cells. The center of each cell will be assigned an appropriately weighted spectrum of particle sizes. During the ensuing transport calculations, each size fraction from each cell will be transported independently. Particle activities will be assigned by the Particle Activity Module program being developed at the Naval Radiological Defense Laboratory. The cell center coordinates, particle size, particle activity, and activity decay constant are the primary inputs to the atmospheric transport portion of the model.

ATMOSPHERIC TRANSPORT

The most important of the major divisions of the prediction system with regard to determination of the final fallout pattern is the atmospheric transport submodel. As with each of the other overall model parts, the transport submodel is being constructed to provide the greatest practicable amount of flexibility and generality of usage. The model is designed to transport fallout particles through a three-dimensional time variant wind field. An outline of the gross features of the submodel is as follows.

A Cartesian coordinate system with origin at ground zero is established. With reference to this coordinate system, grid nets are specified in horizontal planes at arbitrarily spaced intervals in the vertical direction. The grid intervals of different nets are mutually independent. The user provides a data set of wind vectors, arbitrary in number and independent of the grid system, that then is expanded and smoothed to yield interpolated or extrapolated wind vector components (w_x, w_y, w_z) at each grid point. Three interpolation options are available for use in the data expansion calculations. In addition to this so-called macro-wind description system, provision is made for representation of certain special local circulation systems by analytical models. Specifically, models for mountain winds and sea breezes will be provided. The regions controlled by these models are bounded by planes perpendicular to the coordinate axes. Inside these regions, wind vectors are computed for specified circulation model parameters.

Particle trajectories through the atmosphere are computed in jump steps between boundaries defined by the grid-array lines and planes. Lateral particle motion is taken as equal to that of the air currents. Vertical motion is taken as the sum of vertical air current motion and the terminal settling velocity computed for a sphere.

Temporal variation of the wind field is achieved by periodically replacing the entire wind field description data set. The period of data replacement is specified by the user. Topographic variation of ground height is accomplished by specifying elevation heights of blocks in a grid system that can be subdivided indefinitely to

yield any resolution of detail desired. Topography of mountains covered by a mountain wind model cell is described by an analytical mountain shape function. Ground level activity is the sum of activities of deposited cloud cells. A variety of output map options is provided.

COMPUTER PROGRAMMING

The highest practicable degree of modularity is being used in the program construction. This is to allow the greatest possible freedom in providing optional modes and methods of computation, both at the present and in the future. This applies at all levels of organization and construction. Coding is being done exclusively in FORTRAN language. FORTRAN II (IBM 7094) is being used for debugging but this will be converted to FORTRAN IV in the polished version of the program.

ABSTRACT AND SUMMARY

A new concept in fallout models, the DOD Fallout Prediction System, is being designed and constructed to serve as a basis for the next generation of fallout prediction models. The model considers in detail the dynamics of cloud rise and growth and provides for fallout particle transport through a three-dimensional time variant atmosphere that includes analytical wind models of local circulation systems such as mountain winds and sea breezes. The model is being programmed for machine computation in a highly modular and flexible fashion to facilitate research usage of the program. Coding is being done exclusively in FORTRAN language.

Our research effort during the period 1 April to 31 October may be summarized as follows:

1. Cloud Rise Dynamics. The Tech/Ops cloud rise simulation model is composed of two major parts. One accounts for the thermodynamic and hydrodynamic aspects of the cloud rise and growth and provides the basis for simulating the more gross aspects of cloud development. The other accounts for kinematic effects of circulation on distributions of particles in the cloud. An analysis has been developed, that in some respects is patterned after the cloud rise model of Huebsch,[1] to serve as a basis for the dynamic portion of the model. This analysis takes into account thermodynamic effects of the soil content of the cloud, the effects of adiabatic expansion accompanying rise through the hydrostatic atmosphere, the effects of entrainment, and a seemingly important influence of large-scale vortex circulation on cloud rise and growth rate. In support of an investigation into this latter effect, which is a novel contribution to cloud rise dynamics, we have undertaken an extensive study of the variation of vortex circulation strength with altitude.

Studies of the computation methods that form the basis of our circulation kinematics treatment have been performed with the objective of increasing computational efficiency. These studies have resulted in reducing trajectory computation time by a factor of approximately twenty-five.

2. Transport. A static representation of the wind field is provided by an arbitrary three-dimensional array of three-dimensional wind vectors, and temporal variation is achieved by updating this array at selected intervals. To aid the

researcher in his task of preparing wind data, we have provided a number of alternative methods for incorporating extensive sets of real or hypothetical meteorological data into this array. When data are very sparse, the array grid point vector may be given the value of the nearest data point. When data are more extensive, one can use a preferential weighting scheme in which the closest input data are favored. When even more extensive data are available, a three-dimensional least-squares method may be used.

An analysis of the motion of fallout particles in the wind field has shown that the effect of particle inertia at the boundaries between cells can be neglected under all physically realizable circumstances. This work also has resulted in justification to equate the lateral particle velocity to that of the wind velocity. To provide the model with the best means for estimating particle settling rates, a comprehensive review of methods for computing particle settling rates has been performed. The method of Davies (Ref. 6, Appendix A), which is pertinent to spheres, has been selected as most appropriate. A drag slip correction of the form of Cunningham's factor has been adopted.

Local circulation phenomena such as orographic effects and the sea breeze have been investigated in detail. We have been able to derive general expressions for the wind flow over variable terrain and have applied the theory to a single mountain and to a mountain ridge which makes an arbitrary angle with respect to the flow. Within the context of the theory, valleys are treated as inverted mountains. We have also derived expressions for the trajectories of fallout particles over a two-dimensional mountain ridge and have employed these functions to assess the effect of the mountain range's presence on the down-wind deposition of fallout.

A complete review of existing sea-breeze theories has been performed, and the decision has been made to use Defant's[15] linearized model for the fallout computations. We have rendered his theory compatible with the proposed computer program, and we are in the process of developing the numerical procedures that are to be used in the program.

3. Computer Programming. The complete DOD Fallout Prediction System will consist of five semi-independent modules that will be exercised serially. Two

of these are being prepared independently of this project: the Fireball Module and the Particle Activity Module. The Fireball Module is being prepared by Technical Operat ons Research under contract to the Nuclear Defense Laboratory. It supplies a starting time for the cloud rise simulations, an average cloud temperature at the starting time, the soil burden of the cloud in both the vapor and condensed phases, and particle size distributions of condensed phase soil particles. The particle activity program is the responsibility of the Naval Radiological Defense Laboratory and will not be discussed here.

Work on the Fireball Module has been completed. The computer program is particularly simple and will require only a nominal time for execution. The calculation involves serial exercising of a group of subroutines, one for each parameter to be provided in the output.

Because the Cloud Rise Module is still in the research phase of development, it has not been possible to begin detailed work on the cloud rise simulation computer program. Nevertheless, a broad outline of programming strategy has been devised. It is planned to program the cloud development and the particle kinetics portions of the model for closely linked parallel computation. The simulations will be done by following the course of the cloud growth and particle trajectories through a succession of short-time steps. Conventional numerical time-step integration procedures will be used. Significant progress has been made in upgrading the computational efficiency of the particle trajectory computation computer program.

The Transport Module has been divided into three major programs, each of which makes up a separate chain link:

Link 1 - Initialization and control

Link 2 - Wind field description

Link 3 - Particle transport.

At this time preliminary and abbreviated versions of Link 1, 2, and 3 are operative. Link 1 is essentially completed and debugged. Certain computational options remain to be added to Link 2, although the currently available options and

modules are capable of fully exercising the programs of Link 3. Link 3 programming requires a few minor additions and changes for improved efficiency and usefulness. The testing of certain routes and options in Link 3 still remains to be done.

It is the task of the Output Processor Module to accept descriptions of grounded cloud subdivisions, interpret them into a two-dimensional memory array or map image, and then print the resulting array in a form suitable for direct contouring. The interpretation processes required of the Output Processor are the computation of: (1) dose rate "normalized" to H + 1 hours, (2) dose rate at a specified time, (3) dose accumulated between two specified times, and (4) particle mass deposited per unit area. Programming and debugging of the Output Processor Module are completed, and an initial draft of the documentation for the Processor has been written.

CONFERENCES

Table 1 is a summary of the conferences held during this reporting period (1 April 1965 to 31 October 1965).

TABLE 1
SUMMARY OF CONFERENCES

Date	Attendee	Agency Represented*	Conference Location	Purpose
2 April	W. Barr, W. C. Conover, M. Lowenthal, H. Weickmann	ASL	ASL, Fort Monmouth, N. J.	Introductory coordination meeting between ASL and Tech/Ops
	H. G. Norment, T. Schwenke	TOR		
8-9 April	M. Morganthau	AMC	TOR, Burlington, Mass.	Contractor's coordination meeting on DASA subtask NWER 10.058
	W. Barr, W. C. Conover	ASL		
	R. E. Peterson	DASA		
	L. M. Hardin, R. C. Tompkins	NDL		
	S. H. Cassidy, E. C. Evans, III, I. O. Huebsch	NRDL		
	W. D. Lanning, E. T. Clarke, C. Hauer, H. G. Norment, T. W. Schwenke, H. J. Tiller	TOR		
	J. P. Gerrity	TRC		
24 May	H. G. Norment	TOR	Pentagon, Washington, D.C.	Present status report to the Fallout Panel
12 August	W. Barr	ASL	TOR, Burlington, Mass.	Status report on DASA subtask NWER 10.058
	J. W. Cane	DASA		
	L. Hardin	NDL		
	E. T. Clarke, C. Hauer, W. Ing, I. Kohlberg, H. G. Norment, T. Schwenke, H. Tiller, J. Zuckerman	TOR		
30 August	R. C. Tompkins	NDL	TOR, Burlington, Mass.	Coordination conference on computer programming
	S. Cassidy	NRDL		
	W. Ing, H. G. Norment, T. Schwenke, H. Tiller, J. Zuckerman	TOR		
15 September	I. Kohlberg, H. G. Norment	TOR	TRC, Hartford, Conn.	Discussion of mutual interests and progress in attempts to prepare mathematical models of sea-breeze circulation systems
	J. P. Gerrity, J. D. Kangos	TRC		
23 September	W. Barr, W. C. Conover	ASL	TOR, Burlington, Mass.	Conference on fallout model user requirements
	J. W. Cane	DASA		
	L. Hardin, R. C. Tompkins	NDL		
	R. C. Mason, R. C. Simmons	NMCSSC		
	E. T. Clarke, C. Hauer, H. G. Norment, T. Schwenke, H. Tiller	TOR		
19 October	R. C. Tompkins	NDL	RAND, Santa Monica, Calif.	Discussion on progress of DASA subtask NWER 10.058
	R. R. Rapp	RAND		
	H. G. Norment	TOR		
20-21 October	R. C. Tompkins	NDL	NRDL, San Francisco, Calif.	Contractor's coordination meeting on DASA subtask NWER 10.058
	E. C. Evans, III, I. O. Huebsch, S. C. Cassidy	NRDL		
	H. G. Norment	TOR		

*AMC = Army Materiel Command
ASL = Atmospheric Sciences Laboratory
DASA = Defense Atomic Support Agency
NDL = Nuclear Defense Laboratory
NMCSSC = National Military Command System Support Center
NRDL = Naval Radiological Defense Laboratory
TOR = Technical Operations Research
TRC = Travelers Research Center

FACTUAL DATA

CLOUD RISE DYNAMICS

INTRODUCTION

A basic model has been devised that describes the rise and growth of a nuclear cloud during the entrainment controlled phase of its development. This model takes into account thermodynamic effects of the cloud rise through the hydrostatic atmosphere and entrainment of ambient air; it also includes effects of organized vortex circulation on both the cloud rise and disposition of fallout particles in the cloud. Vortex circulatory motion in the cloud is simulated by a three-dimensional ring vortex.[2,3,4] The model depends heavily on observed nuclear cloud rise data for characterization of the kinematics of cloud development.

We have found it convenient and appropriate to divide the development of a nuclear cloud into four phases. These are (in temporal sequence):

1. A fireball phase
2. A pseudo-hydrostatic cloud rise phase
3. An entrainment controlled cloud rise phase
4. A final expansion phase leading to stabilization.

Figure 1 shows these phases with reference to the cloud center height. The fireball phase covers the interval from the detonation time until radiative growth of the fireball has virtually ceased. The prompt effects, including the electromagnetic pulses and the close-in blast, have largely subsided by the end of this period. During phase 2, the fireball is still hot, in fact the second temperature maximum usually occurs early in this phase, but not hot enough for radiation to dominate the cooling process. The fireball begins to rise, and owing to vigorous circulation, to entrain appreciable amounts of ambient air. This causes rapid cooling. In

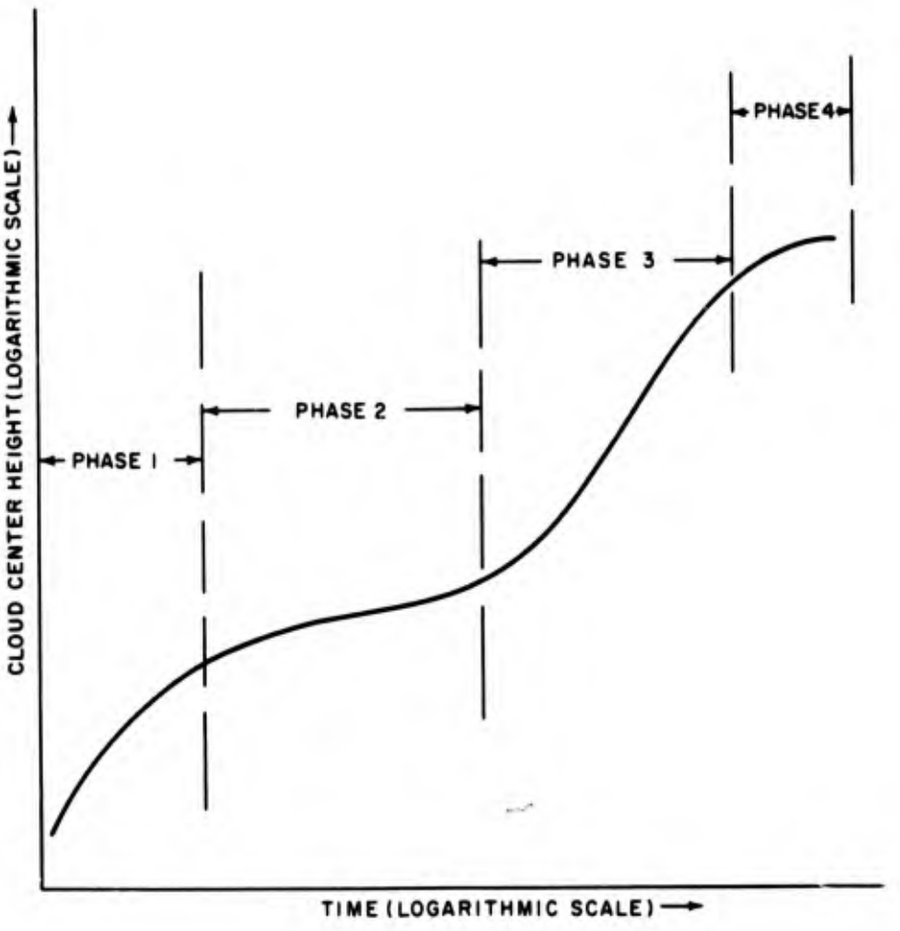

Figure 1. Intervals of the Four Phases of Cloud Development Shown in a Typical Plot of Cloud Center Height vs Time

spite of this entrainment, the cloud appears to rise in a manner that resembles an air bubble rising in water; therefore, we have labeled it the pseudo-hydrostatic rise phase. (It also has been called the hover period.) This behavior results from the fact that the disparity in densities of the cloud and ambient gases ($\rho_{ambient}/\rho_{cloud} > 10$), caused by the high temperature of the cloud, is sufficient to prevent effective momentum transfer from the circulating cloud gases to the surrounding air.[17] At approximately the time of the beginning of phase 3, however, the combined influence of lowered temperature and circulation vigor are sufficient to cause an interaction between the cloud gases and ambient air that

profoundly affects cloud rise and growth. Organized vortex circulation, the structure of which is illustrated in Figure 2, causes an increasingly vigorous engulfment of ambient air into the cloud.* This process continues throughout phase 3. Subsequent to phase 3, cloud behavior is dependent on weapon yield and height of burst. For small detonations at low altitudes, buoyancy and circulation subside together at a time prior to encountering the tropopause. For large detonations, the tropopause is encountered during the cloud rise, and the cloud passes into the stratosphere where the ambient temperature increases with altitude. This so-called temperature inversion results in a rapid loss of cloud buoyancy and causes the cloud rise to cease, while circulatory action (vorticity) and entrainment continue to persist. The residual vorticity then is dissipated by lateral expansion, while the cloud height remains fixed.

Detailed discussions of the physics of vortex rings and the efficacy of vortex ring geometry and circulation to fit observed nuclear cloud behavior have been presented by Norment.[2, 3]

THE INITIAL STATE OF THE NUCLEAR CLOUD

Currently available cloud rise models, including the model presented herein, are applicable only as early as the beginning of the phase 3. Therefore, we have taken the beginning of the phase 3 period as our starting time. Using cloud rise data from Ref. 5, we have determined that the initial time, t_i, is given approximately by

$$t_i = t_{2m}\, 56\, W^{-0.30} \quad ,$$

where t_{2m} is the time of the second temperature maximum, and W is the yield in kilotons; t_{2m} can be evaluated as a function of yield by the equations of Hillendahl[6] or by the relations given in Ref. 7.

*This so-called entrainment process is more appropriately described as a "fluid" uncoiling of the cloud vortex into the ambient air. Magnificent photographs of cross sections of an entraining column of smoke that clearly illustrate the entrainment mechanism have been published by Magarvey and MacLatchy.[18]

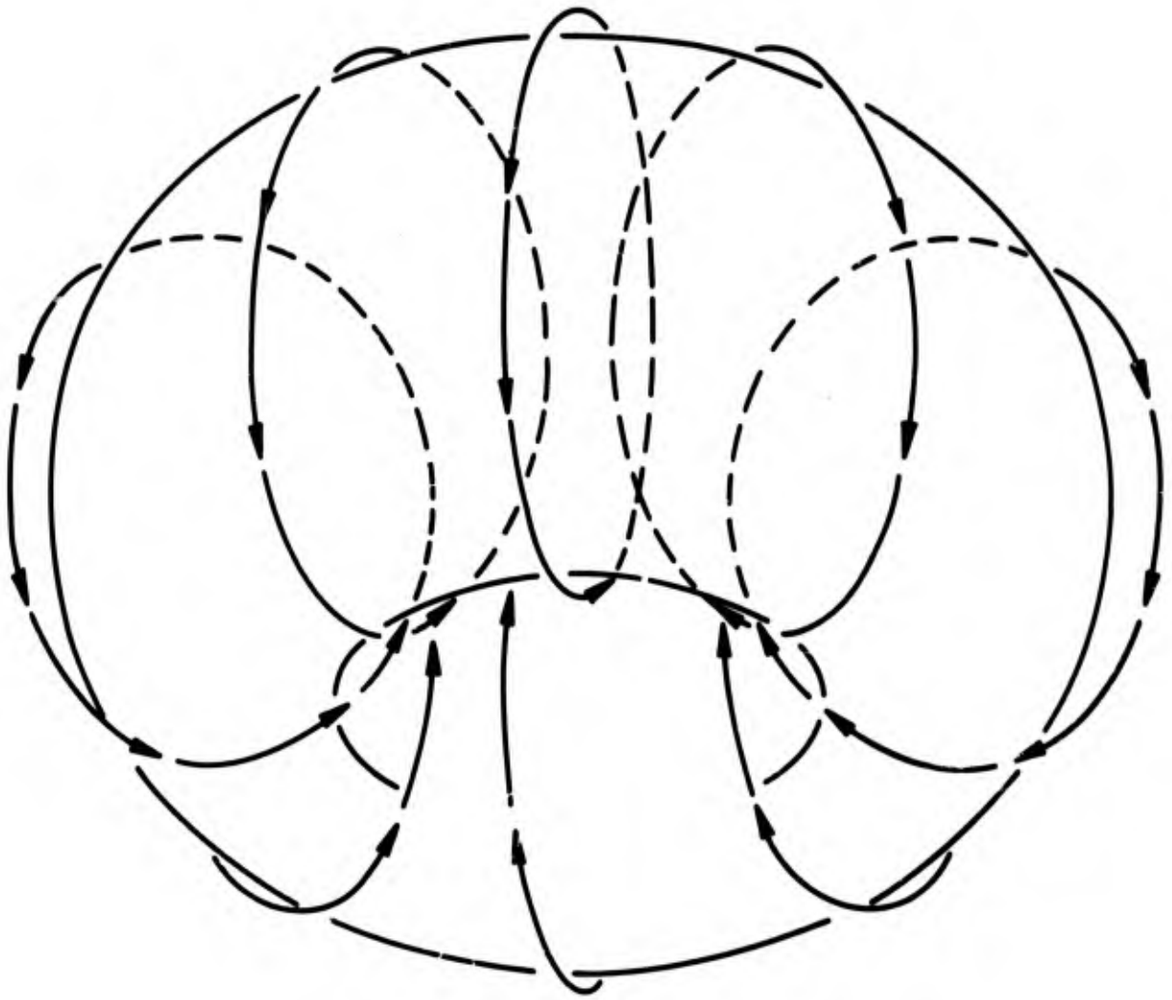

Figure 2. Perspective View of a Rising Nuclear Vortex Ring (Cloud) from a Position Below and to the Side of Ground Zero (Circulation is indicated by the arrowed lines.)

Equations by which the temperature at the initial time and the soil burden of the cloud as a function of yield and height of burst are calculated also have been developed. (This work was supported by the Nuclear Defense Laboratory under Contract DA-18-035-AMC-346(A) and by the Office of Civil Defense under Contract N228(62479)-67712 with the Naval Radiological Defense Laboratory.) The results will be published soon in a final report to the Nuclear Defense Laboratory and, therefore, will not be repeated here.

THE BASIC DYNAMIC MODEL

At times subsequent to t_i, we assume that a nuclear cloud is a buoyantly rising entraining bubble of hot air in pressure equilibrium with the hydrostatic atmosphere

and that radiative loss of heat is not significant. With these assumptions we derive the following general equations from energy balance considerations and the ideal gas equation of state:

$$\frac{dT}{dz} = -(T - T_e)\frac{1}{m}\frac{dm}{dz} - \frac{\rho_e}{\rho}\frac{g}{C_P}M \qquad (1)^*$$

and

$$\frac{dV}{dz} = \frac{1}{\rho}\frac{dm}{dz} + \frac{V}{T}\left(\frac{dT}{dz} + \frac{\rho_e}{\rho}\frac{g}{\mathcal{R}}M\right), \qquad (2)$$

where

V = cloud volume

T = average cloud temperature

T_e = ambient temperature

z = altitude above mean sea level

m = cloud mass

ρ = average cloud density

ρ_e = ambient density

g = acceleration of gravity

C_P = molar specific heat at constant pressure

M = molecular weight of air

$\mathcal{R}$ = universal gas constant.

*This is essentially the same as Eq. (3.4D) of Ref. 1 and Eq. (21) of Ref. 8.

Equations (1 and 2) can be combined and solved for the mass entrainment rate to yield

$$\frac{dm}{dt} = \rho_e \left(\frac{dV}{dz} - \frac{Vg}{\gamma P} \rho_e \right) v \quad , \tag{3}$$

where t is the time; P, the ambient pressure; γ, the specific heat ratio; and v, the cloud rise velocity. We can estimate dV/dz by making use of a well known and widely observed result for entrainment controlled rise of buoyant bubbles through an atmosphere:

$$R = \alpha(z - z') \quad , \tag{4}$$

where R is the bubble radius, α is a constant, and z′ is the value of z at the virtual origin of R as implied by Eq. (4). If we assume that cloud shape similarly is maintained throughout the rise period, we have

$$\frac{dV}{dz} = \frac{3V}{z - z'} \quad , \tag{5}$$

and Eq. (3) becomes

$$\frac{dm}{dt} = \rho_e V \left(\frac{3}{z - z'} - \frac{g\rho_e}{\gamma P} \right) v \quad . \tag{6}$$

Except at very late times, when the cloud is approaching stabilization, the term $g\rho_e/\gamma P$ is negligible compared to $3/(z - z')$, and we may write

$$\frac{dm}{dt} \approx \frac{3\rho_e V}{z - z'} v \quad . \tag{7}$$

Equation (7) is similar to others reported in the literature.[1,9]

To describe a model of the mechanics of cloud rise, the nuclear cloud can be considered either as a bubble of buoyant gas or as a growing vortex ring. Both of

these aspects are important; indeed, they provide complementary representations of the cloud rise and we shall consider both.

A bubble of gas lighter in density than the surrounding ambient air rises because of the buoyancy force on it, whereas its rise is retarded by pressure drag. As the cloud rises, its mass increases by entrainment of ambient air so that the net force on the cloud must be determined by time differentiation of the cloud momentum. The force balance equation of the cloud is

$$\frac{d(mv)}{dt} = V(\rho_e - \rho)\, g - \frac{1}{2}\rho_e v^2 A C_D \quad , \tag{8}$$

where the first and second terms on the right hand side are respectively the buoyancy and drag forces, A is the cross-sectional area of the cloud projected in the direction of motion, and C_D is a dimensionless constant called the drag coefficient. The drag coefficient C_D is a function of both Reynolds number and ellipsoid eccentricity; its value is expected to lie between 1/2 and 1.

After expanding the left hand side of Eq. (8), evaluating A in terms of the cloud radius, and rearranging to the form of the equation of motion of the cloud, we obtain

$$\frac{dv}{dt} = \left(\frac{\rho_e}{\rho} - 1\right) g - \frac{\pi \rho_e v^2 C_D R^2}{2\rho V} - \frac{v^2}{m}\frac{dm}{dz} \quad . \tag{9}$$

We see that the mass entrainment contribution, $\frac{v^2}{m}\frac{dm}{dz}$, effectively adds another drag term to the equation of motion.

To express the equation of motion of a nuclear cloud in terms of vortex ring dynamics we make use of an equation for the impulse of a ring vortex in an ideal fluid given by Lamb.[4] Justification for application of ideal fluid mechanics steady state theory to nuclear vortex rings has been given in Ref. 2 (Chapter II, paragraphs 2 and 3). According to Lamb, the impulse P of a ring vortex of density ρ and radius $\mathcal{R}$ is given by

$$P = \pi \rho \Gamma \mathcal{R}^2 \quad , \tag{10}$$

where Γ is the velocity circulation of the ring vortex. For an ellipsoidal shaped nuclear cloud this may be approximated by the relation

$$P = \pi \epsilon^2 \rho \Gamma R^2 \quad . \tag{11}$$

For a growing nuclear cloud with changing density and constant eccentricity the net force on the cloud is given by

$$\frac{dP}{dt} = \pi\epsilon^2\rho v R^2 \left[\Gamma \left(\frac{1}{R^2} \frac{dR^2}{dz} + \frac{1}{\rho} \frac{d\rho}{dz} \right) + \frac{d\Gamma}{dz} \right] \tag{12}$$

or

$$\frac{dP}{dt} = \pi\epsilon^2\rho v R^2 \left[\Gamma \frac{d\ell n(R^2\rho)}{dz} + \frac{d\Gamma}{dz} \right] , \tag{13}$$

and the equation of motion of the cloud is

$$\frac{dv}{dt} = \frac{\pi\epsilon^2 v R^2}{V} \left[\Gamma \frac{d\ell n(R^2\rho)}{dz} + \frac{d\Gamma}{dz} \right] - \frac{v^2}{m} \frac{dm}{dz} . \tag{14}$$

Equations (1, 6, and 9 or 14) are simplified versions of the basic set of equations required for describing the cloud rise. The major problems remaining are to determine the variation with altitude of the various quantities in Eqs. (9 and 14).

First, however, we shall consider the additional matter of accounting for the presence of soil material in the cloud. A preponderate proportion of the soil material will be in a condensed phase and therefore will serve mainly to ballast and to increase the heat capacity of the cloud. Under the assumption that all soil material is in a condensed phase, Eqs. (1, 2, and 6) can be revised to yield

$$\frac{dT}{dz} = - \left(T - \frac{m_a + m_s q}{m} T_e \right) \frac{1}{m_a + m_s q} \frac{dm}{dz} - \frac{\rho_e}{\rho} \frac{g}{C} , \tag{15}$$

$$\frac{dV}{dz} = \frac{1}{\rho_a} \frac{dm}{dz} + \frac{V}{T} \left(\frac{dT}{dz} + \frac{\rho_e}{\rho_a} \frac{M_a}{\mathcal{R}} g \right) , \tag{16}$$

and

$$\frac{dm}{dz} = m_a \left[\frac{3}{z - z'} + \frac{\rho_e}{P} \left(\frac{\rho_a}{\rho} \frac{\mathcal{R}}{M_a C} - 1 \right) g \right] \Bigg/ \left(1 - \frac{m_a}{m_a + m_s q} + \frac{\rho_a}{\rho} \cdot \frac{\rho_a}{\rho_e} \right) , \tag{17}$$

where the symbols are as defined in Eqs. (1 and 2) except that the subscripts a and s denote air and soil, respectively; the unsubscripted quantities refer to the total cloud, $q = M_a/M_s$ and C is the average specific heat of the cloud.

VARIATION WITH ALTITUDE OF CLOUD RISE PARAMETERS

To determine the cloud growth parameters of Eq. (14), we are making extensive use of cloud rise data in Ref. 5 that have been obtained from movie films of nuclear test shots. (These observed data also are vitally important in checking the efficacy of the theoretical model to reproduce observed cloud behavior.)

During phase 3 of the cloud development (see Figure 1), cloud growth and rise have been observed empirically to proceed by the relation given by Eq. (4),

$$R = \alpha(z - z') \ ,$$

and by

$$z = kt^n \ , \tag{18}$$

where α, k, and n are constants that are unique to each individual shot but can be roughly correlated with weapon yield. Both of these equations, but especially Eq. (18), have been found to fit the observed data with extremely high correlation. (One of the remaining subtasks for the second half of the effort is to relate these equations to atmospheric structure in a useful fashion.)

If we restrict our attention to a particular test shot for which the parameters of Eqs. (4 and 18) have been determined, the only unknown terms in Eq. (14) are those involving Γ, the vortex circulation.* To obtain a relation from which Γ and its rate of change can be determined, we may equate the right hand sides of Eqs. (8 and 12) to obtain

$$\frac{d\Gamma}{dz} + \left(\frac{1}{R^2} \frac{dR^2}{dz} + \frac{1}{\rho} \frac{d\rho}{dz} \right) \Gamma = \frac{1}{\pi \epsilon^2 v} \frac{V}{R^2} \left\{ \left(\frac{\rho_e}{\rho} - 1 \right) g - \frac{\pi \rho_e v^2 R^2 C_D}{2\rho V} \right\}$$

or

$$\frac{d\Gamma}{dz} + \frac{d\ell n(R^2\rho)}{dz} \Gamma = f(z) \ . \tag{19}$$

*v is obtained by differentiation of Eq. (18) with respect to time.

Equation (19) can be integrated to yield

$$\Gamma \rho R^2 = \int_{z_o}^{z} f(z)\rho R^2 dz + \Gamma_o \rho_o R_o^2 \quad , \tag{20}$$

To apply Eq. (20) to determine the change of Γ with time and altitude, it is apparent that an independent estimate of Γ_o must be obtained. A means for accomplishing this, as well as the results of the application of the method to several nuclear test shots, are described in considerable detail in Ref. 3. This procedure, however, is too laborious and demanding of data quality to yield sufficient information to establish variations of Γ over the range of yields and heights of burst desired. More simplified methods, also described in Ref. 3, or others that may be developed, will be applied during the coming months to obtain independent estimates of Γ for as many shots as possible.

Equation (20) was programmed for machine digital calculation to obtain a first order estimate of the behavior of Γ with time and altitude. Values of Γ_o from Ref. 3 in conjunction with estimates of the other model parameters from rise data for real test shots were used in several partial rise simulations. The model has been exercized sufficiently to determine that Γ increases as the cloud rises and grows. This appears to be a physically appropriate result. No results of a final nature, however, can be reported at present.

CLOUD CIRCULATION

The large-scale circulation in a nuclear cloud can be simulated by a three-dimensional ideal fluid vortex ring as described by Lamb.[4] Equations of motion of particles entrained in the cloud have been derived and programmed for machine computation.[2,3] Trajectories of particles of any size moving under the influence of the vortex circulation can be computed. These trajectory computations provide a means for determining the effects of cloud circulation on distributions of particles in the cloud according to particle size and location. It is intended that trajectories of representative particles be computed during the cloud rise and growth simulation phase of the DOD System computations. Since the details of the basic circulation and particle trajectory computation models are adequately presented in Refs. 2 and 3, we shall not repeat them here.

ATMOSPHERIC TRANSPORT OF FALLOUT PARTICLES

INTRODUCTION

The fallout transport module of the DOD Prediction System can be characterized by the terms atomistic, deterministic, and discrete. It is atomistic because the basic element of the module calculations is the fallout particle and, at least in concept, the end results of the model are based on the summation of the effects of individual particles. It is deterministic because the trajectories of individual central particles falling through the atmosphere are uniquely determined by particle and atmospheric properties. It is discrete since the distributions of particles in space, particle size, and radioactivity are divided into discrete parts, the effects of which are associated with representative central particles. The macro-scale atmospheric description used within the transport module is also discrete in that the atmospheric volume of interest during a given time period is divided into subvolumes (cells). Everywhere within a cell the atmospheric properties are considered to be uniform. Thus, the transport module is discrete in space, time, and particle size.

There is within the DOD model more than one system for the description of atmospheric flow. First, we have the macro-scale atmospheric description. In the macro-scale description relatively large cells are employed, and the totality of cells includes a vast volume of atmosphere often on a macro-meteorological scale. Second, we have meso-scale circulation systems. In the meso, or local, atmospheric systems more freedom is allowed in the mode of description. Either much smaller cells, or even a continuous description, may be used. Within each local circulation system, separate and possibly unique particle transport procedures will apply. For practical reasons the DOD model restricts the user to a small number of local circulation systems that are defined within specified boundaries. Where meso- and macro-description systems overlap, the former take precedence since they are capable of greater precision.

WIND CELL CALCULATION METHODS

Transport in a Single Wind Cell

To promote an understanding of the transport calculations of the DOD System, we shall first discuss the transport of a single particle through a single wind cell. Let us consider the two-dimensional example represented in Figure 3 to determine

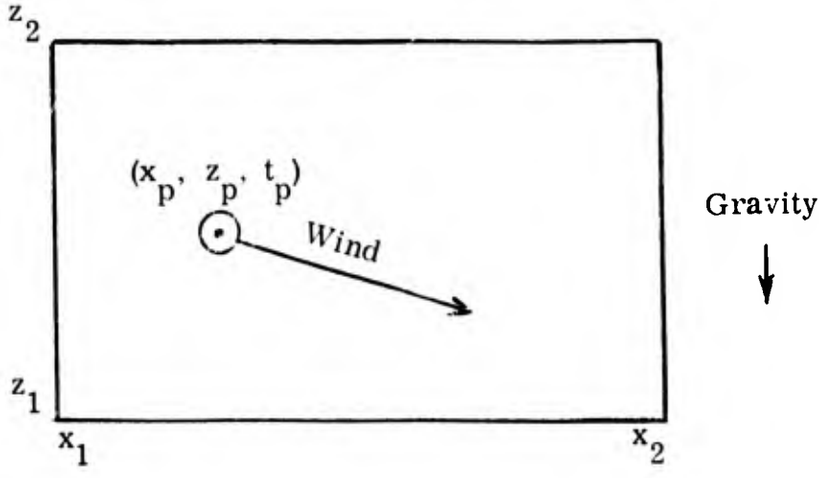

Figure 3. The Wind Cell

the point and time at which a particle originally located at any point x_p, z_p at time t_p will exit from the cell in which it is located. The only forces acting on this particle are gravity and wind drag. Given the particle's size and density, we can compute the particle's terminal velocity (a vertical component). Assuming that the particle's total velocity is equal to the sum of the velocity of the wind and the particle's terminal velocity, we can compute the particle's resultant velocity within the wind cell, and thereby its in-cell trajectory is fully defined since all forces on a particle within a particular cell are taken as constant and independent of position within the cell.

In actual computation we obtain the particle velocity components normal to the bounding planes of the wind cell. We then compute the time at which a boundary intercept would occur in each of the (three) component directions. The earliest of these (three) intercepts indicates the time of exit and also the coordinates of the

exit point. The computation is illustrated, as follows, for the case of a wind vector directed in the positive x axis direction. The distances to boundaries in the x and z directions are given by

$$(x_2 - x_p) \text{ and } (z_p - z_1) \ .$$

For the particular situation illustrated in Figure 3, the times of flight to the x and z bounding planes are

$$t_x = \frac{(x_2 - x_p)}{V_x} \text{ and } t_z = \frac{(z_1 - z_p)}{(V_F + V_z)} \ ,$$

where V_x is the x component of the wind velocity, V_z is the z component of the wind velocity, and V_F is the terminal velocity of the particle and is treated here as a negative quantity. The time increment until exit from the cell is, therefore,

$$t_\epsilon = \text{MIN}(t_x, t_z) \ ,$$

and the particles exit coordinates are

$$x_p^* = x_p + t_\epsilon V_x \ ,$$

$$z_p^* = z_p + t_\epsilon (V_z + V_F) \ .$$

This procedure can be generalized easily to account for: the third dimension, the time limit on the applicability of the current wind description, and particle impact on the topography. Since there are no restrictions placed on the signs and magnitudes of wind vectors, the treatment above is typical but not general and a simple check must be performed at the outset of a computation within a particular cell to determine the proper calculation procedure.

Transport in the Macro-Wind Field

Transport of a single particle through the compartmented wind field is merely an iteration on the single particle-single cell logic. The particle coordinates at

exit from one cell become its initial coordinates for transport through the next cell. In the computer program, transport is always carried out for single particles such that the particle ends up grounded on the topography or positioned in space at a time boundary where it awaits the updating of the wind-field description.

CONSTRUCTION OF THE MACRO-WIND FIELD FROM METEOROLOGICAL DATA

The primary source of wind data to be used in the construction of the wind-field description is derived from atmospheric soundings. The task of converting atmospheric soundings (samplings) into a comprehensive, although discrete, description of the atmosphere is closely analogous to procedures used for weather prediction. Of course, the problem of predicting (in the literal sense) the weather is not new, and fairly sophisticated techniques exist for forecasting purposes. They cannot, however, be relied upon to depict the wind-field description on a meso-meteorological scale. The existing techniques are applicable over large distances in which short-range variations of the wind field are smoothed over. For example, models based on the geostrophic wind approximation attribute the curvature of the wind to the Coriolis effect, which is a relatively large-scale phenomenon (more sophisticated models improve on this approximation). Further investigation on existing models is desirable for the purpose of rendering them suitable over relatively short distances. Because of the extreme complexity of the dynamical weather prediction equations,[10] however, it seems highly unlikely that tangible results are forthcoming in the near future. Despite the limitations of the existing weather prediction models, they can be used to obtain estimates of the wind field for an extremely coarse mesh, say three or four grid points over the entire close-in-fallout range. More expedient methods must be employed to obtain suitable fine-grid wind-field estimates. In the discussion that follows, we present three alternative schemes for expanding a set of input data to a complete three-dimensional wind-field description. The method selected for use in a particular case will be determined by the quantity of data available. The notation used is as follows:

$\vec{R}_i$ = position of i^{th} observed wind velocity vector relative to the wind-field-array grid point $\vec{R}_o$

$\vec{V}_i$ = measured wind velocity at position R_i

$\vec{V}_o$ = wind velocity at a wind-field-array grid point $\vec{R}_o$. $\vec{V}_o$ is to be determined from $\vec{R}_i$ and $\vec{V}_i$.

The Closest Station Method

In this method the velocity at the grid point is assumed to be the same as that of the closest datum point. This will probably be a good approximation if the location of a measurement is sufficiently close to the arbitrary point.

The Preferential Weighting Method

In the preferential weighting method, $\vec{V}_o$ is computed as a weighted average of the velocities at the N nearest data points. The relationship between $\vec{V}_o$ and $\vec{V}_i$ is given by

$$\vec{V}_o = \sum_{i=1}^{N} f_i\left(\vec{R}_1, \vec{R}_2 \ldots \vec{R}_N\right)\vec{V}_i \ , \tag{21}$$

where $f_i(\vec{R}_i, \vec{R}_2, \ldots \vec{R}_N)$ is a weighting factor normalized by the formulation

$$\sum_{i=1}^{N} f_i\left(\vec{R}_1, \vec{R}_2 \ldots \vec{R}_N\right) = 1 \ . \tag{22}$$

A reasonable choice for f_i is

$$f_i = \frac{\left(\frac{1}{\ell_i^2}\right)}{\sum_{k=1}^{N}\left(\frac{1}{\ell_k^2}\right)} \ , \tag{23}$$

in which $\ell_i^2 = x_i^2 + y_i^2 + \alpha z_i^2$, and N = number of sounding stations; α is a constant chosen to be less than unity, so that preferential weighting is given to those sounding stations which are closest in altitude to the arbitrary point. We anticipate much larger variations of the wind velocity in the vertical direction than in the horizontal directions.

The Least-Squares Method

Here, we assume that each velocity component is an analytic function of position. Since the wind velocity in the macro-wind field will not undergo very great spatial variations in a short distance, it becomes possible to approximate each component of the wind velocity by the first few terms of the Taylor expansion taken about the grid point as origin. We then can write

$$u = u_o + (\nabla u)_o \cdot \vec{R} \ ,$$

$$v = v_o + (\nabla v)_o \cdot \vec{R} \ ,$$

and (24)

$$w = w_o + (\nabla w)_o \cdot \vec{R} \ ,$$

where u_o, v_o, and w_o are the x, y, and z components of the wind velocity at the origin. By least-squares fitting of Eq. (24) to the data points, we can determine the twelve unknown constants u_o, v_o, w_o, $(\nabla u)_o \equiv \vec{A}$, $(\nabla v)_o \equiv \vec{B}$, and $(\nabla w)_o \equiv \vec{C}$. Actually, the computation breaks down into three separate parts involving $(u_o, \vec{A})$, $(v_o, \vec{B})$, and $(w_o, \vec{C})$. To illustrate the procedure, we shall outline the method for computing u_o. If U_i denotes the x component of wind velocity at the i^{th} sounding station, the i^{th} residual is given by

$$\xi_i = U_i - u_i = U_i - (u_o + A_x x_i + A_y y_i + A_z z_i) \ . \tag{25}$$

The constants u_o, A_x, A_y, and A_z are determined by the least-squares method[11] by minimizing the functional

$$F(u_o, \vec{A}) = \sum_{i=1}^{N} \xi_i^2 \tag{26}$$

with respect to these four parameters. The four linear equations so deduced are

$$\frac{\partial F}{\partial u_o} = 0 = -\sum U_i + \sum (u_o + \vec{A} \cdot \vec{R}_i) \ , \tag{27}$$

$$\frac{\partial F}{\partial A_x} = 0 = -\sum U_i x_i + \sum (u_o + \vec{A} \cdot \vec{R}_i) x_i \ , \tag{28}$$

$$\frac{\partial F}{\partial A_y} = 0 = -\sum U_i y_i + \sum (u_o + \vec{A} \cdot \vec{R}_i) y_i \ , \tag{29}$$

and

$$\frac{\partial F}{\partial A_z} = 0 = -\sum U_i y_i + \sum (u_o + \vec{A} \cdot \vec{R}_i) z_i \ . \tag{30}$$

Introducing the averaged quantities

$$\bar{u} = \left(\frac{1}{N}\right)\sum U_i \ , \quad \bar{x} = \left(\frac{1}{N}\right)\sum x_i \ , \quad \bar{y} = \left(\frac{1}{N}\right)\sum y_i \ ,$$

$$\bar{z} = \left(\frac{1}{N}\right)\sum z_i \ , \quad \overline{ux} = \left(\frac{1}{N}\right)\sum U_i x_i \ , \quad \overline{uy} = \left(\frac{1}{N}\right)\sum U_i y_i \ ,$$

$$\overline{uz} = \left(\frac{1}{N}\right)\sum U_i z_i \ , \quad \overline{x^2} = \left(\frac{1}{N}\right)\sum x_i x_i \ , \quad \overline{xy} = \left(\frac{1}{N}\right)\sum x_i y_i \ , \tag{31}$$

$$\overline{xz} = \left(\frac{1}{N}\right)\sum x_i z_i \ , \quad \overline{yz} = \left(\frac{1}{N}\right)\sum y_i z_i \ , \quad \overline{y^2} = \left(\frac{1}{N}\right)\sum y_i y_i \ ,$$

$$\overline{z^2} = \left(\frac{1}{N}\right)\sum z_i z_i$$

gives the following matrix equation for u_o and $\vec{A}$:

$$\begin{pmatrix} 1 & \bar{x} & \bar{y} & \bar{z} \\ \bar{x} & \overline{x^2} & \overline{xy} & \overline{xz} \\ \bar{y} & \overline{xy} & \overline{y^2} & \overline{yz} \\ \bar{z} & \overline{xz} & \overline{yz} & \overline{z^2} \end{pmatrix} \begin{pmatrix} u_o \\ A_x \\ A_y \\ A_z \end{pmatrix} = \begin{pmatrix} \bar{u} \\ \overline{ux} \\ \overline{uy} \\ \overline{uz} \end{pmatrix} . \tag{32}$$

By use of conventional matrix inversion techniques, Eq. (32) can be solved for u_o. We have

$$u_o = \gamma_1 \bar{u} + \gamma_2 \overline{ux} + \gamma_3 \overline{uy} + \gamma_4 \overline{uz} , \tag{33}$$

where

$$\gamma_1 = \frac{B^{11}}{|B|} ,$$

$$\gamma_2 = \frac{B^{21}}{|B|} ,$$

$$\gamma_3 = \frac{B^{31}}{|B|} , \tag{34}$$

and

$$\gamma_4 = \frac{B^{41}}{|B|} ,$$

in which $|B|$ denotes the determinent of the matrix Eq. (32). The quantities B^{ki} are the cofactors which equal $(-1)^{i+k}$ times the complimentary minor of the matrix element B_{ki}. It is easy to show that the y and z components of velocity are given by

$$v_o = \gamma_1 \bar{v} + \gamma_2 \overline{vx} + \gamma_3 \overline{vy} + \gamma_4 \overline{vz} \tag{35}$$

and

$$w_o = \gamma_1 \bar{w} + \gamma_2 \overline{wx} + \gamma_3 \overline{wy} + \gamma_4 \overline{wz} \ , \tag{36}$$

where the averaged quantities in Eqs. (35 and 36) are of the same nature as those shown in Eq. (31) with the replacement of U_i with V_i and W_i.

Discussion of Methods

On a purely mathematical basis, it would be desirable to use the least-squares method because it is based on tried and proven experience. However, a minimum of four independent measurements is necessary to render this method applicable. Also, its workability is contingent upon the abundance of closely-spaced sounding stations located in and around the area of interest.

Although the preferential weighting approach is not deduced by rigorous mathematical techniques, it serves to bridge the gap between the least-squares method and the closest-station method. Admittedly, other choices for the weighting function besides $(1/\ell^2)$ are possible and, in fact, should be explored. The preferential-weighting method will be used when the number of sounding stations within the preassigned range is more than one and less than or equal to four; otherwise, the single station approach will be used. It is anticipated that the three alternate methods of computing the wind field on a grid contain sufficient flexibility to render the prediction system a useful research tool.

PARTICLE KINETICS

Motion of Fallout Particles

The fundamental equations which describe the motion of a fallout particle are the momentum equation,

$$\frac{d\vec{V}_p}{dt} = -\left\{ \vec{V}_p(t) - \vec{V}_w\left[\vec{r}(t), t\right] \right\} \phi\left(\left| \vec{V}_p - \vec{V}_w \right| \right) + \vec{G} \ , \tag{37}$$

and the position equation,

$$\frac{d\vec{r}}{dt} = \vec{V}_p \ , \tag{38}$$

where $\vec{V}_p$ and $\vec{V}_w$ are the particle and wind velocity, $\vec{G}$ is the gravitational constant $-G\vec{k}$, and $\phi(|\vec{V}_p - \vec{V}_w|)$ is a friction function so defined that the frictional force per unit mass between the particle and the wind is given by*

$$F = -(\vec{V}_p - \vec{V}_w)\phi \ . \tag{39}$$

Equation (37) is simplified by introducing the relative velocity

$$\vec{\xi} = \vec{V}_p - \vec{V}_w \tag{40}$$

in lieu of $\vec{V}_p$. When Eq. (40) is inserted into Eq. (37), we obtain for $\vec{\xi}$

$$\frac{d\vec{\xi}}{dt} = -\vec{\xi}\phi(|\vec{\xi}|) + \vec{G} - \frac{\partial \vec{V}_w}{\partial t} - \left[(\vec{V}_w + \vec{\xi}) \cdot \nabla\right]\vec{V}_w \ . \tag{41}$$

Except in most unusual and extraordinary cases, the apparent acceleration terms due to the temporal and spatial changes of the wind field are less than $\vec{G}$, the gravitational acceleration. Thus, Eq. (41) reduces to

$$\frac{d\vec{\xi}}{dt} = -\vec{\xi}\phi(|\vec{\xi}|) + \vec{G} \ . \tag{42}$$

In Appendix A we show that both the relative acceleration, $d\vec{\xi}/dt$, and the horizontal components of the relative velocity, $(\vec{\xi}_x, \vec{\xi}_y)$, are negligible. The vertical component of relative velocity is

$$\xi_z = -V_F \ ,$$

---

*A commonly used expression for ϕ in the pressure flow regime is

$$\phi = \frac{1}{2}\frac{C_D}{m}\rho A|\vec{V}_p - \vec{V}_w| = K|\vec{V}_p - \vec{V}_w| \ ,$$

while in the Stokes' law regime ϕ is a constant.

where V_F, the so-called terminal fall velocity, is given by the solution of the equation

$$V_F \phi(V_F) = G \ . \tag{43}$$

Under these circumstances the components of the particle velocity are given by

$$V_{px} = U \ ,$$

$$V_{py} = V \ ,$$

and (44)

$$V_{pz} = - V_F + W \ ,$$

where U, V, and W are the x, y, and z components of the wind velocity. In essence, we have been able to solve the momentum equation for the fallout particle, thus reducing the dynamics of the transport problem to the solution of the position equation. Since originally it was thought necessary to solve both the momentum and position equations, the analytic solution of Eq. (37) reduces the digital computation by a factor of two.

Particle Settling Rates

We have performed a comprehensive survey of methods used for computing particle settling rates, given both in the open literature and in the literature on fallout prediction methods. On the basis of this survey, we have concluded that the equations of Davies[12] for spheres are most appropriate for use in the DOD Fallout Prediction System. The following procedure is used:

1. The dimensionless quantity $C_D R^2$, where C_D is the drag coefficient and R is the Reynolds number, is evaluated by the equation

$$C_D R^2 = \frac{4 g \rho \rho_p d^3}{3 \eta^2} \ , \tag{45}$$

where g is the acceleration of gravity, ρ and ρ_p are the densities of air and particle, d is the particle diameter, and η is the dynamic viscosity of the air.

2. The Reynolds number is evaluated from Davies' polynomials

$$R = \frac{C_D R^2}{24} - 2.3363 \times 10^{-4}\left(C_D R^2\right)^2 + 2.0154 \times 10^{-6}\left(C_D R^2\right)^3 - 6.9105 \times 10^{-9}\left(C_D R^2\right)^4 , \quad C_D R^2 < 140 \tag{46}$$

or

$$\log_{10} R = -1.29536 + 0.986\left(\log_{10} C_D R^2\right) - 0.046677\left(\log_{10} C_D R^2\right)^2 + 0.0011235\left(\log_{10} C_D R^2\right)^3 , \quad 100 < C_D R^2 < 4.5 \times 10^7 . \tag{47}$$

3. The settling velocity V_F is computed from

$$V_F = \frac{R\eta}{\rho d} . \tag{48}$$

4. For small particles at high altitudes, the settling velocity must be multiplied by a drag slip correction, f, where

$$f = 1 + \frac{2.33 \times 10^{-4}}{d\rho} , \tag{49}$$

and d and ρ are in microns and grams per cubic centimeter, respectively.

We conclude that methods used in the past to correct particle fall rates for shape effects in fallout prediction calculations are incorrect. Particles of spherical shape fall at a rate that is the maximum for particles of equivalent volume of all

shapes. In addition, irregularity of shape can cause deviation of particle trajectories from the vertical in still air. It is known that both of these effects become more pronounced with increase in Reynolds number. Unfortunately, so little experimental work has been done for particles in the pressure flow range (i.e., for large Reynolds numbers) that the importance of these effects to fallout prediction calculations cannot be precisely determined. Additional studies of these effects should be performed to resolve the issue.

Appendix B presents the details of our study and a comparison of particle settling rate computation methods. A cursory treatment of turbulent diffusion effects on fallout particles are also included.

LOCAL CIRCULATION SYSTEMS

Orographic Effects

It has been recognized for some time that orographic effects influence the ultimate distribution of radioactivity resulting from a tropospheric nuclear explosion. The vertical lifting of light debris over mountains can extend the fallout range beyond the usual expectations. Gradual but extended depressions will shorten it.

The need to develop a mathematical model of orographic flow which can be rendered compatible with machine computations of fallout arises principally from the lack of sufficient meteorological data, at this time, to yield a satisfactory time and space dependent picture of the wind field. Although sounding stations at 14-mile intervals are planned in the near future (Army Integrated Meteorological System), it is questionable whether even this will be sufficient to account for local variations of the wind field.

A perturbation theory based model has been developed to compute the changes in the wind field caused by orographic effects, such as mountains and valleys. The model is predicted on the assumption of the existence of a uniform, steady velocity field which would otherwise exist in the absence of the ground disturbance. The vertical attenuation constant of the perturbed velocity field is coupled to the periodicity of the ground variation through a dispersion relationship derived from

a system of linear differential equations with constant coefficients. In general, the dispersion relationship is of 2nd degree in k_z, the vertical attenuation constant. and its dependence on k_x and k_y, the wave numbers for the horizontal ground variations, becomes greatly simplified upon neglect of the Coriolis effect. Roughly speaking, this limits the applicability of the theory to ground variations less than ($4\ u_{mph}$) in extent, where u_{mph} is the unperturbed horizontal component of wind velocity in miles per hour. For most practical cases involving tropospheric fallout, this restriction is not severe since sounding stations are presumed to exist at reasonable distances from each other. Moreover, for small u_{mph}, orographic effects can be neglected since the motion of a fallout particle will be nearly vertical, descending with the so-called terminal velocity, V_F.

From a theoretical point of view, this investigation is a modified extension of the earlier work of Queney,[13, 14] but there are differences which render somewhat different results. Although both models utilize perturbation theory to include the effects of variable terrain, there is a distinct conceptual difference between them arising from the choice of the dependent variables. Queney deals with the displaced trajectories of the streamlines as the fundamental physical quantities of interest (which seems to introduce extra degrees of complexity into the problem), while we treat the changes in the velocity field. Our method of attack permits more refined criteria for establishing the validity of the calculation and leads quite naturally to a generalization to three-dimensional systems, which are more frequently encountered than the two-dimensional idealizations of Queney. Moreover, we show that a perturbation theory model for the hydrodynamics does not necessarily imply the applicability of superposition of ground disturbances, a result which does not seem to have been recognized earlier. This is a distinct problem. However, we are able to demonstrate that the superposition hypothesis can serve as the basis of an iterative scheme for computing the velocity field to an arbitrary degree of accuracy consistent with the initial premises of the perturbation method. In certain two-dimensional cases, there does not appear to be much difference between Queney's results and ours.

The relevancy of this model for fallout prediction is considered in the sense that it renders a description of the wind in regions where meteorological data are not readily available. In order to use the theory, it is necessary to deduce an

appropriate wind velocity, u_o, which is supposed to exist in the absence of the particular topographical disturbance. The quantity u_o either can be obtained by a direct measurement from a single meteorological station or suitably constructed from the measurements of a group of nearby sounding stations.

The overall validity of the model is based upon the applicability of the non-turbulent hydrodynamics equations. Consequently, the theory will not yield an accurate description of the wind field within the boundary layer at the earth's surface. There is much uncertainty as to the extent of this layer since it depends on a multitude of physical processes acting in conjunction with each other. For example, the height of the boundary layer over an ocean surface is around 300 ft, the magnitude of which is manifested by the patterns of soaring gulls. If we tentatively use this as a measure of the magnitude of the boundary layer over "non-violent" topographical effects, then for practical purposes, it becomes possible to render the theory applicable over all space since the fallout pattern will not be substantially modified by wind field uncertainties in the lower few hundred feet.

Soluble mathematical models of airflow in the troposphere must in some measure be removed from reality because of the enormous complexity of the actual physical system. Despite this inherent limitation, the non-turbulent models of airflow can be useful for fallout calculations if they at least semi-quantitatively describe the salient features of the particular aerodynamics. The utility of such models can best be evaluated by comparison with suitable experiments.

A detailed analysis, describing the theory of airflow over mountains, valleys, plateaus, and similar terrain under stationary and quasi-stationary wind conditions, is included in Appendix C of this report. We describe the pertinent geometrical details, the perturbation theory, the applications of the theory to specific geometries, and the relevance of our results to the general problem of fallout. In addition, calculations of fallout particle trajectories are made for a two-dimensional mountain ridge, thus permitting some assessment of the importance of this obstacle on the downstream distribution.

Here, we shall present the results for a single mountain and a mountain ridge whose crest-line is not perpendicular to the flow. The x direction points along u_o (the direction of the unperturbed flow), the y axis is perpendicular to u_o, and the

z axis points in the direction of the zenith. The functions u(x, y, z), v(x, y, z), and w(x, y, z) denote the x, y, and z components of the wind velocity.

Investigations have shown that a suitable representation for a mountain is

$$z = f(x, y) = \frac{h(a^3)}{(a^2 + r^2)^{3/2}} , \tag{50}$$

where z is the elevation of the mountain, h is the maximum elevation of the mountain, a is the width, and r is the horizontal distance from the center of the mountain, i. e.,

$$r^2 = x^2 + y^2 . \tag{51}$$

The components of velocity are given by

$$u(x, y, z) = u_o \left[1 + (a^2 h) \frac{(y^2 + \lambda^2 - 2x^2)}{(r^2 + \lambda^2)^{5/2}} \right] , \tag{52}$$

$$v(x, y, z) = 3u_o(a^2 h) \frac{xy}{(r^2 + \lambda^2)^{5/2}} , \tag{53}$$

and

$$w(x, y, z) = -3u_o(a^2 h) \frac{\lambda x}{(r^2 + \lambda^2)^{5/2}} , \tag{54}$$

where

$$\lambda = (z + a) .$$

A limitation of the theory is that the ratio (h/a), which is, roughly speaking, the average slope of the mountain, must be less than unity.

In the case of a three-dimensional mountain ridge not perpendicular to the flow, the line depicting the crest of the mountain is at an angle γ with respect to the direction of the unperturbed flow (see Figure C-2 in Appendix C). The crest-line is assumed to be of infinite length, and in the rotated coordinate system (x', y') it is parallel to the y' axis. The elevation of the ridge, z, is given by

$$z = \frac{h}{1 + (x'/a)^2} , \tag{55}$$

where h is the maximum elevation of the ridge, and a its width; x and y are related to x' and y' by the equations

$$x = x' \cos\gamma - y' \sin\gamma \quad \text{and} \quad x' = x \cos\gamma + y \sin\gamma ,$$

and (56)

$$y = x' \sin\gamma + y' \cos\gamma \quad \text{and} \quad y' = -x \sin\gamma + y \cos\gamma .$$

Using the previous notation for the components for u, v, and w, we have

$$u = u_o - u_o(ah) \cos^2\gamma \frac{\left[(x \cos\gamma + y \sin\gamma)^2 - \lambda^2\right]}{\left[(x \cos\gamma + y \sin\gamma)^2 + \lambda^2\right]^2} , \tag{57}$$

$$v = -u_o(ah) \cos\gamma \sin\gamma \frac{\left[(x \cos\gamma + y \sin\gamma)^2 - \lambda^2\right]}{\left[(x \cos\gamma + y \sin\gamma)^2 + \lambda^2\right]^2} , \tag{58}$$

and

$$w = -2u_o(ah)\lambda \cos\gamma \frac{\left[(x\cos\gamma + y\sin\gamma)\right]}{\left[(x\cos\gamma + y\sin\gamma)^2 + \lambda^2\right]^2} , \qquad (59)$$

where

$$\lambda = z + a .$$

It should be noted that u, v, and w really depend on $x' = x\cos\gamma + y\sin\gamma$, so that the origin of the (x, y) coordinate system can be located anywhere along the crest-line. For convenience it will be located at the center of the crest-line in the actual computations.

The Sea Breeze

An extensive evaluation and review of existing sea-breeze theories is rendered in Appendix D, the results of which may be summarized as follows.

The linearized model of the sea-breeze as developed by Defant[15] has been selected as the most suitable model for the sea-breeze for two reasons: (1) it gives good agreement with experimental observation, and (2) the resulting analytical expressions for the components of the sea-breeze are relatively simple from a computational standpoint. Defant approaches the sea breeze circulation problem in the sense of Lord Rayleigh's convection theory,[16] the dynamics of which are governed by the continuity equation, the three momentum equations, the equation of state, and the heat-diffusion equation. By neglecting density variations in the continuity equation, and including them in the momentum equations since they modify the action of gravity, it becomes possible to construct a vorticity function from which the components of velocity in a plane perpendicular to the coast can be determined. Included in Defant's model is the assumption of an infinitely long coastline which points in the y direction; variations of velocity in this direction are neglected. The x axis is perpendicular to the coast and positive inland, while the z axis denotes the vertical.

Although the fundamental equations which describe the system are non-linear, in the sense that they depend on products of the dynamic meteorological variables, it becomes possible to linearize the equations by a perturbation theory technique. As pointed out in Appendix D, this procedure cannot unequivocably be justified, but apparently it leads to results which are consistent with observation. The perturbation methods lead to a set of coupled linear partial differential equations with constant coefficients, which can readily be solved by the variables-separable technique. The boundary conditions are:

$$\text{at } z = 0, \quad \theta = e^{i\Omega t}\Delta T \sin \lambda x, \quad w = 0$$

$$\text{at } z = \infty, \quad \theta = 0, \quad w = 0,$$

where λ equals π/L, L is the extent of the sea breeze, Ω is the frequency of the sideral day which equals 7.3×10^{-5} sec^{-1}, ΔT is the temperature differential, and x extends from $-(L/2)$ to $(L/2)$. The theory leads to the following expressions for the potential temperature θ and for u, v, and w, the x, y and z components of the wind velocity.

$$\theta = \Delta T \sin \lambda x \left[e^{-g_2 z} \cos(\Omega t + h_2 z) + e^{-g_1 z} A \cos(\Omega t + h_1 z + \phi) \right.$$
$$\left. - e^{-g_2 z} A \cos(\Omega t + h_2 z + \phi) \right], \tag{60}$$

$$u = -\frac{\Delta T \cos \lambda x}{\lambda} B \left[P_1 e^{-g_1 z} \cos(\Omega t + h_1 z + \psi - S_1) \right.$$
$$\left. - P_2 e^{-g_2 z} \cos(\Omega t + h_2 z + \psi - S_2) \right], \tag{61}$$

$$v = \frac{\Delta T \cos \lambda x}{\lambda} BQ \left[P_1 e^{-g_1 z} \cos(\Omega t + h_1 z + \bar{\psi} - S_1) \right.$$

$$\left. - P_2 e^{-g_2 z} \cos(\Omega t + h_2 z + \bar{\psi}\, S_2) \right] , \tag{62}$$

$$w = \Delta T \sin \lambda x B \left[e^{-g_1 z} \cos(\Omega t + h_1 z + \psi) - e^{-g_2 z} \cos(\Omega t + h_2 z + \psi) \right] . \tag{63}$$

The constants which appear in the foregoing expressions are determined from the physical parameters in the system such as L, Ω, the Guldberg-Mohn friction parameter σ, the Coriolis parameter f, the kinematic eddy viscosity K, and the unperturbed potential temperature and potential temperature gradient.

THE COMPUTER PROGRAM

SYSTEM PHILOSOPHY

A model for use in fallout prediction research must be extremely flexible if it is to be successful. One of the prime objectives of a research model is sensitivity testing to identify and to some extent quantify the variables that are important for the prediction of fallout effects. The paucity and inconsistency of observed data on fallout effects and the fallout environment dictate that the model must provide a framework for analysis, and, therefore, it must be given the capability of providing a detailed theory of fallout prediction.

Design requirements have called for flexibility in regard to the extent and precision of the prediction, the research objective, the submodels used, and also speed of operation. In regard to computer programming, we must interpret flexibility to mean the ability to deal with various overall forms of the whole model, alternative submodels and submodel programs, variable extent and precision in input and output data sets, and submodel options for modeling, computation, and display. This interpretation implies that the program of the DOD fallout research model must have all the attributes of a computational system, rather than merely a computer program. Specifically, there must be a program execution monitor system or program

which provides the data environment for all other programs of the whole model. As the system executive of the DOD model, we make use of the FORTRAN Monitor System's CHAIN link feature. The CHAIN feature, which is given only terse description in most FORTRAN manuals, basically allows one to link a number of FORTRAN programs (with subroutines) together in any sequence or in loops and sequences.

The task of the DOD Fallout Prediction System is to provide a detailed modeling of events beginning with a nuclear detonation and ending with radioactive decay of ground deposited debris material. A physically reasonable and scientifically defensible division of the complete modeling task is clearly required, since the events taking place are complex and an extensive treatment of each is needed. We have chosen the subdivision scheme illustrated in Figure 4 to represent the required total model. This figure shows a sequence of logically separate modules which in total cover the complete phenomenon of interest. The Fireball Module begins with basic weapon and environmental parameters and ends with the beginning of entrainment controlled cloud rise. The Cloud Rise Module then develops from these results a description of the distribution of fallout particles after cloud rise circulation is no longer important. The Particle Activity Module assigns radioactivity to the particles on the basis of information supplied by the preceding models. The Transport Module accounts for the effect of atmospheric motion and results in a distribution of fallout debris on the ground. The Output Processor Module interprets the results of the Transport Module in light of user requests for particular tabulations. We also have established a set of intermediate results that follow each module computation. Some computation modules may be bypassed entirely by simply replacing them with intermediate results generated synthetically or by a previous calculation.

In the DOD model computer system there is a group of programs corresponding to each of the major subdivisions shown in Figure 4. These program groups are executed essentially in the sequence shown to make a fallout prediction. However, since each of these program groups requires extensive computation and is

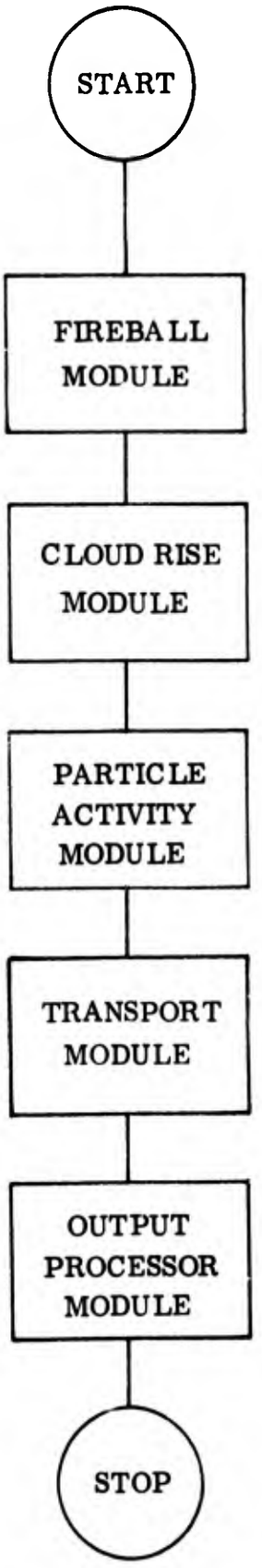

Figure 4. DOD Model Computer System

expensive to execute, experience dictates that the sequence be arranged so that it might be stopped and restarted anywhere in the chain of models. Thus, while the basic program execution sequence is that shown in Figure 4, a more complete picture of the model is given by Figure 5, which shows the intermediate results produced and the inputs required at each stage of the model. Figure 5 and its supporting documentation define the linkage between the modules and indicate, as well, the stop and restart points that have been designed into the DOD model.

In the following sections, we shall discuss the modules. The Fireball Module and the Particle Activity Module are being constructed independently of this contract; nevertheless, the Fireball Module will be described in sufficient detail to clarify its position in relation to the overall model. The Particle Activity Module will not be discussed.

THE FIREBALL MODULE

The purpose of this module is to supply a set of initial conditions to serve as primary inputs to the Cloud Rise Module. These are an initial time, average cloud temperature at the initial time, mass of the soil burden in the vapor and condensed phases, and size distribution parameters of fallout particles. The calculation involves serial exercising of a group of subroutines, one for each parameter to be provided in the output. Input is weapon yield, height (or depth) of burst, and soil category (siliceous or calcareous). Both the analysis and programming are being done by Technical Operations Research under contract DA 18-035-AMC-346(A) to the Nuclear Defense Laboratory.

THE CLOUD RISE MODULE

The Tech/Ops Cloud Rise Module can be considered to consist of two component parts: (1) the dynamics submodel, and (2) the particle circulation submodel. These submodels are closely linked, however, with flow of considerable information from

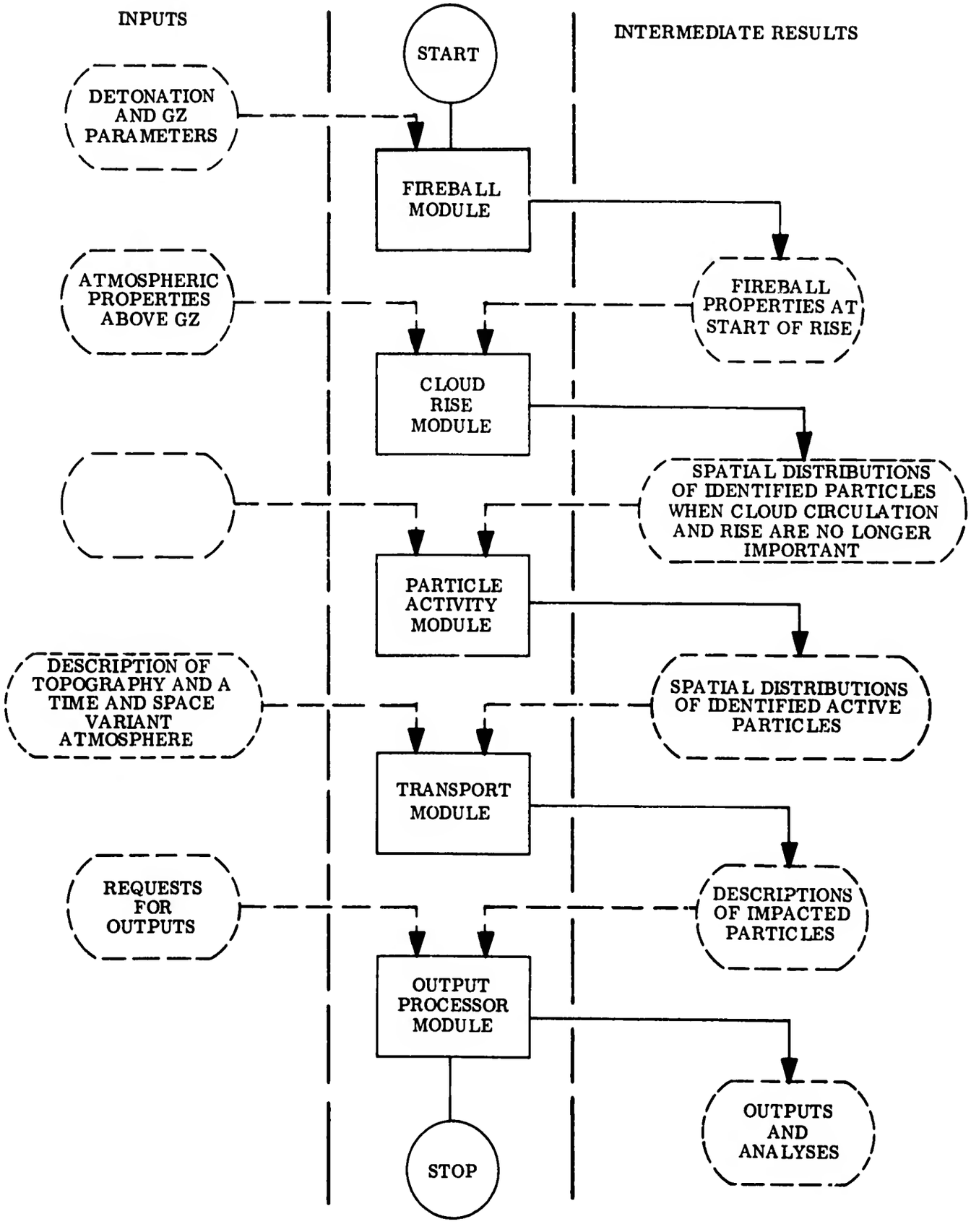

Figure 5. Data Flow in the Program Sequence

the dynamics portion to the particle circulation portion. Starting with the initial conditions specified by the Fireball Module, the differential equations of cloud rise and growth in the dynamics submodel and the differential equations of particle motion in the circulation submodel are solved numerically at each step of a succession of short time-steps. In this manner, the time profile data on cloud size, height, temperature, and content will be accumulated at the same time the particle trajectories are determined. As implied above, the two submodels will be run in parallel.

Upon reaching a condition that has been selected as representing stabilization, i.e., when the cloud rise is complete and turbulence has subsided to a low level, the particle data obtained from the circulation program will be smoothed and expanded to an essentially continuous distribution in space, the cloud will be sectioned three-dimensionally into cells, and then each cell center will be corrected for horizontal cloud drift. The center of each cell will be assigned an appropriately weighted spectrum of particle sizes. During the ensuing transport calculations each size fraction from a cell will be transported independently. Particle activities will be assigned by the Particle Activity Module program being developed at the Naval Radiological Defense Laboratory. A preliminary flow chart of the Cloud Rise Module organization is shown in Figure 6. Theoretical studies on the dynamics portion of the model are incomplete at the time of this writing, so that programming of this submodel is still in the planning stage. On the other hand, the particle circulation submodel is in an advanced stage of development.

THE TRANSPORT MODULE

The specific purpose of the transport program is to accept a list of fallout particle properties and positions, and mathematically transport these particles through a temporally and spatially varying wind velocity field until they land on the ground or until the researchers interests are satisfied. The transport module has been divided for sake of flexibility and ease of construction into three major programs, each of which makes a separate chain link. These three links have the following general purposes:

Link 1. Initialization and control
Link 2. Wind field description
Link 3. Particle transport.

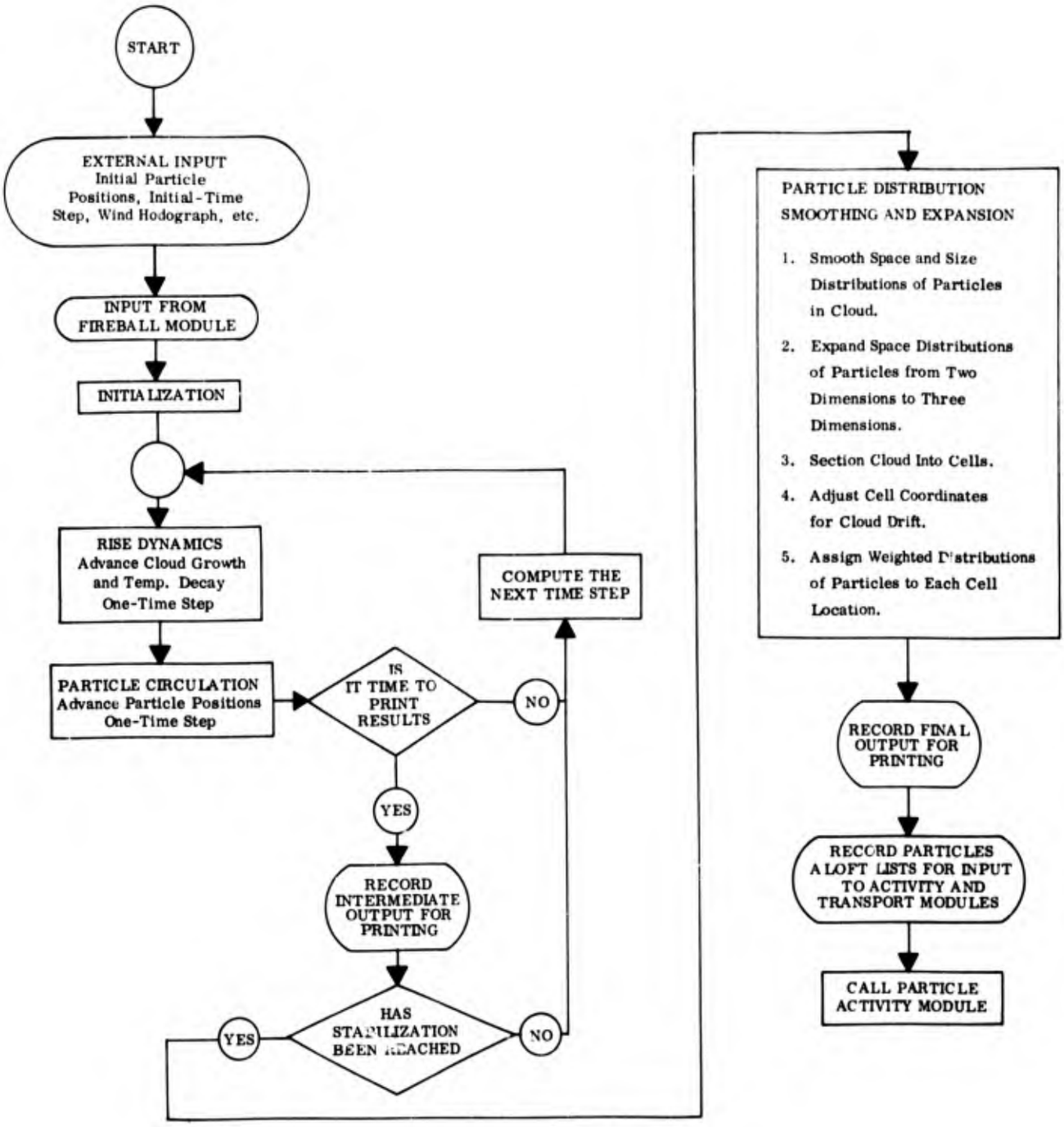

Figure 6. Preliminary Organization Flow Chart for the Cloud Rise Module

Figure 7 shows the arrangement in which the computations required during the transport period are grouped for execution. Note that final exit from Link 1, the transport executive, is made via a subroutine to a fourth and final chain link, the Output Processor. Figure 8 is a flow chart of the general program logic of the transport module. This simplified representation shows in some detail the hierarchy of computation loops that make up the transport logic. A simpler representation of this hierarchy is given in Figure 9, which shows a nested set of five loops. In the outermost loop, there is a test to determine if the specified temporal extent of the transport has been achieved, and, if not, an updated version of the wind-field description is computed. In the next lower hierarchy level, a part of a multi-part wind-field description is brought into the computer (if a multi-part description is in use) in order to transport particles which have gone beyond the in-core part of the description. In the third level of the hierarchy, the topographic description is treated like the multi-part wind description (if required). In the particles aloft list loop, individual particle descriptions are given sequential attention, and in the actual transport code the individual fallout particle is transported until it reaches either the ground or some boundary at which in-core data are insufficient to move it further. Figure 10 represents schematically the flow of information from secondary (tape) memory to primary (core) memory and back during an extensive run of the transport program. Using Figure 10 as a guide, let us consider the sequence of data flows.

Initially, only the particles (input) and topography tapes contain any information, and only the transport codes themselves are in primary memory. The initialization and control program (Link 1) reads identification information from the particles (input) tape, writes comments on the system output tape, and then, if required, loads the topography arrays from a previously prepared topography tape.* At this point the wind-field description program (Link 2) is called and a wind-field description is generated. This description is generated directly (and completely) into the wind arrays in primary memory by the current versions of

*A special program has been written to aid the researcher in preparing topography tapes from topographic maps or other sources. The user may, however, specify a planar topography and bypass the use of a detailed topographic tape.

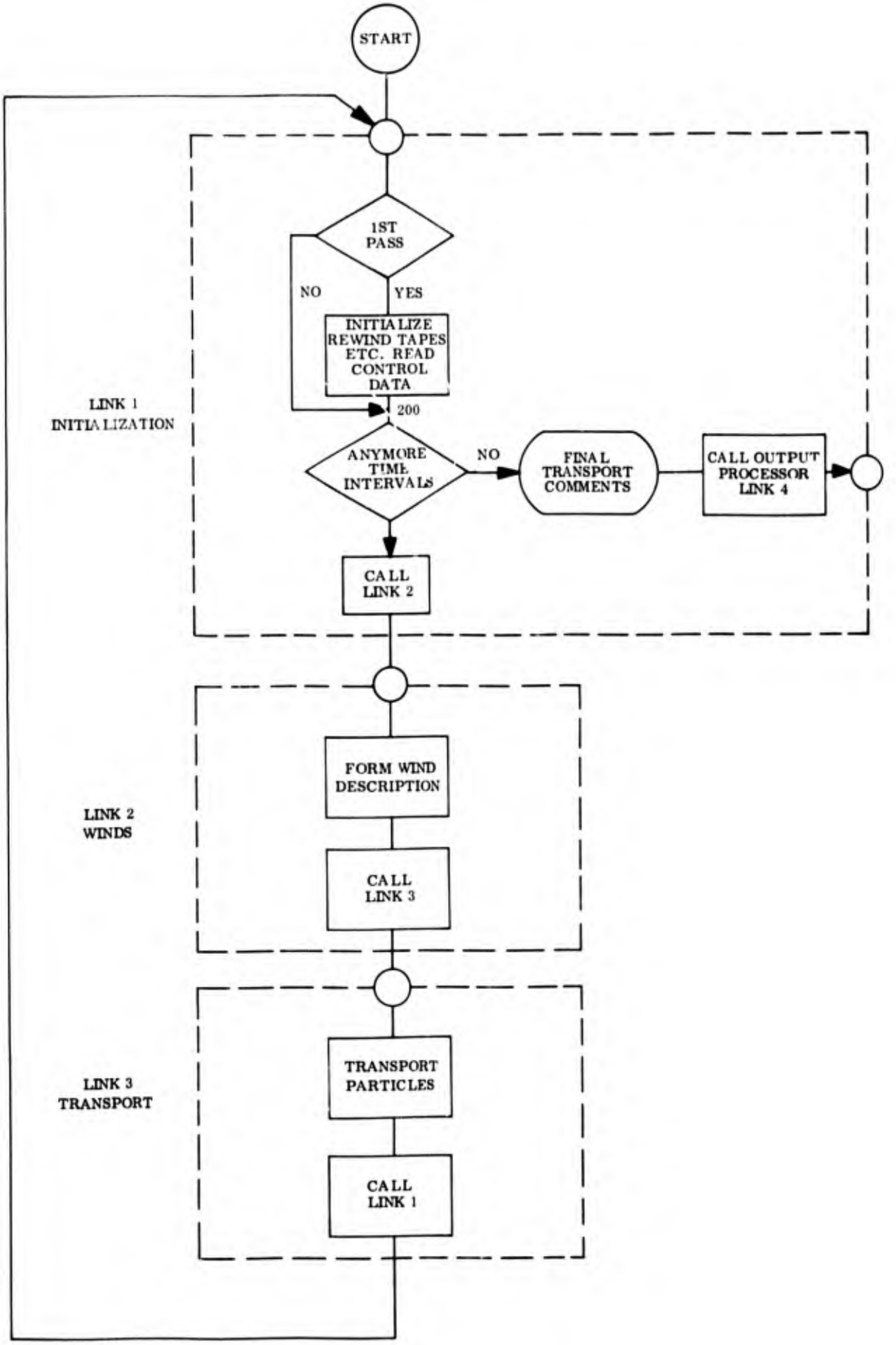

Figure 7. Chain Link Arrangement for Transport Module

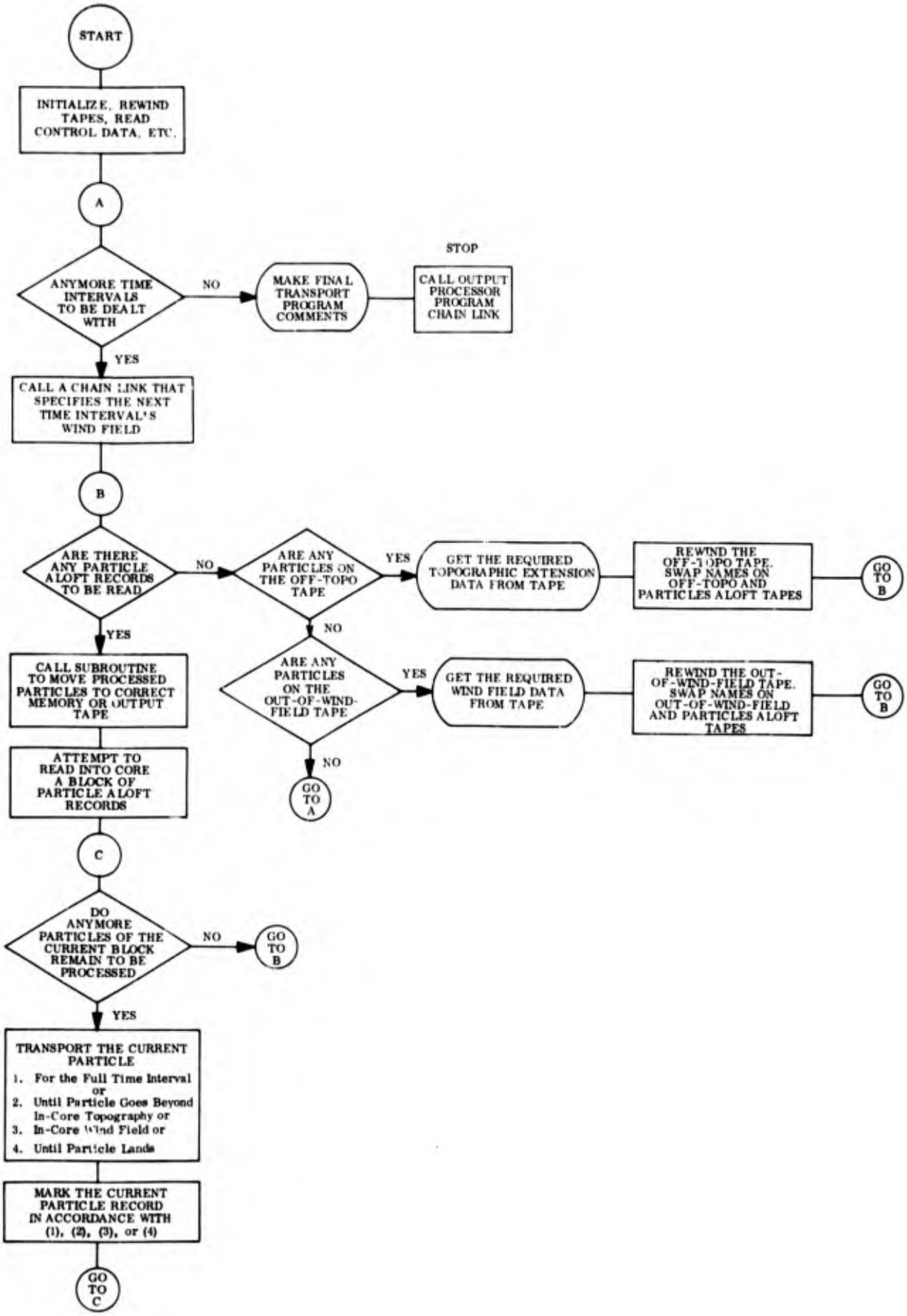

Figure 8. General Flow Chart of Transport Program

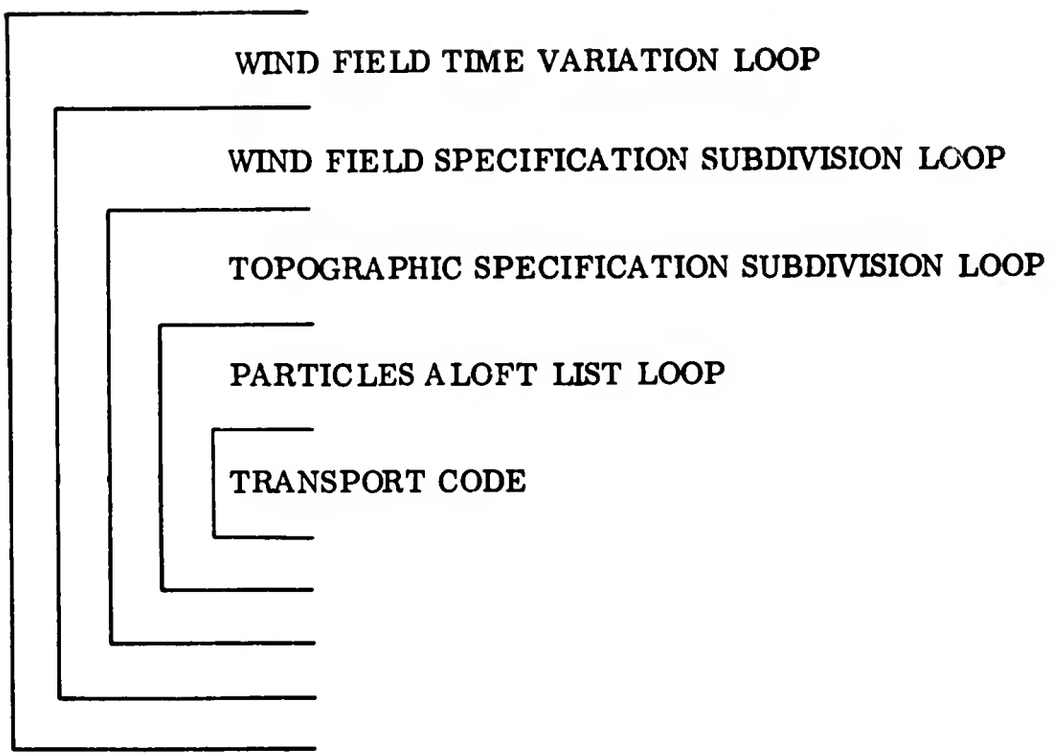

Figure 9. Transport Module Loops

Link 2. However, if future requirements warrant, a modified version of Link 2 might produce a more extensive description of the wind field and be forced to store part of it on tape. In either case, when Link 2 is completed, the wind arrays are loaded and a "map" of the wind tape (if any) has been produced and stored in primary memory.

Next, we enter Link 3, the actual transport program, and read a part of the particles (input) tape into primary memory. The particle descriptions are then transported one at a time until one of five possible conditions arises. These conditions, which may be thought of as boundaries, are:

1. The particle drifts beyond the area for which a topographic height has been specified in core. In this case the particle's description is marked so that it will be eventually written onto the "off-topo" tape.

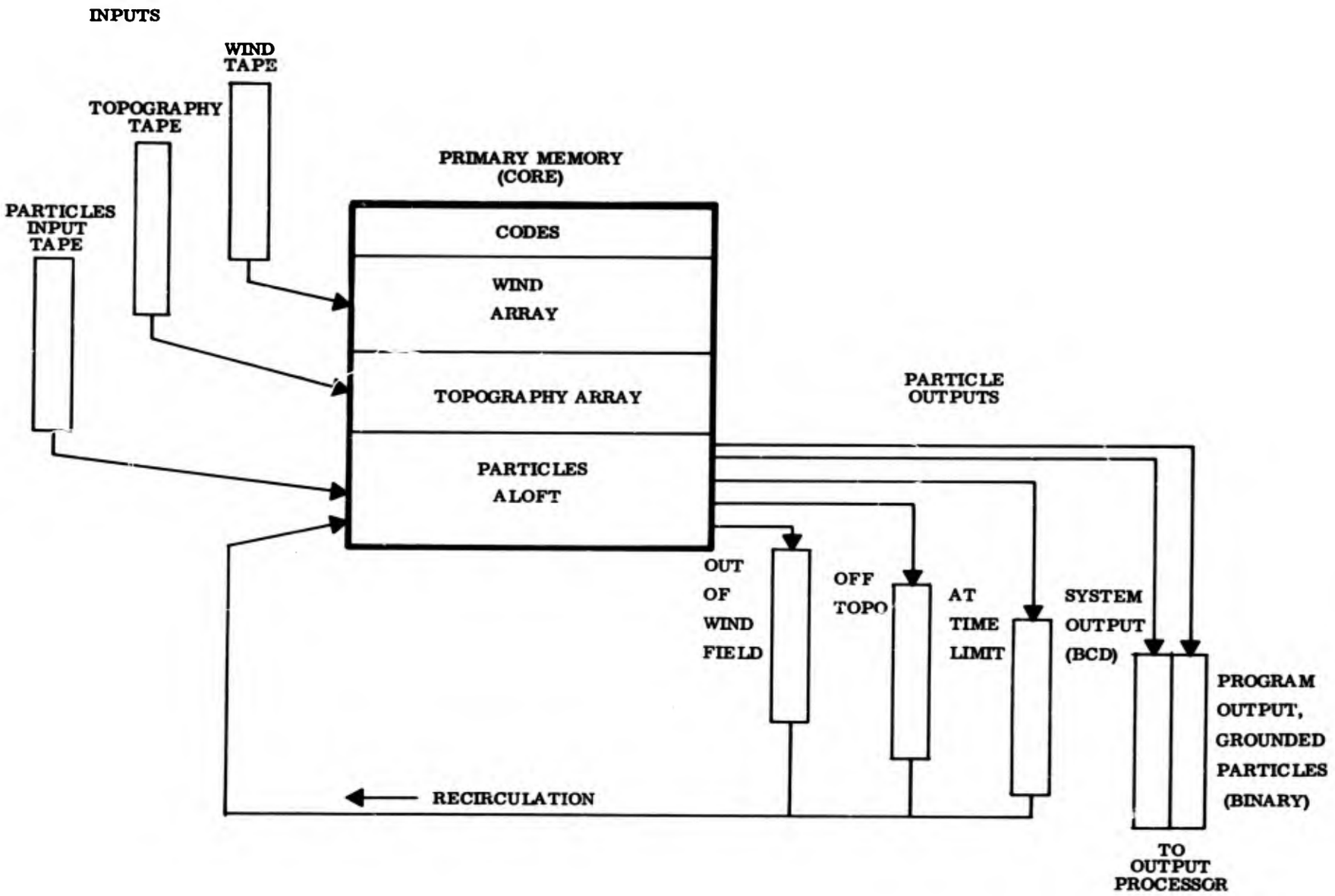

Figure 10. Transport Program Data Flow

2. The particle drifts beyond the region for which the wind velocity field has been specified in core. In this case the description is marked to go on the "out-of-wind-field" tape.

3. The particle encounters neither of the previously mentioned boundaries and is still aloft at the time when the wind field description must be updated to achieve discrete temporal variability of the wind field. In this case the description is marked to go on the "time boundary" tape.

4. The particle becomes grounded on the topography. In this case the particle description is marked so that it eventually is written on the "program output tape" which is used as an input to the Output Processor.

5. The particle drifts beyond the entire secondary as well as primary memory region of specification for either topography or winds. In this case the description is marked to be written on to the "system output tape" and is removed from the transport process.

When the entire block of descriptions has been read into memory and processed, the next block of particle descriptions is read into memory and processed. After all particle descriptions on the original input tape have been processed, treatment of the data (if any) on the three recirculation tapes begins. First, if any descriptions were written on the "off-topo" tape, a new block of topographic data is read in, and the "off-topo" tape is put into the position (symbolically) of the original particles input tape. Processing continues as before, and eventually the condition will obtain that at the end of a pass no descriptions will be found on the "off-topo" tape. Under this condition we proceed to consider the "out-of-wind-field" tape in a manner analogous to "off-topo." The treatment given to the "time boundary" tape is similar, but when all particles that are still aloft are on the "time boundary" tape, a new description of the wind field must be computed. Before each call of the wind-field program (Link 2) a check is made to see if the transport time limit has been exceeded, and if it has been, a termination procedure is executed to record the final status of memory.

Obviously, many details and options have been omitted in the foregoing discussion. At this time it must suffice to say that there is still some development work to be done to the main transport loop, and upon its completion the detailed documentation of the transport program can be carried out.

THE OUTPUT PROCESSOR MODULE

The Basic Operation of the Output Processor

The Output Processor of the DOD Fallout Prediction System is a very flexible, highly modular computer program for use in the interpretation of data representing grounded subdivisions of the radioactive cloud. It accepts descriptions of grounded cloud subdivisions, interprets them into a two-dimensional memory array or map image, and then prints the resulting array in a form suitable for viewing as a map. The interpretation processes required of the Output Processor are the computation of: (1) dose rate "normalized" to H + 1 hour, (2) dose rate at a specified time, (3) dose accumulated between two specified times, and (4) particle mass deposited per unit area.

The apparent simplicity of the foregoing task specification may lead one erroneously to believe that the Output Processor is a straightforward and even trivial program. However, the requirement for flexibility and adaptability in dealing with large input and output data sets has led to a rather large and complex but hopefully useful program. The approach that was followed was dictated both by our contractual work statement and also by our own understanding of the status of fallout prediction research. The following statements outline this approach:

1. Great flexibility in program use should be sought in terms of the nature of computations and tasks and in terms of the degree of precision in both modeling and display.

2. The Output Processor should be capable of handling a large set of grounded particle data; the size of this set might exceed available memory space by many times.

3. The position and scale factor of the map should be under the direct control of the researcher. (This gives the user or researcher the ability to produce maps of any desired scale

factor for superposition on other maps and enables him to achieve either a microscopic or a macroscopic view of the fallout field.)

4. The Output Processor should be capable of handling output maps containing a larger number of map grid points than can be represented in the computer memory at one time.

5. In general, it was desired that the Output Processor be simple to use and be reasonably foolproof and automatic with respect to its internal operations. (Since the sizes of input and output data sets were assumed to be widely varying, this led us to a certain amount of essentially "dimension free" programming with the objective of making it unnecessary in most situations for the user to explicitly modify memory allocations (dimension statements) and recompile programs in order to change the program's scale of operation.)

Flexibility and Modularity

Flexibility of a kind can be achieved in complex computer programs through the use of modular construction. To provide the user with a program having a functional modularity of construction allows him great latitude in making modifications within the context of the defined set of subroutine functions or purposes. However, modularity can generate considerable inter-program communication and debugging problems particularly if there are few logically simple functional subdivisions in the task to be accomplished by the program. From the practical point of view, in conventional FORTRAN systems the achievement of program flexibility through module replacement means that the user must frequently modify the composition of decks of binary and symbolic cards, which is both time consuming and costly.

To achieve program flexibility through the coding of a number of options into a single program is sometimes wise. Such attempts, however, often fail because the programmer must anticipate user requirements (which are often not even known to

the user), and he often guesses wrong. Yet, where important options are seen to be needed and alternative treatments are available, internal program options are very practical.

For a prediction system, one which is to be capable of aiding the researcher in his many and varied tasks, no single approach to flexibility is sufficient; consequently, we have designed the system of programs with three modes of flexibility. These are program modularity, parameter controlled options, and as a mid-ground between these two, prepared code insertion points. In the basic model of the fallout process, and where possible within its programs, functional subroutines have been defined to operate wherever functions can be clearly seen. For example, within the Output Processor there is a subroutine (CALC) with the primary function of interpreting grounded cloud subdivisions into a two-dimensional array, and a separate subroutine (MAP) with the function of composing and displaying the computational results. These functional subroutines may be relatively easily replaced by other modules having similar purposes. As an example of the second mode of flexibility, in CALC all currently required computational tasks have already been accounted for and these computational alternatives are treated as parameter-controlled options within the program. In order to select one of the available computational options, the user need only punch on an input card the appropriate numerical value for an input parameter, in this case the parameter NREQ (see Appendix E). Furthermore, provision has been made in the CALC option selection procedure (as well as in those of other programs) for the future inclusion of other computational option codes with little or no modification to the control programming within the subroutine. Such insertion points are noted in the flow charts and card listings and represent the third mode of program flexibility.

Use of the Output Processor

A preliminary version of the card input description of the User's Manual for the Output Processor is presented in Appendix E. The primary input to the Output Processor is the magnetic tape of grounded particle descriptions that is produced by the Transport Module. For each included central particle which represents a cloud subdivision, this tape contains the two horizontal coordinates of its impact

point, its time of input, the central particle size, and a particle class identification number. The tape also contains a table of particle properties indexed on the particle class identification number. These properties are:

1. The mass per horizontal unit area covered by the cloud subdivision at the time of its definition
2. The dose rate increment that would be observed at the center of the subdivision at time H + 1 hour
3. The radioactivity decay rate of the particle class.

In addition to this primary input, the user must communicate to the program his wishes regarding the kind of output computation and its form of presentation. He must also provide run identification information and information on certain important computer features. These latter inputs are necessary to allow the program to adapt to some degree to different computer environments.

The following algebraic sentence characterizes the Output Processor:

Particle impact data

\+ computer characteristics and run identification
\+ presentation characteristics
\+ computation option specification
\+ display option specification
⇨ desired presentation.

By computer characteristics we mean simply the identifiers of magnetic tape units that are available for temporary use by the Output Processor and the character spacing constants for the off-line printer. The run identifier is an arbitrary 71 character symbol which the user can set to identify and associate outputs and inputs. The presentation characteristics are at this time merely the description of the geographical limits and data point density of a map which is to be produced as output. Computation option means the choice of which of the six (at this time) alternative output quantities should be computed and displayed. Display option means the choice of a particular printer map format or eventually some format on

another kind of output device. A listing and brief discussion of each of the major options for computation and display which exist in the Output Processor are:

1. Printed Descriptions of Impacted Particles

   Under this option the content of the grounded particles tape may be printed in a form analogous to that in which it exists on the transport tape (IPOUT). While this option is valuable in checking the execution of experimental transport codes, it is also useful in providing a hard and readable copy of the result of transport production runs.

2. Computational Options

   a. Count of grounded cloud subdivisions. This optional computation was of primary value in debugging the Output Processor but may also be of considerable value to the researcher in assessing the statistical validity of a computed map quantity at any particular point on the map.

   b. Dose rate "normalized" to time H + 1 hour. This is the recognized standard mathematical construct for the comparison of fallout patterns.

   c. Dose rate at time H + T1. This is actually the estimated dose rate at the specified time taking into account the impact times of all cloud subdivisions.

   d. Dose accumulated from time H + T1 to infinity. This is the estimated dose as integrated from time H + T1 or particle impact time, whichever is later.

   e. Dose accumulated from time H + T1 to time H + T2. This is the estimated dose as integrated from time H + T1 or particle impact time (whichever is later) to time H + T2.

   f. Total mass deposited. This is the estimate of the mass of fallout, both radioactive and inert, deposited on the map during the entire fallout period.

g. Total mass deposited between times T1 and T2. This is the estimate of the total mass, both active and inert, deposited during the specified interval.

3. The Undistorted Map Option

In specifying the scale factor of the output map, it is possible for the user to specify separate grid point intervals for the North-South and East-West directions. Thus he may in general obtain as an output a distorted mapping of the situation represented by the fallout model. By using the undistorted map option the user requests the assistance of the program in setting the grid intervals so that a conventional undistorted map will be produced. However, he must still specify the map's scale factor.

4. Display Options

Two display options exist at this time in the Output Processor. These options, which can be characterized as the two-line E-format and the two-line F 11.3-format, are explained and illustrated below for a single data point.

a. The two-line E-format

NNNNNN
±V.VVV

interpreted as

$\pm V.VVV \times 10^{NNNNNN}$.

b. The two-line F 11.3-format

NNNNNN
±V.VVV

interpreted as

± NNNNNNV.VVV .

The Output Processor has been arranged to accept as input a sequence of requests for processing. This was deemed appropriate because of the large number

of different quantities which might be of interest to the researcher now and after further development of the program and also because of the usual turn-around time delays which plague the users of computer centers operating in the batch processing mode. Rather than handling requests on a one-per-run basis, unlimited sequences of requests are accepted. Figure 11 shows the general flow logic of the Output Processor.

The user may specify the geographical limits for a sequence of output maps, and for each set of map limits he may specify a sequence of computation requests. Thus, the card input deck is hierarchical in construction with two levels in its hierarchy. Because of the severe limitation of high-speed memory space during the output processing, it was not practical to process more than one map request at a time. At present, the grounded particles data tape must be passed once for each map request. If and when non-map requests are added to the list of possible processing tasks, it may become desirable to remove this one-pass-per-request restriction.

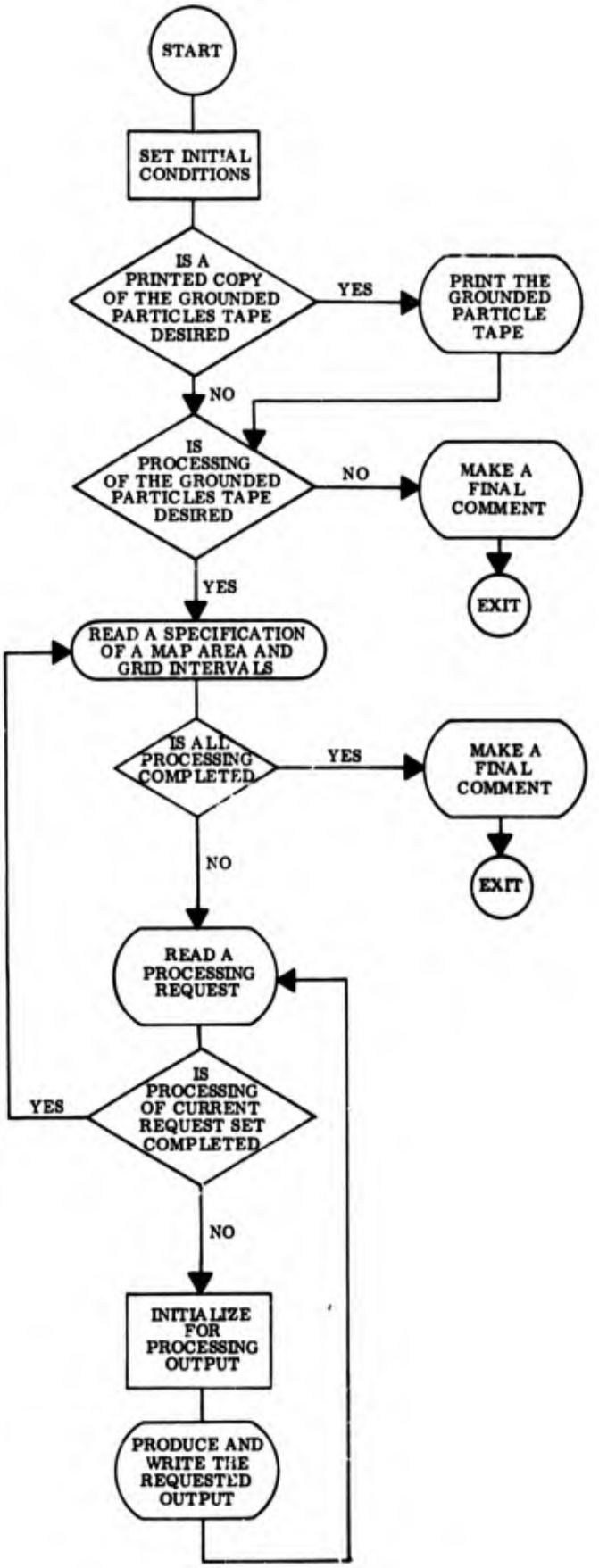

Figure 11. Output Processor General Logic

CONCLUSIONS

Substantial research and development progress has been made on the design of an improved land fallout prediction system. Research on cloud rise dynamics is advancing satisfactorily, and the research effort in atmospheric transport of fallout is essentially completed. An overall strategy for preparation of the computer program has been devised, and the coding and debugging are well advanced in the areas of atmospheric transport and output processing.

PROGRAM FOR NEXT INTERVAL

CLOUD RISE DYNAMICS

In the remaining period of this effort, the cloud rise and growth model must be upgraded to account for effects of variation of yield, height of burst, and soil burden. To do this requires that the variation with these quantities of many of the critical model parameters be studied and quantitatively determined. The final phase of the cloud development, phase 4 in Figure 1, also must be studied and represented by an appropriate physical model. Finally, the several models must be combined and programmed for machine computation as a link in the computing system of the DOD Fallout Prediction System.

TRANSPORT

Subtasks planned for completion in the remaining six months period are.

1. Complete the verification of the sea-breeze model.
2. Develop sub-routines for incorporating the orographic-effects model and the sea-breeze model in the computer program.
3. Investigate the effects of air turbulence on the transport of fallout particles. Up to now, this aspect of the problem has been neglected under the assumption that the dispersion in the trajectory of an individual fallout particle caused by the randomness or turbulence of the air is small. Arguments have also been rendered to the effect that although turbulence may cause a significant trajectory smearout for a single particle, the net effect will average out to zero. We will evaluate these conjectures during the remaining period of the contract.

COMPUTER PROGRAMMING

The programming efforts to be carried out on the DOD Fallout Prediction System are summarized as follows:

1. Virtually all of the programming on the cloud rise program remains to be done.

2. In relation to the three major programs of the transport module, only minor adjustments need to be made in the Link 1 program, and documentation remains to be written. Two wind vector interpolation options must be added to the Link 2 program. The orographic-flow model and the sea-breeze model must be programmed in their entirety. In the Link 3 program, testing of the existing code operating with a horizontally and temporally variant wind description remains to be done. Minor modifications must be made to the basic transport loop of the program to allow for the inclusion of one or more local wind system programs. This is primarily a matter of establishing communication and control conventions between Links 2 and 3. After making these programming modifications and additions, the Link 3 documentation will be written.

3. No important additions or modifications to the Output Processor (Link 4) are foreseen. Only final testing in assembly with other DOD Model programs and second draft documentation remain to be done.

REFERENCES

1. I.O. Huebsch, "The Development of a Water-Surface-Burst Fallout Model: The Rise and Expansion of the Atomic Cloud," U.S. Naval Radiological Defense Laboratory, Report No. USNRDL-TR-741, 23 April 1964

2. H.G. Norment, "Research on Circulation in Nuclear Clouds," Technical Operations Research, Report No. TO-B 63-102, 1 December 1963.

3. H.G. Norment, "Research on Circulation in Nuclear Clouds, II(U)," Technical Operations Research, Report No. TO-B 64-102, 1 November 1964.(Conf.-FRD)

4. H. Lamb, "Hydrodynamics," Sixth edition (New York, N.Y.: Dover Publications, 1932), Sec. 162.

5. Unpublished Document on Cloud Characteristics, Edgerton, Germeshausen and Grier Report No. ET-833, prepared on contract AT(29-1)1183. (Secret-FRD)

6. R.W. Hillendahl, "Characteristics of the Thermal Radiation from Nuclear Detonation (U)," Vol. III, U.S. Naval Radiological Defense Laboratory, Report No. TR-383, 30 June 1959. (Secret RD)

7. S. Glasstone, ed., "The Effects of Nuclear Weapons" (Washington, D.C., U.S. Atomic Energy Commission, 1962), Sec. 2.116.

8. R.R. Rapp and R.E. Huschke, "On the Behavior of Large Hot Bubbles in the Atmosphere," The RAND Corporation, Report RM-3605-DASA, June 1963. (Secret RD)

9. G.I. Taylor, "Dynamics of a Mass of Hot Gas Rising in Air," U.S. Atomic Energy Commission, Report No. MDDC-919, 16 March 1945.

10. P.D. Thompson, "Numerical Weather Analysis and Prediction" (New York, N.Y.: The MacMillan Company, 1961).

11. J.B. Scarborough, "Numerical Mathematical Analysis," Fifth Edition (Baltimore, Maryland: The Johns Hopkins Press, 1962).

12. C.N. Davies, "Definitive Equations for the Fluid Resistance of Spheres," Proc. Phys. Soc. (London) 57, 259 (1945).

13. P. Queney, "Theory of Perturbations in Stratified Currents with Applications to Air Flow over Mountain Barriers," Miscellaneous Reports No. 23, Department of Meteorology, University of Chicago (1947).

14. P. Queney, "The Problem of Air Flow over Mountains: A Summary of Theoretical Studies," Bull. Am. Meteorol. Soc. 29, 16 (1948).

15. F. Defant, "Theorie der Land-und Seewinde," Arch. Meteorol. Geophys. Bioklimatol. 2, 404 (1950)

16. Lord Rayleigh, "On Convection Currents in a Horizontal Layer of Fluid when the Higher Temperature is on the Under Side," Phil. Mag. 32, 529 (1916).

17. G.K. Batchelor, "Heat Convection and Buoyancy Effects in Fluids," Quart. J. Roy. Meteorol. Soc. 80, 339 (1954).

18. R.H. Magarvey and C.S. MacLatchy, "The Formation and Structure of Vortex Rings," Canadian J. Phys. 42, 678 (1964).

APPENDIX A

THE MOTION OF FALLOUT PARTICLES IN A WIND FIELD

INTRODUCTION

In the following sections, we render a simplified way of treating the motion of fallout particles in wind fields usually encountered in the migratory period from cloud rise to ultimate delivery on the earth's surface. In particular, we demonstrate that the horizontal components of the relative acceleration of the fallout particle with respect to wind velocity are negligible at every point in space and time. It will be shown that the foregoing assertion permits the horizontal displacement of the fallout particle to be determined from the equations

$$\frac{dx}{dt} = u\left[\vec{r}(t),\ t\right] \tag{1}$$

and

$$\frac{dy}{dt} = v\left[\vec{r}(t),\ t\right] \quad , \tag{2}$$

while the equation for the vertical displacement is given by

$$\frac{dz}{dt} = -V_F + w\left[\vec{r}(t),\ t\right] \quad . \tag{3}$$

In the above notation, $\vec{r} = \vec{i}x + \vec{j}y + \vec{k}z$ is the particle position; u, v, and w are the x, y, and z components of the wind velocity; and V_F is the so-called particle fall velocity defined later in the text.

The description of the particle trajectory as given by Eqs. (1 to 3) represents a substantial reduction (by at least a factor of two) in machine running time as opposed to the system of equations that would have otherwise resulted. In general, the motion of a particle is determined from the six equations,

$$\begin{aligned} (dV_i/dt) &= F_i, \qquad (i = x, y, z) \\ (dX_i/dt) &= V_i, \qquad (i = x, y, z) \quad . \end{aligned} \tag{4}$$

The reduction of Eq. (4) to the set given by Eqs. (1 to 3) results from the approximate solution of the force equation. The uncertainties introduced by our treatment, which are evaluated in a later section, are found to be quite negligible for reasonable wind fields.

THE DYNAMICS OF PARTICLE MOTION

The motion of a fallout particle in the wind is given by

$$\frac{d\vec{V}_p(t)}{dt} = -\left(\vec{V}_p(t) - \vec{V}_w\left[\vec{r}(t),\ t\right]\right)\phi\left(\left|\vec{V}_p - \vec{V}_w\right|\right) + \vec{G} \tag{5}$$

and

$$\frac{d\vec{r}}{dt} = \vec{V}_p \ , \tag{6}$$

where

$\vec{V}_p$ = particle velocity,

$\vec{V}_w$ = wind velocity,

$\vec{G}$ = gravitational force = $-G\vec{k}$,

$\phi(|\vec{V}_p - \vec{V}_w|)$ = a friction function defined in such a way that the frictional force per unit mass between the particle and wind is given by:

$$\vec{F} = -(\vec{V}_p - \vec{V}_w)\,\phi \ .$$

A common expression for ϕ, valid for large Reynolds numbers, is

$$\phi = \frac{1}{2}\frac{C_D}{m}\rho A\,\left|\vec{V}_p - \vec{V}_w\right| = K\left|\vec{V}_p - \vec{V}_w\right| \ , \tag{7}$$

whereas in the Stokes' law regime ϕ = constant. Here C_D is the drag coefficient, ρ is the air density, m is the particle mass, and A is the cross-sectional area of the particle perpendicular to its direction of motion.

Equation (5) is simplified by introducing the relative velocity

$$\vec{\xi} = \vec{V}_p - \vec{V}_w \ , \tag{8}$$

from which we obtain the equation for the relative acceleration:

$$\frac{d\vec{\xi}}{dt} = -\vec{\xi}\,\phi(|\vec{\xi}|) + G - \frac{\partial \vec{V}_w}{\partial t} - (\vec{V}_w \cdot \nabla)\,\vec{V}_w - (\vec{\xi} \cdot \nabla)\,\vec{V}_w \ . \tag{9}$$

Although Eq. (9) may seem rather imposing, the predominance of the gravitational force as opposed to the other terms in the expression, coupled with the negligibility of the inertia term as compared to the friction force, renders a relatively simple solution. We shall show in the next section that

$$\begin{aligned} (d\vec{\xi}/dt) &\approx 0 \ , \\ \xi_x &\approx 0 \ , \\ \xi_y &\approx 0 \ , \\ \xi_z &= -V_F \ , \end{aligned} \tag{10}$$

where V_F is the fall velocity which satisfies the equation $V_F\phi(V_F) = G$. These assertions imply that the horizontal components of fallout particle velocity are given by

$$\begin{aligned} V_{px} &\simeq u \ , \\ V_{py} &\simeq v \ ; \end{aligned}$$

the vertical velocity, by

$$V_{pz} = -V_F + w \ .$$

SIMPLIFICATION OF THE FORCE EQUATION

Since the analytic justification for the neglect of the relative acceleration is difficult to achieve in the differential equation form (as given by Eq. 9), we shall

show that the relative acceleration is indeed negligible by breaking up the velocity field into cells and looking at the dynamics in each cell (see Figure A-1). For mathematical simplicity, we shall consider a two-dimensional cell structure in which the positive z axis is the vertical and the x axis is the horizontal.

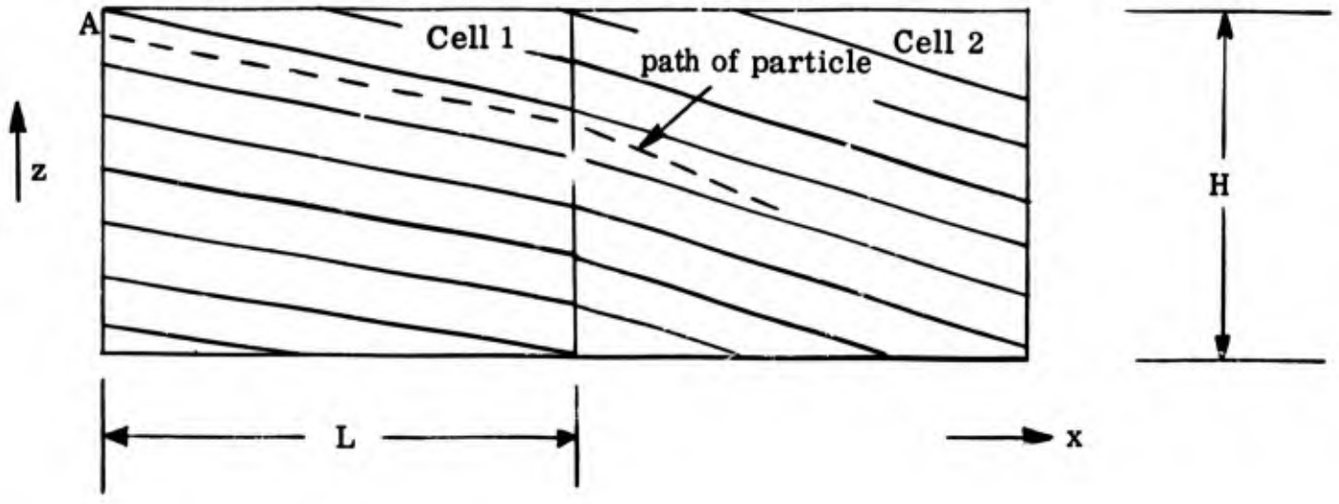

Figure A-1. Cell-Particle Motion

Consider two adjacent cells of length, L, and height, H. The diagonal lines are the direction of the wind field. We assume that within each cell the velocity in a particular direction is uniform, but can change with time in a preassigned way. The mathematical description of the velocity is thus given by

u_1, u_2 = x component of wind velocity in cells 1 and 2,

w_1, w_2 = z component of wind velocity in cells 1 and 2,

$$\frac{\partial u_1}{\partial x} = \frac{\partial u_2}{\partial x} = \frac{\partial w_1}{\partial x} = \frac{\partial w_2}{\partial x} = \frac{\partial u_1}{\partial z} = \frac{\partial u_2}{\partial z} = \frac{\partial w_1}{\partial z} = \frac{\partial w_2}{\partial z} = 0 \ ,$$

$$\frac{\partial}{\partial t} \rightarrow \frac{d}{dt} \neq 0 \ .$$

Since the spatial derivatives are absent within each cell, the equation of motion is

$$\frac{d\vec{V}_p(t)}{dt} = -\left(\vec{V}_p(t) - \vec{V}_w(t)\right) \phi\left(\left|\vec{V}_p - \vec{V}_w\right|\right) + \vec{G} \ . \qquad (11)$$

Introducing the relative velocity

$$\vec{\xi} = \vec{V}_p - \vec{V}_w \tag{12}$$

gives

$$\frac{d\vec{\xi}}{dt} = -\vec{\xi}\,\phi(|\vec{\xi}|) - \frac{d\vec{V}_w(t)}{dt} + \vec{G} \quad . \tag{13}$$

If we assume that $(d\vec{\xi}/dt)$ is negligible, we imply that the relative velocity in each cell is determined from the equation

$$\vec{\xi}\,\phi(|\vec{\xi}|) = \vec{G} - d\vec{V}_w(t)/dt \quad . \tag{14}$$

The solution of Eq. (14) gives $\vec{\xi}$ as a function of t. We denote the solution of the foregoing algebraic equation by $\vec{\xi}_\ell(t)$, and one possible criterion for the negligibility of $(d\vec{\xi}/dt)$ is the comparison of $(d\vec{\xi}_\ell/dt)$ with the other terms in Eq. (13). This is not, however, an ironclad rule since a very steep ramp function for $(d\vec{V}_w(t)/dt)$ will render a time independent $\vec{\xi}_\ell(t)$, whose derivative will be identically zero. On the other hand, the exact solution to Eq. (13) will give time dependent transients whose derivatives may be substantially different from zero.

For reasonable values of $(d\vec{V}_w/dt)$, we shall initially show that $(d\vec{\xi}/dt)$ is negligible by comparing Eqs. (13 and 14) for a proposed digital solution to the problem in which the time variation of $(d\vec{V}_w/dt)$ is given by a series of step functions. We write Eq. (13) in its component form:

$$\frac{d\xi_z}{dt} = -\xi_z\phi(|\xi|) - \frac{dw}{dt} - G \quad , \tag{15}$$

$$\frac{d\xi_x}{dt} = -\xi_x\phi(|\xi|) - \frac{du}{dt} \quad , \tag{16}$$

where

$$\xi = \left(\xi_x^2 + \xi_z^2\right)^{1/2} \quad .$$

Let us suppose that at time t = 0 the fallout particle enters cell 1 with initial relative velocity components, ξ_{zo} and ξ_{xo}. For a period of time T_1, the components of wind velocity are assumed not to change, so that the equations of motion are:

$$\frac{d\xi_z}{dt} = -\xi_z \phi(|\xi|) - G, \tag{17}$$

$$\frac{d\xi_x}{dt} = -\xi_x \phi(|\xi|), \qquad \text{for} \quad 0 \leq t \leq T_1 \ . \tag{18}$$

Let us take for our initial conditions $\xi_{xo} = 0$, and $\xi_{zo} = 0$. Thus, the only equation to be solved is

$$\frac{d\xi_z}{dt} = -\xi_z \phi(|\xi_z|) - G \ . \tag{19}$$

Using a proposed form of $\phi(|\xi_z|)$ equal to

$$\frac{1}{2} \frac{C_D}{m} \rho A \, |\xi_z| = K \, |\xi_z| \ , \tag{20}$$

and letting

$$\lambda = -\xi_z \ ,$$

give us

$$-\frac{d\lambda}{dt} = \lambda^2 K - G$$

or

$$\int_o^{\lambda} \frac{d\lambda'}{G - K\lambda'^2} = t \ , \tag{21}$$

from which the solution becomes

$$\xi_z = -V_F \tanh\left(\frac{Gt}{V_F}\right) , \tag{22}$$

where V_F is the so-called fall velocity, determined from the solution of the equation

$$KV_F^2 = G . \tag{23}$$

This, of course, is the solution of Eq. (17) when $(d\xi_z/dt) = 0$. The asymptotic value of ξ_z will be reached when $(Gt/V_F) \sim 2$ (tanh $2 \sim 0.96$), or a time t_c equal to

$$\bar{t} \sim 2(V_F/G) = 2t_c; \qquad t_c = (V_F/G) . \tag{24}$$

For a 1000-μ particle at 10^3 ft, $(V_F/G) = 0.806$ yielding 1.6 sec for $\bar{t}$, while for the lightest particles it will assume values in the millisecond range. The vertical displacement in time t is given by

$$d = V_F \int_0^t \tanh\left(\frac{Gt'}{V_F}\right) dt' = \frac{V_F^2}{G} \int_0^{Gt/V_F} \tanh x\,dx = \frac{V_F^2}{G} \log(\cosh x) , \tag{25}$$

which for $t = 2t_c$ is approximately given by

$$d \sim \frac{V_F^2}{G} = t_c V_F .$$

We thus see that for times less than two seconds the equilibrium fall velocity is reached; this is achieved in distances small compared with the other pertinent dimensions in the system. On the basis of these calculations, we can now relax the imposition that the horizontal components of velocity change in stepwise fashion,

and seek to solve Eq. (16) almost exactly. This equation permits a relatively simple solution in the case where ξ_x turns out to be much less than V_F. In this case, $\phi(|\xi|)$ is with good approximation given by

$$\phi(\xi) \simeq \frac{G}{V_F} = \frac{1}{t_c} \quad . \tag{26}$$

Equation (16) thus becomes

$$\frac{d\xi_x}{dt} = -\frac{\xi_x}{t_c} - \frac{du}{dt} \quad . \tag{27}$$

Using the initial condition, $\xi_{xo} = 0$, we find that the solution of Eq. (27) is given by

$$\xi_x = -e^{-t/t_c} \int_o^t e^{t'/t_c} \frac{du}{dt'} dt' \quad , \tag{28}$$

$$\xi_x = -e^{-t/t_c} \left\{ t_c \left[e^{t/t_c} \left(\frac{du}{dt}\right) - \left(\frac{du}{dt}\right)_{t=0} \right] - t_c \int_o^t e^{t'/t_c} \left(\frac{d^2u}{dt'^2}\right) dt' \right\} \quad , \tag{29}$$

or

$$\xi_x = -t_c \left(\frac{du}{dt}\right) + t_c e^{-t/t_c} \left(\frac{du}{dt}\right)_{t=0} + t_c e^{-t/t_c} \int_o^t e^{t'/t_c} \left(\frac{d^2u}{dt'^2}\right) dt' \quad . \tag{30}$$

The first term in Eq. (30) is the solution of Eq. (27) when $(d\xi_x/dt) = 0$. The second term in Eq. (30) becomes small in any event for $t > t_c$, while the last term will always be small because (d^2u/dt^2) is itself a small quantity. Moreover, even for

a finite number of discontinuities in (du/dt), the $\exp(-t/t_c)$ factor renders the last term in Eq. (30) negligible for $t > t_c$. The validity of Eq. (30) is predicated on the supposition that $|\xi_x|$ be less than V_F, which is mathematically stated as

$$t_c \left|\frac{du}{dt}\right| < V_F \tag{31}$$

or

$$\frac{1}{G} \left|\frac{du}{dt}\right| < 1 \ . \tag{32}$$

The foregoing inequality is well satisfied without exception.

In summary, we find that the neglect of $(d\xi_z/dt)$ and $(d\xi_x/dt)$ is well justified after an insignificantly small time. The axial and horizontal relative velocity components are given by

$$\xi_z = -V_F \ , \tag{33}$$

and

$$\xi_x = -\frac{V_F}{G} \frac{du}{dt} \ . \tag{34}$$

For Eqs. (33 and 34) to be meaningful, the size of the first cell must be substantially greater than the distance corresponding to the damping time for the transients. That is

$$L > ut_c \ ,$$

and

$$H > (V_F + w)\, t_c \text{ (44 ft for a 1000-}\mu\text{ particle with } w = 0) \ . \tag{35}$$

We now consider what happens when the particle crosses a vertical interface, as shown in Figure A-1. At the 1-2 interface, there are discontinuities both in u and w, so that both ξ_x and ξ_y experience discontinuous changes. These discontinuities result from the physical requirement that the particle velocity remains

continuous. If time t = 0 is now established at the boundary, then ξ_x and ξ_z have initial values which are different from zero. It readily follows that

$$\xi_{xo} = u^{(1)} - u^{(2)} = \Delta u \tag{36}$$

and

$$\xi_{zo} = -V_F + w^{(1)} - w^{(2)} = -V_F + \Delta w \ , \tag{37}$$

where Δu and Δw are the discontinuous changes in horizontal and vertical wind velocity at the 1-2 boundary. In order to easily demonstrate the negligibility of transient effects resulting from the inclusion of $(d\xi_x/dt)$ and $(d\xi_z/dt)$, it is desirable to make Δu and Δw less than V_F so that $\phi(|\xi|)$ is still given by

$$\phi(|\xi|) = \frac{G}{V_F} \ .$$

This permits an analytical solution for ξ_x and ξ_z. As in the previous case, the result, of course, gives transients which diminish in less than a few seconds. However, Δu and Δw are not really independent parameters; they depend on the curvature of the wind field. We have*

$$\Delta u = \left(\overline{\frac{\partial u}{\partial x}}\right) \Delta L \ , \tag{38}$$

and

$$\Delta w = \left(\overline{\frac{\partial w}{\partial x}}\right) \Delta L \ , \tag{39}$$

*Strictly speaking, we should write

$$\Delta u = \left(\frac{\partial u}{\partial x}\right) \Delta L + \left(\frac{\partial u}{\partial z}\right) \Delta z'$$

$$\Delta w = \left(\frac{\partial w}{\partial x}\right) \Delta L + \left(\frac{\partial w}{\partial z}\right) \Delta z' \ ,$$

where $\Delta z'$ is the vertical distance traversed in cell 1. However, there is no loss in generality since the pursuant arguments which apply to Eqs. (38 and 39) are also valid when the more exact expressions are used.

where $\overline{(\partial u/\partial x)}$ and $\overline{(\partial w/\partial x)}$ are the average partial derivatives over cell 1. The condition that

$$\Delta u << V_F \quad \text{and} \quad \Delta w << V_F \tag{40}$$

thus becomes

$$\overline{\frac{\partial u}{\partial x}} << \frac{V_F}{L}; \qquad \overline{\frac{\partial w}{\partial x}} << \frac{V_F}{L} \ . \tag{41}$$

On the other hand, we have $L >> ut_c$ (from Eq. 35), which thus establishes the inequalities,

$$\frac{V_F}{\overline{(\partial u/\partial x)}} >> ut_c \quad \text{and} \quad \frac{V_F}{\overline{(\partial w/\partial x)}} >> ut_c \ ;$$

or in simpler terms,

$$u\overline{(\partial u/\partial x)} << G \quad \text{and} \quad u\overline{(\partial w/\partial x)} << G \ . \tag{42}$$

These inequalities will be easily satisfied with the possible exception of the most violent tornadoes and cyclones.

The analysis just presented for the transition across a vertical interface can be shown to be applicable when applied to a transition across a horizontal interface.

CONCLUSION

By proposing a cell model for the solution of the equations of motion for a fall-out particle, we have been able to show that the relative acceleration of the particle with respect to the local wind velocity is negligible. The relative velocity is greatest in the vertical direction and is, with very good approximation, given by

$$V_F \phi(V_F) = G \ .$$

The friction function $\phi(V_F)$ depends on z through its dependence on air density. Hence, the fall velocity, V_F, depends on z. Also within the framework of a cell structure, we find that the horizontal component of the relative velocity is given by

$$\xi_x = \frac{V_F}{G} \frac{du}{dt} .$$

The relative displacement associated with ξ_x is

$$\delta = \int_o^t \xi_x dt = \frac{V_F}{G} \left[u(t) - u(o) \right] ,$$

which is extremely small since $t_c = (V_F/G)$ is at the most a few seconds. On the other hand, the absolute horizontal displacement is

$$x = \int_o^t u(t)\, dt + \delta .$$

We readily see that the relative displacement will be small compared to the total displacement, so that ξ_x itself can be considered negligible.

The conclusions derived from the proposed cell model solution to the problem can be considered quite general, because the model is supposed to accurately represent the wind field. We therefore conclude that the displacement of a fallout particle is given by the solution of the equations

$$\begin{aligned} \frac{dx}{dt} &= u\left[\vec{r}(t),\ t\right] , \\ \frac{dy}{dt} &= v\left[\vec{r}(t),\ t\right] , \\ \frac{dz}{dt} &= -V_F(Z) + w\left[\vec{r}(t),\ t\right] . \end{aligned} \tag{43}$$

APPENDIX B

PARTICLE SETTLING RATES

INTRODUCTION

A detailed examination of the current generation of fallout models reveals that there is a great multiplicity of methods for calculating particle settling rates. In fact, there are about as many particle settling rate calculation methods as there are fallout models. We have made a survey of these methods as well as a survey of the open literature, and we have concluded that this multiplicity is unwarranted. The open literature on the subject of particle dynamics is extensive and provides results of excellent and comprehensive studies that are readily applicable to fallout work. Much of the best work in this field has been almost completely ignored by workers charged with fallout prediction calculations, which undoubtedly has resulted in the confusion and multiplicity of methods.

In this appendix, we shall consider those problems of the settling of spheres and irregular particles through the atmosphere that pertain to fallout transport calculations. In addition, we shall briefly discuss the effects of turbulent diffusion. Results of computations of particle settling rates by four methods are presented so that comparisons between them can be made.

SETTLING OF SPHERES THROUGH THE ATMOSPHERE

The dynamics of terminal settling (i.e., steady-state settling) of a sphere through a fluid is amenable to treatment by the principle of mechanical similarity. That is to say, the unique properties of the particular fluid and particle under consideration can be combined to yield dimensionless numbers that adequately express the state of the system but effectively remove many of the experimental particulars. In this manner, a particular experiment can yield a result of much wider range of applicability than would be possible otherwise. The dimensionless parameter of most interest here is the Reynolds number: the ratio of inertial force to viscous force.

For a sphere in motion relative to a fluid, the Reynolds number R is conventionally given as

$$R = \frac{\rho dV}{\eta} , \tag{1}$$

where ρ and η are the fluid density and dynamic viscosity, d is the sphere diameter, and V is the velocity of the sphere relative to the fluid. For cases where the Reynolds number is small ($R \leq 0.05$) viscous forces predominate, and the force of resistance of the fluid to the motion of the particle (i.e., the drag force) is given by Stokes' law

$$D = 3\pi\eta dV \tag{2}$$

or in terms of the Reynolds number

$$D = \frac{3\pi\eta^2 R}{\rho} . \tag{3}$$

For steady-state settling under the force of gravity, the drag force for a particle of mass m must equal the gravity force, mg, so that for a particle of density ρ_p

$$\frac{\pi}{6} d^3 g(\rho_p - \rho) = 3\pi\eta dV_F ,$$

where g is the acceleration of gravity. Therefore, we find that when Stokes' law holds, the terminal velocity varies as the square of the particle diameter according to the simple relation

$$V_F = \frac{g(\rho_p - \rho)d^2}{18\eta} . \tag{4}$$

This relation can be solved for the diameter as a function of Reynolds number to yield

$$d \approx \left(\frac{18\eta^2}{g\rho\rho_p} R\right)^{1/3} . \tag{5}$$

Since Stokes' law is accurate for Reynolds numbers no larger than about 0.05, a critical diameter d_c is readily found from Eq. (5), by using representative particle

and atmospheric properties, that is the maximum particle size for which Stokes' law holds. Assuming $\rho_p = 2.25$ g cm^{-3} along with atmospheric properties of the U.S. Standard Atmosphere, 1962,[1] we obtain the critical diameters given in Table B-1. It is apparent that most particles that contribute significantly to local

TABLE B-1

CRITICAL PARTICLE DIAMETER VS ALTITUDE

Altitude (m)	d_c (μ)
0	22
2,000	23
5,000	25
10,000	28
20,000	45
30,000	79

fallout have diameters larger than the critical diameter. Unfortunately, there is no method as simple and direct as Stokes' law for obtaining terminal velocities for large spheres, and it is necessary to employ experimentally determined data to obtain settling rates of the required accuracy.

For cases where the Reynolds number is large, inertial forces (pressure) become dominant in determining the drag, and the drag force is given by Newton's law

$$D = \frac{1}{2} \rho V^2 S C_D \ , \qquad (6)$$

where S is the area of the particle projected in the direction of motion and C_D is a variable dimensionless quantity called the drag coefficient. The quantity $\rho V^2/2$ is a measure of the so-called dynamic pressure on the particle, so that its product

with S yields a measure of the inertial force of resistance on the particle. For a sphere, Eq. (6) becomes

$$D = \frac{\pi}{8} \rho V^2 d^2 C_D \quad . \tag{7}$$

In terms of the Reynolds number, the relation becomes

$$D = \frac{\pi}{8} \frac{\eta^2}{\rho} C_D R^2 \quad . \tag{8}$$

For terminal gravity settling of particles, we can equate D with mg and obtain directly from Eqs. (7 and 8) the relations

$$V_F = \sqrt{\frac{4\rho_p g}{3\rho C_D}\, d} \tag{9}$$

and

$$C_D R^2 = \frac{4g\rho\rho_p d^3}{3\eta^2} \quad , \tag{10}$$

where we have taken $(\rho_p - \rho) \approx \rho_p$. In Eq. (9) we see that the terminal velocity now varies as the square root of the diameter, and in Eq. (10) we have a relation for $C_D R^2$ that is independent of the particle velocity. This latter equation is of great importance in calculating terminal velocities for spheres for Reynolds numbers beyond the range of Stokes' law. The reason for this will become apparent a little later.

As mentioned earlier, the drag coefficient C_D is not constant. Indeed, it varies over many orders of magnitude as a function of the Reynolds number. Aerodynamicists long ago made many measurements of fluid drag on spheres, and these data have been accumulated in several references and used to determine consensus curves relating C_D with R. Figure B-1 represents one such plot.[2] It is apparent that the agreement of the many determinations is excellent and that as a result drag coefficients are adequately known for spheres. The downward break in the curve at about R = 100,000 is the so-called drag crises. Reynolds numbers of this magnitude are not encountered in fallout calculations, so we need not be concerned with it.

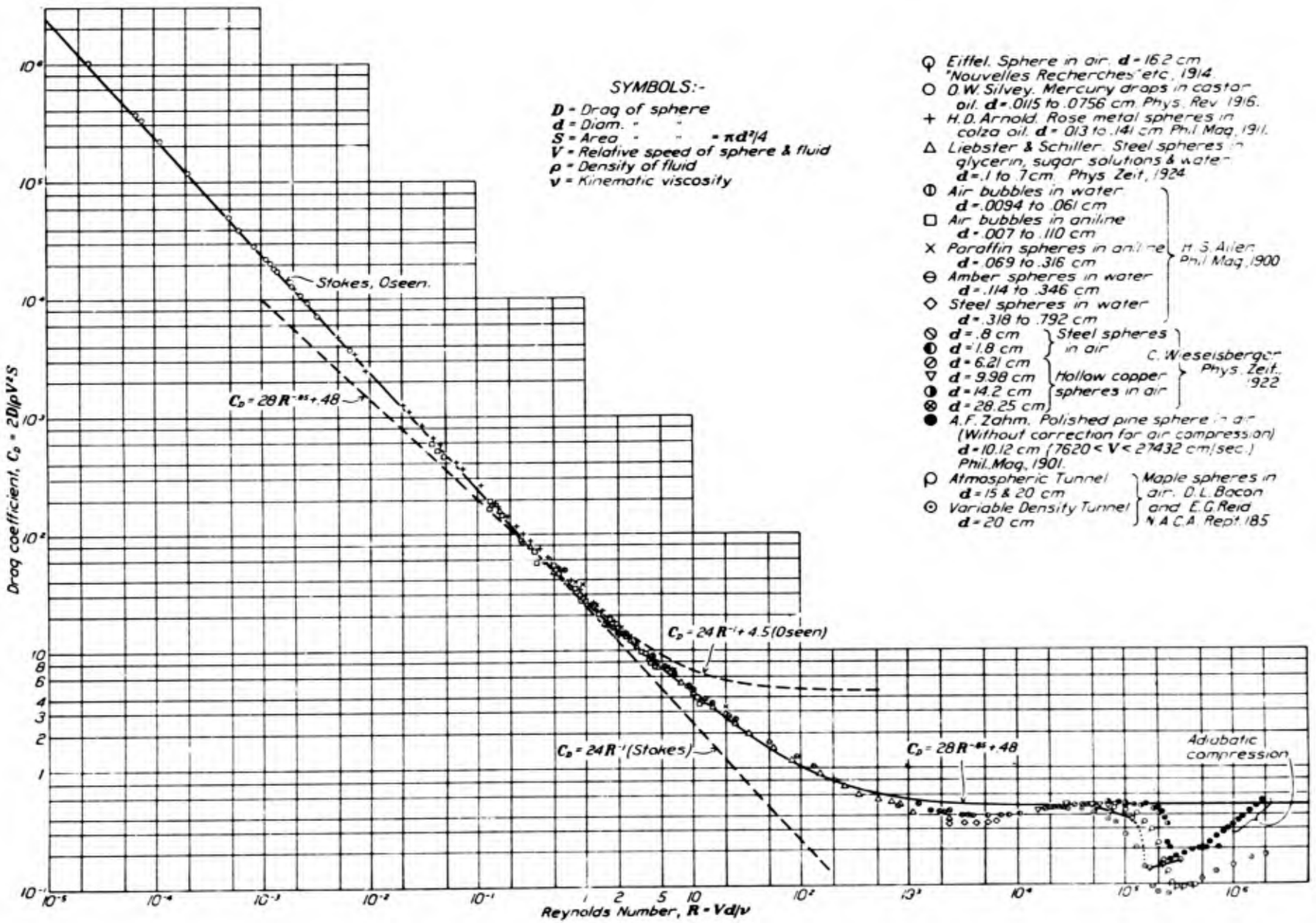

Figure B-1. Drag Coefficient for a Sphere in Steady Translation Through a Viscous Fluid (From Zahm in Ref. 2)

A fruitful scheme for determining particle settling rates is based on the relation of $C_D R^2$, as expressed in Eq. (10), which is independent of velocity. Thus, by making use of the data of Figure B-1, we can express R as a function of $C_D R^2$. Since $C_D R^2$ is readily calculated from known properties of the particle and fluid, the Reynolds number can be determined, and hence the velocity (see Eq. 1). This procedure was discovered independently by many investigators.[3, 4, 5] The work that is both most useful and most accurate is that of Davies.[6] Davies fitted two least squares polynomials to selected data in such a manner that Stokes' law is approached at the low end of the range, and high accuracy is maintained out to R = 10,000 at the high end. These polynomials are

$$R = \frac{C_D R^2}{24} - 2.3363 \times 10^{-4} \left(C_D R^2\right)^2 + 2.0154 \times 10^{-6} \left(C_D R^2\right)^3 - 6.9105 \times 10^{-9} \left(C_D R^2\right)^4, \quad R < 4 \text{ or } C_D R^2 < 140 \tag{11}$$

and

$$\log_{10} R = -1.29536 + 0.986 \left(\log_{10} C_D R^2\right) - 0.046677 \left(\log_{10} C_D R^2\right)^2 + 0.0011235 \left(\log_{10} C_D R^2\right)^3, \quad 3 < R < 10,000 \text{ or } 100 < C_D R^2 < 4.5 \times 10^7. \tag{12}$$

COMPARISON OF METHODS CURRENTLY USED

Several alternative methods currently in use for calculating terminal velocities are as follows. The fallout models developed at The RAND Corporation use empirical equations devised by Hastings:[7]

$$V_F = \frac{r^2}{\left[2.9527 \times 10^3 + 6.199 r^{3/2} \exp(-1.148 \times 10^{-4} z)\right]}, \tag{13}$$

*Note that as $C_D R^2$ becomes small $R \approx C_D R^2/24$. This relation can easily be shown to be equivalent to Stokes' law.

where r is the particle radius in microns, z is the altitude in meters, and V_F is the terminal velocity in meters per second. Recently, Hedman[8] published a unique procedure for calculating settling velocities for spheres that, like Hastings' method, requires knowledge only of altitude and particle size. Hedman's equations are

$$V_F = \frac{B_s \rho_p d^2}{D_r^x} , \tag{14}$$

where

$$D_r = \frac{53.17 \rho_p^{1/3} d}{D_s} ,$$

$$x = 0, \text{ when } D_r \leq 53\ \mu$$

$$= 0.074230 (\log D_r)^2 - 0.120553 (\log D_r) - 0.013022, \text{ when } 53\ \mu < D_r \leq 800\ \mu$$

$$= 0.009011 (\log D_r)^2 + 0.231346 (\log D_r) - 0.483577, \text{ when } 800\ \mu < D_r \leq 5500\ \mu,$$

$$B_s = 10^{-4}(0.5762 \times 10^{-4} z^2 + 0.4938 \times 10^{-2} z + 0.9984), \text{ for } 0 \leq z \leq 36.2$$

$$= 10^{-4}(0.0050 \times 10^{-4} z^2 - 0.0165 \times 10^{-2} z + 1.2578), \text{ for } 36.2 \leq z \leq 65.6$$

$$= 10^{-4}(0.0178 \times 10^{-4} z^2 - 0.1796 \times 10^{-2} z + 1.3593), \text{ for } 65.6 < z \leq 100 ,$$

$$D_s = 26.92 \times 10^{-4} z^2 + 31.67 \times 10^{-2} z + 52.41, \text{ for } 0 \leq z \leq 36.2$$

$$= 106.90 \times 10^{-4} z^2 + 28.12 \times 10^{-2} z + 43.38, \text{ for } 36.2 < z \leq 65.6$$

$$= 187.50 \times 10^{-4} z^2 - 66.08 \times 10^{-2} z + 77.77, \text{ for } 65.6 < z \leq 100 .$$

In Eq. (14) d is in microns; z, in thousands of feet; ρ_p, in grams per cubic centimeter; and V_F, in feet per second. Average atmospheric conditions are assumed.

An equation, used for many years at the Naval Radiological Defense Laboratory and in the Anderson D-Model fallout predictor,[9] is attributed to Ksanda:*

$$V_F = \frac{1.325 b \eta}{\rho} \log_{10}^3 (bd + 1.163) , \tag{15}$$

*The derivation of this equation has never been published.

where

$$b = \left[\frac{2g\rho(\rho_p - \rho)}{\eta^2} \right]^{1/3} \quad \text{in CGS units .}$$

Equation (15) is reported to yield settling rates for irregular particles (cylinders of diameter d and length 2d falling lengthwise without tumbling).[9, 10]

To compare the accuracies of the methods described above, we have calculated terminal velocities over ranges of particle size and altitude appropriate for fallout work. The results are given in Table B-2. Davies' values are taken as our standard. The most surprising feature of these results is that the Ksanda equation overestimates the settling rates for small particles by as much as a factor of two. Since the Ksanda calculations are for irregular particles (cylinders), the velocities should be underestimated because, as we shall see later, falling rates for spheres are greater than for bodies of equal volume of any other shape. Actually, in obtaining the results reported in Table B-2, the diameters given in the column headings were used directly in Ksanda's equation. If the diameter for a sphere of equivalent volume is used, the settling rates computed from Eq. (15) becomes even higher. Hedman's equations yield results that agree quite well with those of Davies, while Hastings' results are good for the small particles but are significantly in error for the larger particles. Of course, in using the methods of Hedman and Hastings, there is the disadvantage that the atmospheric properties cannot be altered since these have been incorporated in the empirical equations.

SETTLING OF IRREGULAR PARTICLES THROUGH THE ATMOSPHERE

An excellent discussion of the effects of particle shape on settling rate is given by Fuchs.[11] According to Fuchs, theoretical studies of the settling of non-spherical particles have been carried out only for ellipsoids and for viscous flow (Stokes' law) conditions. A few experimental studies have been made, however, for particles of a variety of shapes, as well as for ellipsoids, and for both viscous flow and pressure flow conditions. The next four paragraphs are based on the discussion in Fuchs' book.

TABLE B-2

PARTICLE SETTLING RATES (cm sec^{-1}) AS A FUNCTION OF SIZE AND ALTITUDE BY FOUR METHODS

(Properties of the U.S. Standard Atmosphere, 1962 are used.[1] The settling rates are not corrected for drag slip, which becomes important at high altitudes for small particles.)

Altitude (m)	Method	Particle Diameter (μ)				
		10	50	100	500	1000
2,000	Davies	0.710	16.65	53.83	372.9	693.2
	Hedman	0.709	16.91	52.39	393.9	709.2
	Hastings	0.831	17.51	53.25	278.6	430.7
	Ksanda	1.442	23.68	64.16	361.3	628.0
5,000	Davies	0.753	17.84	58.31	422.2	793.7
	Hedman	0.751	18.24	57.21	447.3	813.7
	Hastings	0.836	18.44	59.71	373.0	595.4
	Ksanda	1.551	25.82	71.07	412.3	722.8
10,000	Davies	0.841	20.24	67.84	530.2	1017.
	Hedman	0.838	20.97	67.23	563.0	1045.
	Hastings	0.840	19.54	68.53	582.6	1002.
	Ksanda	1.782	30.25	85.65	525.2	936.
20,000	Davies	0.863	21.37	80.66	851.3	1786.
	Hedman	0.857	21.42	82.95	936.8	2014.
	Hastings	0.845	20.62	78.78	1153.3	2518.
	Ksanda	2.157	36.21	114.3	899.1	1728.
30,000	Davies	0.831	20.74	81.99	1244.	2902.
	Hedman	0.823	20.57	82.28	1275.	3147.
	Hastings	0.846	20.99	82.71	1673.	4839.
	Ksanda	2.844	39.15	134.35	1414.	3006.

Fuchs defines a dynamic shape factor, χ, that is the ratio of the resistance of a given particle to that of a spherical particle of equivalent volume:

$$\chi = \frac{D}{D_{(sphere)}} \quad . \tag{16}$$

Shape factor values, calculated for ellipsoids under viscous flow conditions,[11, 12] indicate that in extreme cases χ can be as high as 15. For small velocities an ellipsoidal particle can maintain any orientation in flow. For a case where the motion is directed toward or near the direction of the ellipsoidal major axis, χ can be less than one. On the other hand, for a large number of particles in random orientations, the average χ is essentially always greater than or equal to one.[12] For particles less symmetrical than an ellipsoid, only special orientations are stable.

A feature characteristic of the settling of non-spherical particles is that the resistance force is not co-linear with the direction of motion. Thus, in general, for a non-spherical particle in an arbitrary orientation, an unbalanced torque will develop that will tend to rotate the particle toward a position of torque balance. Apparently, this preferred orientation is the one of maximum drag resistance. For example, plates and needles tend to orient with their sides of maximum dimension perpendicular to the direction of flow, and regular polyhedra orient with one face perpendicular to the direction of flow. This orientation force increases with Reynolds number until at R values from 10 to 100 the orientation is complete. Variation of χ with Reynolds number at large values of R (i.e., under pressure flow conditions) has not been adequately studied. According to Fuchs it is known, however, that χ remains constant up to a certain value of R and then begins to increase rapidly. This increase is caused by the creation of vortices and, therefore, begins sooner for particles with sharper edges. For cubes and octahedra, it begins when R is about 100, whereas it begins at about 10 for tetrahedra and thin discs falling in the horizontal position.

On the basis of the work summarized above, it is possible to make the generalization that spherical particles settle with less drag resistance than particles of equal volume of any other shape. This means that of all particles of a given volume, the spherical particle will settle with maximum velocity.

In addition to its influence on settling speed, particle shape has a significant affect on the settling trajectory. As R becomes larger, the deviation of the resistance force from that of the direction of fall becomes larger until finally the particle trajectory begins to deviate from the vertical. For sufficiently large R, the particles begin to slip sideways or glide, and the trajectories become spiral or zigzag. The average deviation of coal ash particles from the vertical during a fall of 100 cm was 0.45 for a particle of 80-μ diameter and 1.4 cm for a particle of 300-μ diameter. (Of course, this dispersion is in addition to that caused by turbulent diffusion.)

Rapp and Sartor[13] performed particle settling experiments using simulated irregular fallout particles. The particles consisted of large plastic spheres with smaller plastic spheres or hemispheres adhering to them. Settling times of the particles through mineral oil were observed. Their results correspond to a range of fallout particle sizes with an upper limit of about 100-μ diameter under sea-level atmospheric conditions. They detected no significant deviation from the consensus C_D vs R curve (given in Ref. 14) with the exception of several extremely irregular particles, which happened to be rather small, for which the fall velocity was found to be about 80% that of spheres of equivalent volume. The effect of surface roughness on flow resistance of spheres is discussed by Hoerner.[15] The value of R at the onset of the drag crises (see Figure B-1) is markedly influenced by surface roughness: the greater the surface roughness, the lower the R value at which the drag crisis occurs. Otherwise, there does not appear to be an appreciable effect.

In several of the currently used fallout models, attempts are made to correct particle fall rates for shape effects. The Anderson D-Model uses an equation that is designed to give settling rates of cylinders of diameter d and length 2d. The effectiveness of this equation is discussed on pp. B-7 et seq. A fallout model developed by the Ford Instrument Company[16] multiplies particle settling velocities by a shape factor, S, that is computed from the equations:

$$\begin{aligned} S &= 0.71465 + 0.010277\ \ell n(R)\ ,\quad 10^{-4} \leq R \leq 0.24 \\ S &= 0.73518 + 0.024673\ \ell n(R)\ ,\quad 0.24 < R < 800 \\ S &= 0.820788 + 0.011858\ \ell n(R)\ ,\quad 800 \leq R \leq 10^{4}\ . \end{aligned} \tag{17}$$

From a value of about 0.62 at the low end of the R range, S increases to a value of about 0.92 at the upper end. Apparently these equations are derived from some results quoted by Dallavalle,[17] who, in turn, obtained his results from the work of Martin.[18, 19]

Martin performed his experiments on a pilot plant scale, using quartz sand powdered in a tube mill. Sand batches varying in weight from 75 g to 45 lb were size fractionated in air elutriator tubes. Figure B-2 shows the essential features

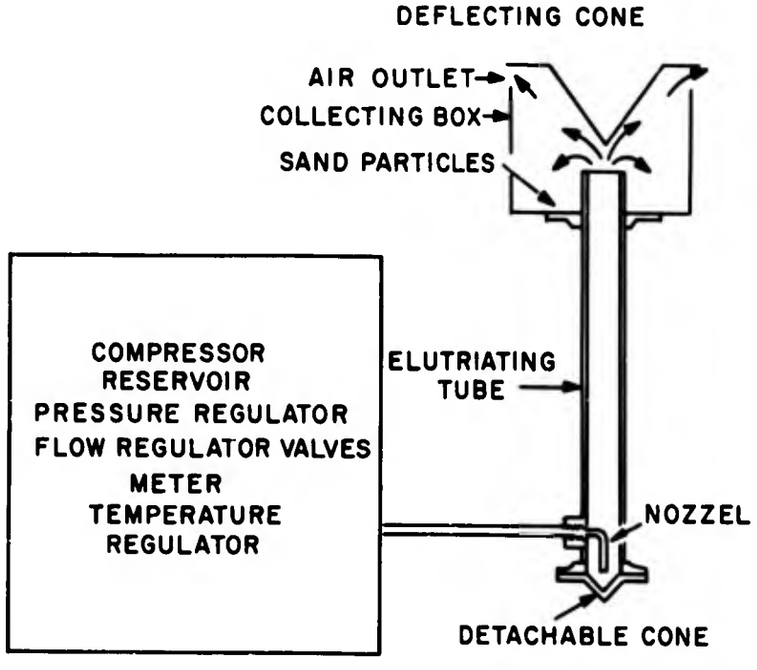

Figure B-2. Elutriator Apparatus (According to Martin in Ref. 18)

of the apparatus. The elutriator tube inside diameters varied from 2 to 6 in.; lengths were 5 to 6 ft. The experimental procedure was as follows. A batch of powdered sand was placed in the cone at the bottom of the elutriator tube and then blasted by a regulated jet of air from the nozzle. The airflow rate was carefully adjusted and controlled so that the finest portion of sand in the batch was barely able to lift over the top of the tube and then settle into the collector at the top. Flow was continued until separation was complete. In this manner a batch of powdered sand was separated into a large number of size fractions. Size measurements of each fraction were done microscopically by a method that today is a classic

in its field. Using Eqs. (1 and 10), we have calculated Reynolds numbers and drag coefficients from Martin's data, which he grouped under two categories, streamline flow and turbulent flow, and these are plotted in Figure B-3 along with the consensus

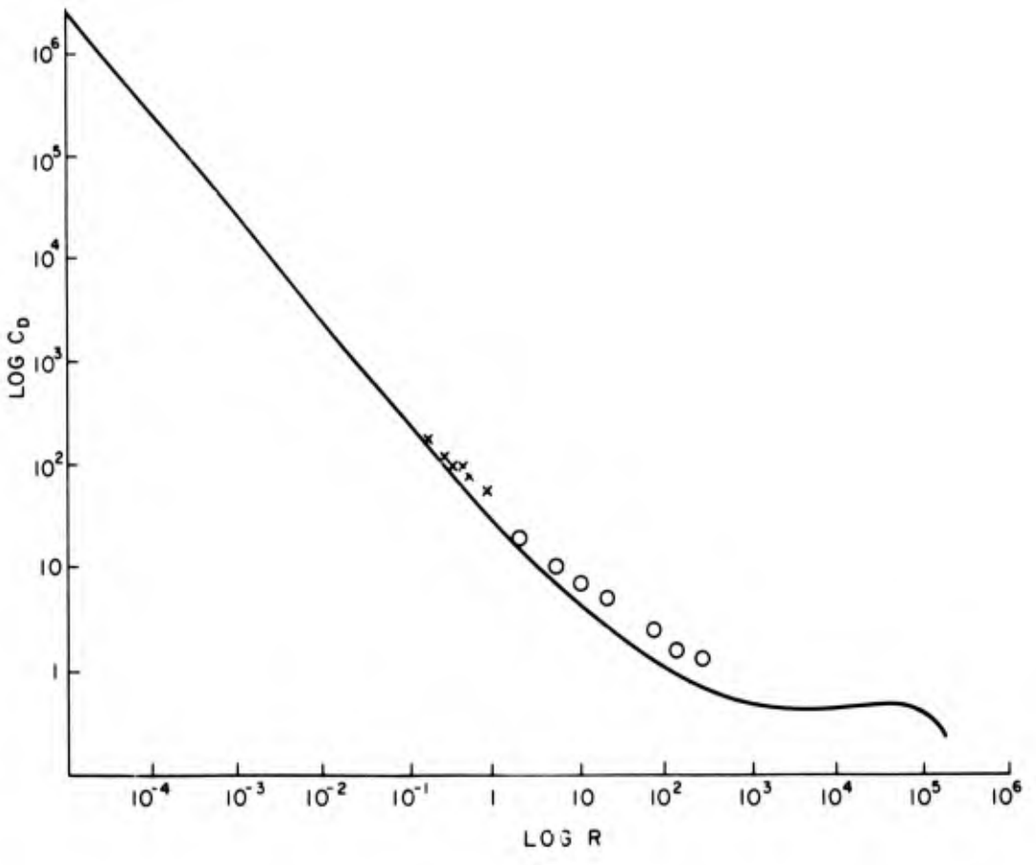

Figure B-3. Comparison of Martin's Data for Irregular Quartz with Consensus Curve of Figure B-1 (The plotted points represent Martin's data; the crosses are for streamline flow, and the circles for turbulent flow.)

curve of Figure B-1. Relative to spheres, Martin's quartz yielded lower settling velocities, and consequently higher drag coefficients. Calculations of the Reynolds numbers[20] for airflow in the elutriator tubes shows that for the turbulent flow data the critical Reynolds number ($R \approx 1000$) is exceeded, whereas for the streamline flow data it is not.

Martin's results were interpreted as being caused by the effect of irregular particle shape. No doubt, irregularity of particle shape is a contributing factor, but the major contributor most probably was from another source. Martin's experiments were performed under conditions that ensured the presence of extremely vigorous turbulence even for the cases of "streamline flow." The entire stream of air was jetted into the bottom of the elutriator tube to stir and carry aloft the sand collected there. The fact that the Reynolds numbers were below the critical value for the "streamline flow" cases, merely ensured that the turbulence eventually would damp out at some downstream point—provided that the tube was long enough. For the turbulent flow cases, vigorous turbulence certainly prevailed throughout the length of the elutriator tube. In a turbulent stream of air of the sort that prevailed in Martin's elutriator tubes, one would expect that air velocities within the eddies would be higher than the velocity computed using the volume throughput and tube diameter. Since Martin used the latter method, his velocities are too small, and it is apparent immediately why his results differ so greatly from the results of other investigators who performed their experiments under truly streamline flow conditions. No correction of the data for the effects of turbulence was made by Martin.

Alpha quartz is a polymeric silicon oxide with three dimensional cross-linking of silicon-oxygen chemical bonds. There are no outstandingly pronounced preferred cleavage planes, such as is found in mica, for example, so that after crushing in a ball mill one would expect particles that are irregular but with a fairly compact shape. In such a case, shape effects on particle settling rates would be expected to be more of the "surface roughness" type and would not be expected to cause deviations as large as those found in Martin's data. Furthermore, we would expect the effect to increase with Reynolds number, not to decrease as required by the Ford Instrument Company corrections.

We conclude, therefore, that the deviation of Martin's results from those expected for spheres is caused mainly by the effects of turbulence, not particle shape. This interpretation is supported by the results of Rapp and Sartor[13] which overlap those of Martin but do not show a comparable effect.

Because of the paucity of studies in the area of shape effects on particle settling rates, it is not clear at this time just how important these effects are in determining deviations in settling speed and trajectories of the larger fallout particles. On the one hand, one might be tempted to ignore these effects since most radioactive fallout particles observed thus far are fairly compact in shape;[21, 22] on the other hand, the larger particles are radiologically the most significant, and available information indicates that these are affected by particle shape the most. It is apparent then that these problems need additional study.

DRAG SLIP CORRECTION

When the mean free path of gas molecules is the same order of magnitude as the particle size, as can happen for small particles at high altitudes, the drag resistance becomes less than that predicted by Stokes' law. To correct for this effect, the Stokes' law terminal velocities are multiplied by a factor f of the form

$$f = 1 + \frac{\ell}{r}\left(A + Be^{-br/\ell}\right) ,$$

where r is the particle radius and ℓ is the air mean free path. Experimental determinations of the constants are summarized by Davies.[6] The equation selected by Davies as best representing the data is

$$f = 1 + \frac{\ell}{r}\left(1.257 + 0.400\, e^{-1.10\, r/\ell}\right) . \qquad (18)$$

The mean free path, ℓ, can be obtained from

$$\ell = \frac{1}{\sqrt{2}\, \pi n \sigma^2} , \qquad (19)$$

where n is the number of gas molecules per unit volume and σ is the molecular diameter of gas molecules. If we assume air to be composed of 28.1% nitrogen, 20.1% oxygen, and 1% argon, we obtain a weighted average value for σ of 3.42×10^{-8} cm. (Molecular diameter data are from Ref. 23.) In terms of air density the mean free path becomes

$$\ell = \frac{0.927 \times 10^{-4}}{\rho} \text{ (micron)} .$$

At an altitude of 30 km (98,000 ft), $\ell \approx 4.5\ \mu$. It is apparent that the exponential term in Eq. (18) can be neglected since particles smaller than approximately 25 μ radius are not considered to contribute significantly to local fallout.

We arrive thus at the slip correction equation,

$$f = 1 + \frac{2.33 \times 10^{-4}}{d\rho} , \tag{20}$$

where d is the particle diameter in microns and ρ is the air density in grams per cubic centimeters. Equation (20) has the form of the Cunningham slip equation (Ref. 11, p. 25 ff).

TURBULENT DIFFUSION OF FALLOUT PARTICLES

The study of diffusion of free falling particles in the atmosphere by turbulence and convection is still in its infancy; this is probably the main reason it has received so little attention in fallout studies. In referring to methods for calculating settling rates such as those presented above, Fuchs (p. 34, Ref. 11) emphasizes that the formulas must be used with caution, because the presence of turbulence and convection currents completely changes the nature of settling. From this we might infer that turbulent diffusion of fallout particles is a matter of considerable significance.

It has been found that a close analogy exists between macro-turbulent diffusion and Brownian molecular diffusion. Therefore, we can express the relation between the mean displacement of a particle caused by turbulent diffusion, $\bar{x}$, and time, t, by an equation of the form

$$\bar{x}^2 = 2D_t t , \tag{21}$$

where D_t is defined as a coefficient of turbulent diffusion. This equation is pertinent to a frame of reference that is stationary relative to the ground. It does not properly account for the movement of atmospheric turbulence on an overriding air current. Accordingly, a relative eddy diffusion coefficient, D_L, has been defined that is pertinent to a frame of reference moving with the prevailing air currents.

Sutton[24] has shown that for large scale diffusion in the atmosphere, the molecular diffusion type of law should be replaced by an equation

$$\bar{x}^2 = C^2(Ut)^m \ , \tag{22}$$

where C is a generalized diffusion coefficient, m has a value of about 1.75, and U is the prevailing average wind velocity. C and D_L are related by the equation

$$D_L = \frac{C^2}{4}(Ut)^{m-1} U \ . \tag{23}$$

The available theory and data appear to be applicable only to the lowest portion of the atmosphere. Extensive additional work (especially experimental) is necessary to determine realistic values for these diffusion coefficients.

An interesting equation reported by Fuchs (see p. 286, Ref. 11) and due to Davies[25] gives the concentration distribution in a deposit of coarse particles that originated in a cloud at height H:

$$n(x, y) = \frac{Q \cos\theta}{\pi C^2 L^m} \exp\left(-\frac{y^2 \cos^2\theta + x^2}{C^2 L^m}\right), \tag{24}$$

where x and y are coordinates on the earth's surface with the origin at the center of the cloud. Q is the mass of the cloud; θ, the angle between the line of descent of the cloud and the vertical ($\theta = \tan^{-1} U/V_s$); L, the length of the path ($= H/\cos\theta$); and C, the averaged Sutton coefficient. Experiments with clouds of water droplets ($r \approx 0.5$ mm) descending from heights of 300 to 1500 m in a normal gradient were claimed by Davies to be in good agreement with Eq. (24); C was determined from special experiments.

The importance of turbulent diffusion to fallout predictions is a somewhat controversial issue. So little quantitative information is available that there is insufficient basis for rendering a decision on the matter, and sufficient additional work in this area should be done to resolve the issue.

CONCLUSION

Fall velocities in any specified atmosphere should be computed by the method of Davies:[6]

$$V_F = \frac{R\eta}{\rho d} , \tag{25}$$

where, according to Eqs. (11, 12, and 10),

$$R = \frac{C_D R^2}{24} - 2.3363 \times 10^{-4}\left(C_D R^2\right)^2 + 2.0154 \times 10^{-6}\left(C_D R^2\right)^3$$

$$- 6.9105 \times 10^{-9}\left(C_D R^2\right)^4 , \quad R < 4 \text{ or } C_D R^2 < 140 ;$$

$$\log_{10} R = -1.29536 + 0.986\left(\log_{10} C_D R^2\right) - 0.046677\left(\log_{10} C_D R^2\right)^2$$

$$+ 0.0011235\left(\log_{10} C_D R^2\right)^3 , \quad 3 < R < 10,000 \text{ or } 100 < C_D R^2 < 4.5 \times 10^7 ;$$

$$C_D R^2 = \frac{4g\rho\rho_p d^3}{3\eta^2} .$$

To correct for drag slip at very high altitudes, the velocity computed from Eq. (25) is multiplied by the factor (Eq. 20),

$$f = 1 + \frac{2.33 \times 10^{-4}}{d\rho} ,$$

where d is in microns and ρ is in grams per cubic centimeters.

Methods of correcting fall velocities for particle shape effects employed by currently available fallout models are incorrect. It is known that the effect of shape

and surface irregularities is such as to decrease the settling rate below that of spheres of equivalent volume in all cases. Furthermore, at high Reynolds numbers, unsymmetrical particles are known to deviate from vertical trajectories. These effects must be studied further to determine their degree of importance in fallout predictions and to provide data for use in accounting for them. Additional work also should be done in the area of turbulent diffusion of fallout particles. In particular, estimates of coefficients of turbulent diffusion of fallout particles in the atmosphere should be made.

REFERENCES

1. "Handbook of Geophysics and Space Environments," ed. S. L. Valley (Bedford, Mass.: Air Force Cambridge Research Laboratories, Office of Aerospace Research, U.S. Air Force, 1965).
2. A. F. Zahm, "Flow and Drag Formulas for Simple Quadrics," National Advisory Committee for Aeronautics, Report No. 253, U.S. Government Printing Office, Washington, 1927.
3. I. Langmuir, "The Production of Rain by a Chain Reaction in Cumulus Clouds at Temperatures Above Freezing," J. Meteorol. 5, 179 (1948).
4. J. E. McDonald, "An Aid to the Computation of Terminal Fall Velocities of Spheres," J. Meteorol. 17, 463 (1960).
5. R. R. Rapp, "The Vertical Motion of Solid Spheres in the Atmospheres," The RAND Corporation, Report No. P-1921, 18 February 1960.
6. C. N. Davies, "Definitive Equations for the Fluid Resistance of Spheres," Proc. Phys. Soc. (London) 57, 259 (1945).
7. R. R. Rapp, The RAND Corporation, private communication.
8. F. A. Hedman, "Calculation of Free-Fall Velocity of Spherical Particles at Various Altitudes," National Military Command System Support Center, Technical Report No. TR-1-65, 1 March 1965.
9. A. D. Anderson, "A Theory for Close-In Fallout from Land-Surface Nuclear Bursts," J. Meteorol. 18, 431 (1961).

10. J. J. Birch, "Schemes for Computing Particle Settling Rates," Appendix to University of California Report TM-CD Project Series 2 Issue 3J, "Deposit Location Predictions for a Single Fallout Particle," by D. C. Kleinecke, 15 May 1961.

11. N. A. Fuchs, "The Mechanics of Aerosols," Translated from the Russian by R. E. Daisley and M. Fuchs and edited by C. N. Davies, Revised and Enlarged Edition (New York, N. Y.: The MacMillan Company, 1964).

12. C. N. Davies, "Shape of Small Particles," Nature 201, 905 (1964).

13. R. R. Rapp and J. D. Sartor, "Rate of Fall Through the Atmosphere of Irregularly Shaped Particles," The RAND Corporation Report RM-2006 (AD 150665), 1 November 1957.

14. W. Wien and F. Harnes, "Handbuch der Experimentalphysik," Band 4, Teil Z, (Leipzig: Akademische Verlagsgesellschaft M. B. H.. 1932), pp. 340-380.

15. S. F. Hoerner, "Fluid-Dynamic Drag" (Published by the Author, 148 Busteed Drive, Midland Park, New Jersey, 1958), pp. 2-9 and 3-8.

16. R. Bailey et al., "Fallout Predictor," Ford Instrument Company, Quarterly Report No. 6, Contract No. DA-36-039SC-78185 to the U.S. Army Signal Research and Development Laboratory, 15 January 1960.

17. J. M. Dallavalle, "Micromeritics" (New York, N. Y.: Pitman Publishing Co., 1948), pp. 20 ff.

18. G. Martin, "Researches on the Theory of Fine Grinding. Part IV. On the Air Analysis of Large Quantities of Crushed Sand," Trans. Brit. Ceram. Soc. 25, 226 (1926).

19. G. Martin, "Researches on the Theory of Fine Grinding. Part VI. On the Diameters of Irregularly Shaped Crushed Sand Particles Lifted by Air Currents of Different Speeds and Different Temperatures," Trans. Brit. Ceram. Soc. 26, 21 (1926-27).

20. L. Prandtl and O. G. Tietjens, "Applied Hydro- and Aeromechanics" (New York, N. Y.: Dover Publications, 1934), sections 23 and 24.

21. C. E. Adams, N. H. Farlow, and W. R. Schell, "The Compositions, Structures, and Origins of Radioactive Fallout Particles," U.S. Naval Radiological Defense Laboratory, Report No. TR-209 (AD 160 395), 3 February 1958.

22. R. D. Cadle, "The Effects of Soil, Yield, and Scaled Depth on Contamination from Atomic Bombs," Standford Research Institute Project CU-641, 29 June 1953. (Secret RD)

23. J. O. Hirschfelder, C. F. Curtiss, and R. B. Bird, "Molecular Theory of Gases and Liquids" (New York, N. Y.: John Wiley & Sons, 1954), p. 545.

24. O. G. Sutton, "A Theory of Eddy Diffusion in the Atmosphere," Proc. Roy. Soc. A135, 143 (1932).

25. D. R. Davies, Proc. Cambridge Phil. Soc. 46, 500 (1950).

BLANK PAGE

APPENDIX C

THEORY OF OROGRAPHIC FLOW WITH APPLICATION TO TROPOSPHERIC FALLOUT

GEOMETRIC CONSIDERATIONS

The geometric origin of our coordinate system is established at "ground zero," the point at which the detonation occurs. The x direction points from west-to-east; the y direction, north. The z axis is the direction of the zenith. The components of the earth's angular velocity along the x, y, and z directions are given by

$$\begin{aligned} \Omega_z &= \Omega \sin \theta \ , \\ \Omega_x &= 0 \ , \\ \Omega_y &= \Omega \cos \theta \ , \end{aligned} \tag{1}$$

where θ is the latitude, and Ω equals 0.73×10^{-4} $\sec^{-1}$. For the problem of short-range fallout, Ω_z and Ω_y can be considered constant, which is consistent with neglecting the curvature of the earth. If u, v, and w are the x, y, and z directions of the wind, then the corresponding components of the Coriolis force,

$$\vec{F} = 2\vec{v} \times \vec{\Omega} \ , \tag{2}$$

are given by

$$\begin{aligned} F_x &= 2(v\Omega_z - w\Omega_y) = 2\Omega(v \sin \theta - w \cos \theta) \ , \\ F_y &= -2u\Omega_z = -2\Omega u \sin \theta \ , \\ F_z &= 2u\Omega_y = 2\Omega u \cos \theta \ . \end{aligned} \tag{3}$$

In many situations, the orographic effects are better described in a coordinate system which is obtained from the established system through a rotation γ about

the z axis. This is shown in Figure C-1 where $\bar{x}$ and $\bar{y}$ are the new rectangular axes. The components of $\bar{\Omega}$ in this coordinate system are given by

$$\begin{aligned} \bar{\Omega}_y &= \Omega_y \cos\gamma \ , \\ \bar{\Omega}_x &= \Omega_y \sin\gamma \ , \\ \bar{\Omega}_z &= \Omega_x \ . \end{aligned} \tag{4}$$

The components of the wind field are related to each other by the well known formulas

$$\begin{aligned} \bar{u} &= u\cos\gamma + v\sin\gamma \quad \text{and} \quad u = \bar{u}\cos\gamma - \bar{v}\sin\gamma \ , \\ \bar{v} &= v\cos\gamma - u\sin\gamma \quad \text{and} \quad v = \bar{u}\sin\gamma + \bar{v}\cos\gamma \ , \\ \bar{w} &= w \ . \end{aligned} \tag{5}$$

The components of the Coriolis force in the $\bar{x}$, $\bar{y}$, and $\bar{z}$ system are readily given by application of Eq. (2).

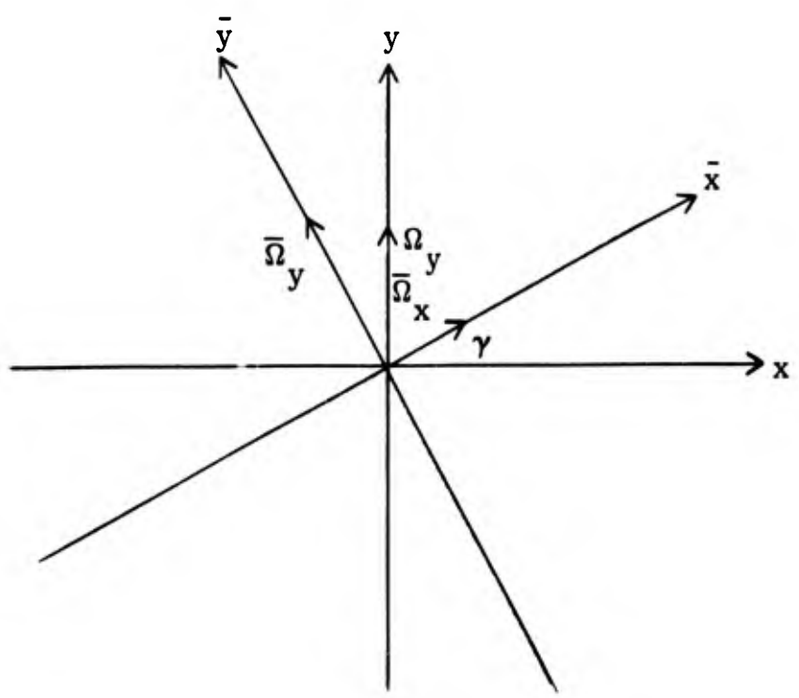

Figure C-1. Rotation of Coordinate System ($\bar{x}$, $\bar{y}$, $\bar{z}$)

The perturbation method for treating orographic effects, as outlined in the next section, is greatly simplified by orienting the axis so that the undisturbed flow points in the $\bar{x}$ direction. After the perturbed velocity field is computed, it can be related to the established coordinate system by the relationships previously established. For brevity, the coordinate system used will be labeled x, y, z instead of its true designation, $\bar{x}$, $\bar{y}$, $\bar{z}$.

THEORY OF OROGRAPHIC DISTURBANCES

The description of airflow over variable terrain can be realized by assuming that the changes in topography can be treated as a small perturbation on the wind field. It is postulated that if the ground were flat, the wind velocity, u, would be constant both in position and time. Orographic effects, such as mountains and valleys, then cause the wind field to change in a determined way, as computed from the perturbation theory.

The origin of the coordinate system is established at a suitable point in the vicinity of the region whose orographic effects on the wind field are to be computed. Assuming that for all times the thermodynamic process which describes the flow of air is isentropic, the relationship between pressure P and air-mass density ρ is given by

$$\left(\frac{P}{P_E}\right) = \left(\frac{\rho}{\rho_E}\right)^{\gamma} = \left(\frac{T}{T_E}\right)^{\frac{\gamma}{1-\gamma}}, \tag{6}$$

where P_E, ρ_E, and T_E are the pressure, mass density, and temperature at the origin in the unperturbed case. These quantities are further related to each other by the ideal gas law,

$$P_E = \left(\frac{\rho_E k T_E}{m}\right), \tag{7}$$

where k is the Boltzmann constant ($k = 1.38 \times 10^{-16}$ erg deg^{-1}), and m is the mass of the air molecule. The two equations which describe the aerodynamics are the continuity equation and the momentum equation:

$$\frac{\partial \rho}{\partial t} + \nabla \cdot (\rho \vec{v}) = 0 \tag{8}$$

and

$$\frac{d\vec{v}}{dt} = 2\vec{v} \times \vec{\Omega} - \nabla\psi + \vec{G} \ , \tag{9}$$

where $\vec{G}$ is the gravity force and is equal to $-G\vec{k}$, and ψ is a potential obtained by combining the term, $(1/\rho)\,\nabla P$, with Eq. (6).

$$\psi = \frac{P_E}{\rho_E^{\gamma}} \left(\frac{\gamma}{\gamma - 1}\right) \rho^{(\gamma - 1)} \ . \tag{10}$$

We assume that a steady state exists in which there is only one uniform (spatially homogeneous) component of velocity, u_o, which is parallel to the x direction. The system of equations then reduces to

$$0 = -\frac{\partial \psi}{\partial x} \ , \tag{11}$$

$$0 = -2u_o\Omega_z - \frac{\partial \psi}{\partial y} \ , \tag{12}$$

$$0 = 2u_o\Omega_y - \frac{\partial \psi}{\partial z} - G \ . \tag{13}$$

The general solution to Eqs. (11 to 13) is given by

$$\psi = Ay + Bz + C \ , \tag{14}$$

which, when substituted into the foregoing equations, gives

$$A = -2u_o\Omega_z \ , \tag{15}$$

$$B = -G + 2u_o\Omega_y \simeq -G \ , \tag{16}$$

$$C = \left(\frac{\gamma}{\gamma - 1}\right)\frac{P_E}{\rho_E} = \left(\frac{\gamma}{\gamma - 1}\right)\left(\frac{kT_E}{m}\right) = \psi(y=0,\ z=0)$$
$$= c_s^2/(\gamma - 1) \ , \tag{17}$$

where c_s is the speed of sound and equals 3.4×10^4 cm sec^{-1} under STP conditions.

The coefficient A has the dimensions of acceleration but is several orders of magnitude smaller than G, thereby showing that the predominant density change is in the z direction. For a 100 mph wind, $u_o = 4400$ cm sec^{-1} so that the acceleration $(-2u_o\Omega_z)$ is at the most 0.64 cm sec^{-2}. A rough measure of the y dimension over which density variations become important can be obtained from the relationship (with $\gamma = 1.4$)

$$y_c \equiv \left|\frac{C}{A}\right| = \frac{11.6 \times 10^8}{(0.4)(2u\Omega_z)} = \left(\frac{29 \times 10^8}{2u\Omega_z}\right) \text{cm} \ . \tag{18}$$

Using the maximum realizable value of $2u\Omega = 0.6$ gives

$$y_c \sim 0.5 \times 10^{10} \text{ cm} \sim 0.3 \times 10^5 \text{ miles} \ . \tag{19}$$

On the other hand, the characteristic z dimension over which density changes become important is likewise given by

$$z_c = \left|\frac{C}{B}\right| \approx \frac{29 \times 10^8}{980} = 3 \times 10^6 \text{ cm} = 20 \text{ miles} \ . \tag{20}$$

The orographic effects considered in the close-in fallout problem are presumed to extend not more than a few hundred miles so that horizontal variations in the steady state caused by the Coriolis effect can be neglected. This will not necessarily be true in the perturbed case where the curvature of the wind field caused by the variable terrain becomes important.

The initial state of the system is given by

$$\vec{v} = \vec{i}u_o \tag{21}$$

and

$$\rho = \rho_o(z) = \rho_E(1 - z/z_c)^{(1/(\gamma-1))} = \rho_E(1 - \alpha z)^{(1/(\gamma-1))} , \tag{22}$$

where

$$\alpha = \frac{1}{z_c} = \frac{1}{3 \times 10^6} = 0.3 \times 10^{-6} \text{ cm}^{-1} \quad (\text{for } \gamma = 1.4) . \tag{23}$$

If attention is further confined to the troposphere ($z \leq 2$ miles $= 0.32 \times 10^6$ cm), the variation of density with altitude is approximated by

$$\rho_o(z) \simeq \rho_E\left[1 - \left(\frac{\alpha}{\gamma - 1}\right)z\right] = \rho_E(1 - \beta z) \simeq \rho_E e^{-\beta z} , \tag{24}$$

where β is defined as the tropospheric density attenuation constant,

$$\beta = \left(\frac{\alpha}{\gamma - 1}\right) = 2.5\alpha = 0.75 \times 10^{-6} \text{ cm}^{-1} . \tag{25}$$

Actually, β is given by

$$\left(\frac{1}{\gamma - 1}\right)\frac{1}{z_c} = \frac{mG}{\gamma k T_E} ,$$

which is observed to be not very sensitive to the choice of γ between 1 and 1.4 (the range of polytropic processes).

We now assume that the three components of velocity and density become modified by the topographical nonhomogeneities. The perturbed quantities are assumed to be related to the unperturbed ones by

$$
\begin{aligned}
u_p &= u_o + \bar{u} \ , \\
v_p &= \bar{v} \ , \\
w_p &= \bar{w} \ , \\
\rho_p &= \rho_o + \bar{\rho} \ , \\
\psi_p &= \psi_o + \bar{\psi} \ .
\end{aligned}
\tag{26}
$$

Substituting Eq. (26) into Eqs. (8 and 9) and neglecting second order effects, such as $\bar{\rho}\,\bar{w}$ and $\bar{v}\,\bar{w}$, give, under stationary conditions $(\partial/\partial t = 0)$,

$$
\rho_o\left(\frac{\partial \bar{u}}{\partial x} + \frac{\partial \bar{v}}{\partial y} + \frac{\partial \bar{w}}{\partial z}\right) + u_o \frac{\partial}{\partial x}\bar{\rho} + \bar{w}\frac{\partial}{\partial z}\rho_o = 0 \ , \tag{27}
$$

$$
u_o \frac{\partial \bar{u}}{\partial x} = 2\left(\bar{v}\Omega_z - \bar{w}\Omega_y\right) - \frac{\partial \bar{\psi}}{\partial x} \ , \tag{28}
$$

$$
u_o \frac{\partial \bar{v}}{\partial x} = 2\left(\bar{w}\Omega_x - \bar{u}\Omega_z\right) - \frac{\partial \bar{\psi}}{\partial y} \ , \tag{29}
$$

$$
u_o \frac{\partial \bar{w}}{\partial x} = 2\left(\bar{u}\Omega_y - \bar{v}\Omega_x\right) - \frac{\partial \bar{\psi}}{\partial z} \ . \tag{30}
$$

For mathematical convenience, it is desirable to deal with a function, η, related to the initial density ρ_o by the formula

$$
\eta = \frac{\bar{\rho}}{\rho_o} \ . \tag{31}
$$

In terms of η, $\bar{\psi}$ is given by

$$\bar{\psi} = \psi(\rho_o + \bar{\rho}) - \psi(\rho_o)$$

$$= \gamma \frac{P_E}{\rho_E^{\gamma}} \rho_o^{\gamma - 1} \eta \, . \tag{32}$$

Using the exact expression for ρ_c,

$$\rho_o^{\gamma - 1} = \rho_E^{\gamma - 1} (1 - \alpha z) \, ,$$

gives

$$\bar{\psi} = \frac{\gamma k T_E}{m} (1 - \alpha z) \eta \, ;$$

while the derivatives of $\bar{\psi}$ are

$$\frac{\partial \bar{\psi}}{\partial x} = \frac{\gamma k T_E}{m} (1 - \alpha z) \frac{\partial \eta}{\partial x} \, ; \quad \frac{\partial \bar{\psi}}{\partial y} = \frac{\gamma k T_E}{m} (1 - \alpha z) \frac{\partial \eta}{\partial y} \, ,$$

and

$$\frac{\partial \bar{\psi}}{\partial z} = -(\gamma - 1) G \eta + \frac{\gamma k T_E}{m} (1 - \alpha z) \frac{\partial \eta}{\partial z} \, . \tag{33}$$

The object at this point is to reduce Eqs. (27 to 30) to a system of linear equations with constant coefficients. This can readily be accomplished by restricting the calculation to values of z much less than z_c so that $(1 - \alpha z) = (1 - z/z_c) \simeq 1$. Also, within this range, $\ln \rho_o = \ln \rho_E - \beta z$, thereby reducing Eqs. (27 to 30) to the following set:

$$\left(\frac{\partial \bar{u}}{\partial x} + \frac{\partial \bar{v}}{\partial y} + \frac{\partial \bar{w}}{\partial z} \right) + u_o \frac{\partial}{\partial x} \eta - \beta \bar{w} = 0 \, , \tag{34}$$

$$u_o \frac{\partial \bar{u}}{\partial x} = 2\left(\bar{v}\Omega_z - \bar{w}\Omega_y\right) - \left(\frac{\gamma k T_E}{m}\right) \frac{\partial \eta}{\partial x} , \tag{35}$$

$$u_o \frac{\partial \bar{v}}{\partial x} = 2\left(\bar{w}\Omega_x - \bar{u}\Omega_z\right) - \left(\frac{\gamma k T_E}{m}\right) \frac{\partial \eta}{\partial y} , \tag{36}$$

$$u_o \frac{\partial \bar{w}}{\partial x} = 2\left(\bar{u}\Omega_y - \bar{v}\Omega_x\right) + (\gamma - 1)G\eta - \left(\frac{\gamma k T_E}{m}\right) \frac{\partial \eta}{\partial z} , \tag{37}$$

where

$$\beta = \frac{mG}{\gamma k T_E} \quad \text{or} \quad \frac{\gamma k T_E}{m} = \frac{G}{\beta} .$$

Equations (34 and 37) relate the perturbed quantities to one another, while the absolute scale of the perturbations will be obtained from the new boundary conditions. We now assume that each of the perturbed quantities can be expressed by an expansion of plane waves.

$$\begin{aligned} \bar{u} &= \int A(\vec{k})\, e^{i\vec{k}\cdot\vec{r}}\, d^3k , \\ \bar{v} &= \int B(\vec{k})\, e^{i\vec{k}\cdot\vec{r}}\, d^3k , \\ \bar{w} &= \int C(\vec{k})\, e^{i\vec{k}\cdot\vec{r}}\, d^3k , \\ \eta &= \int D(\vec{k})\, e^{i\vec{k}\cdot\vec{r}}\, d^3k , \end{aligned} \tag{38}$$

where

$$d^3k = dk_x dk_y dk_z .$$

Substituting Eq. (38) into Eqs. (34 to 37) leads to the dispersion relationship between the "allowed" wave numbers. Thus, we have

$$\begin{pmatrix} ik_x & ik_y & (ik_z - \beta) & iu_o k_x \\ ik_x u_o & -2\Omega_z & 2\Omega_y & (ik_x G/\beta) \\ 2\Omega_z & ik_x u_o & -2\Omega_x & (ik_y G/\beta) \\ -2\Omega_y & 2\Omega_x & ik_x u_o & \left[(1-\gamma)G + (ik_z G/\beta)\right] \end{pmatrix} \begin{pmatrix} A \\ B \\ C \\ D \end{pmatrix} = 0 . \qquad (39)$$

The only non-trivial solutions to Eq. (39) occur when the determinant of the matrix equals zero. This establishes a connection between k_x, k_y, and k_z. The so-called dispersion relationship can be interpreted in several ways depending on which component(s) of the wave vector $\vec{k}$ can be preassigned. It is at this point that the pertinent physical factors are introduced into the problem. Since the topography can be resolved into periodic components of x and y, we must necessarily regard k_x and k_y as real numbers. The dispersion relationship is then interpreted as

$$k_z = k_z(k_x, k_y) . \qquad (40)$$

For each set of values (k_x, k_y), there will be two solutions of Eq. (40), corresponding to the roots of the equation which results when the determinant of the matrix (Eq. 39) is set equal to zero. Since the number of solutions of Eq. (40) is finite, we can contract the description of the Fourier components of the field quantities. For example, $\bar{w}$ now becomes

$$\bar{w}(x, y, z) = \sum_{\mu = 1, 2} \iint C_\mu(k_x, k_y)\, e^{ik_x x}\, e^{ik_y y}\, e^{ik_z^\mu(k_x, k_y) z}\, dk_y dk_x ,$$

where k_z^{μ} stands for the μ^{th} root of Eq. (40). Setting the determinant of Eq. (39) equal to zero leads to the dispersion relationship

$$ak_z^2 + b(ik_z) + c = 0 \ , \tag{41}$$

where

$$a = \sigma\left(k_x^2 u_o^2 - \Omega^2 \omega_x^2\right) \ ,$$

$$b = \sigma\left[\gamma\beta k_x^2 u_o^2 + 2\Omega k_x k_y u_o \omega_x + \Omega^2\left(2ik_x\omega_z\omega_x + 2ik_y\omega_z\omega_y - \gamma\beta\omega_z^2\right)\right],$$

$$c = k_x^2 u_o^2\left[\sigma\left(k_x^2 + k_y^2\right) - u_o^2 k_x^2 + (1-\gamma)\sigma\beta^2\right]$$

$$+ \Omega\beta\sigma\left[2k_x^2\omega_y u_o - \gamma\left(\omega_y u_o k_x^2 - \omega_x u_o k_x k_y\right)\right]$$

$$+ \Omega^2\left[4k_x^2 u_o^2 - \sigma\left(k_x\omega_x + k_y\omega_y\right)^2 - \omega_z^2(1-\gamma)\sigma\beta^2\right.$$

$$\left. - \beta\sigma\gamma\left(ik_x\omega_x\omega_y + ik_y\omega_y\omega_z\right)\right] \ ,$$

in which

$$\omega_x = \frac{2\Omega_x}{\Omega} \ ,$$

$$\omega_y = \frac{2\Omega_y}{\Omega} \ ,$$

$$\omega_z = \frac{2\Omega_z}{\Omega} \ ,$$

$$\sigma = \left(\frac{G}{\beta}\right) \ .$$

We shall now examine the coefficients in the dispersion relationship—namely a, b, and c—to determine the conditions on the velocity and wavelength for which the Coriolis effect can be neglected. Since we are primarily interested in short-range effects, we shall freely make use of the assumed inequality,

$$\sqrt{k_x^2 + k_y^2} >> \beta = 0.75 \times 10^{-6} \text{ cm}^{-1} , \tag{42}$$

which signifies that the wavelength of the horizontal variations in the terrain is less than the $2\pi\beta^{-1}$, or approximately 50 miles.

The Coriolis effect can be neglected in the coefficient a provided that

$$|k_x| u_o >> \Omega , \tag{43}$$

or equivalently

$$\frac{u_o}{\Omega} >> \frac{1}{|k_x|} = \frac{L_x}{2\pi} , \tag{44}$$

where L_x is a representative wavelength in the x direction. The distance (u_o/Ω) equals

$$\frac{u_o}{\Omega} = d = (60 \times 10^4 \, u_{mph}) \text{ cm} = (3.8 \, u_{mph}) \text{ miles} , \tag{45}$$

where u_{mph} is the wind velocity in miles per hour. We shall assume the inequality of Eq. (44) to hold in our analysis. Equation (44) will not be satisfied when the unperturbed velocity is too large, or both a small u_o and large L_x are combined. However, these conditions are not important relevant to fallout considerations. If L_x is large, the disturbance cannot be considered as a local effect; hence, additional meteorological information will be available, thus precluding the utility of the perturbation methods considered here. If u_o is small, orographic effects will not be important since the motion of the fallout particle will be essentially vertical, descending with the so-called terminal velocity (i.e., the irregularities in the terrain on the fallout particles will not have far-reaching effects).

The importance of the Coriolis effect in the second coefficient of the dispersion relationship, b, can be assessed by independently comparing the magnitude of the first-to-second terms, and the first-to-third terms in the foregoing expansion of b in powers of Ω. The magnitude of the first-to-second term is

$$\frac{\gamma \beta k_x^2 u_o^2}{2\Omega |k_x| \, |k_y| u_o \omega_x} \sim \left(\frac{|k_x| u_o}{\Omega}\right)\left(\frac{\beta}{|k_y|}\right) = \left(\frac{d}{L_x}\right) \beta L_y \, , \tag{46}$$

neglecting the unimportant numerical factors. Unlike the simple inequality depicted by Eq. (44), Eq. (43) will be greater than unity when a combination of conditions is met. Substituting Eq. (45) into Eq. (46) gives the following inequality which must be satisfied for neglecting the Coriolis effect.

$$0.46\left(\frac{L_y}{L_x}\right) u_{mph} >> 1 \, . \tag{47}$$

For one-dimensional problems in which the transverse ground variations are neglected $\left[(L_y/L_x) \rightarrow \infty\right]$, Eq. (47) is obviously satisfied. Even when (L_y/L_x) is less than unity, the inequality of Eq. (47) can still be maintained with reasonable wind velocities. Since, in the applications of our theory, we treat only those cases for which

$$L_y \geq L_x \, , \tag{48}$$

we accept the validity of Eq. (47). Using Eq. (42) together with the assumed relationship $L_y \geq L_x$ gives for the ratio of the first-to-third terms in the expression for b

$$\left(\frac{k_x^2 u_o^2}{\Omega^2}\right) \frac{\beta}{|k_x|} = \frac{(2\pi) d^2}{L_x \beta} \, . \tag{49}$$

The relationship between the unperturbed wind velocity and wavelength L_x is thus given by

$$2\pi(1.8) u_{mph}^2 >> L_x \, . \tag{50}$$

The cases for which $L_x > 2\pi(1.8)\, u_{mph}^2$ are physically uninteresting for the same reasons discussed in reference to Eq. (44). Recalling that

$$\sigma = \frac{G}{\beta} = \frac{(980)}{0.75 \times 10^{-6}} = 1.3 \times 10^{9}\ \text{cm}^{-2}\ \text{sec}^{-2}\ ,$$

which is overwhelmingly larger than u_o^2 $\left[\sigma >> u_o^2\right]$, and using Eqs. (42 and 49), neglecting minor numerical factors, we have the following approximate expression for c in powers of Ω:

$$c \simeq k_x^2 u_o^2 \sigma\left(k_x^2 + k_y^2\right) + \Omega\beta\sigma u_o k_x^2 + \Omega^2 \sigma k_x^2\ .$$

Examination of this expression shows that the Coriolis effect can be neglected if

$$\frac{k_x^2 u_o^2\left(k_x^2 + k_y^2\right)}{\Omega\beta u_o k_x^2} = \frac{u_o\left(k_x^2 + k_y^2\right)}{\Omega\beta} > 1 \qquad (51)$$

and

$$\frac{k_x^2 u_o^2\left(k_x^2 + k_y^2\right)}{\Omega^2 k_x^2} = \frac{u_o^2\left(k_x^2 + k_y^2\right)}{\Omega^2} > 1\ . \qquad (52)$$

Equations (51 and 52) are readily observed to be satisfied in light of the previous discussion.

Henceforth, although we shall restrict our calculations to the regime where the Coriolis force is negligible, the mathematical techniques which will be developed for treating orographic flow can be extended to include this effect.

Since Eq. (39) is homogeneous, the absolute magnitudes of the functions $A(\vec{k})$, $B(\vec{k})$, $C(\vec{k})$, and $D(\vec{k})$ cannot be determined, but their relationship to each other can. For mathematical convenience, it is desirable to eliminate $D(\vec{k})$ and deal only with the Fourier transforms of the velocity components of the wind velocity. Thus, we obtain the equation

$$\begin{pmatrix} b_{11} & b_{12} & b_{13} \\ b_{21} & b_{22} & b_{23} \\ b_{31} & b_{32} & b_{33} \end{pmatrix} \begin{pmatrix} A \\ B \\ C \end{pmatrix} = 0 , \tag{53}$$

where the b_{ik}'s are the elements of a matrix $\tilde{b}$ and are given by

$$\begin{aligned}
b_{11} &= ik_x\xi + iu_o k_x \Omega\omega_y , \\
b_{12} &= ik_y\xi - iu_o k_x \Omega\omega_x , \\
b_{13} &= (ik_z - \beta)\xi + (u_o k_x)^2 , \\
b_{21} &= (ik_x u_o)\xi + ik_x \sigma\Omega\omega_y , \\
b_{22} &= -\Omega\omega_z\xi - (ik_x\sigma)\Omega\omega_x , \\
b_{23} &= \Omega\omega_y\xi - (ik_x\sigma)(ik_x u_o) , \\
b_{31} &= \Omega\omega_z\xi + (ik_y\sigma)\Omega\omega_y , \\
b_{32} &= ik_x u_o\xi - (ik_y\sigma)\Omega\omega_x , \\
b_{33} &= -\Omega\omega_x\xi + k_x k_y \sigma u_o ,
\end{aligned} \tag{54}$$

in which $\xi = (1-\gamma)G + (ik_z\sigma)$ and $\sigma = (G/\beta)$.

The dispersion relationship derived by setting the determinant of $\tilde{b}$ equal to zero is necessarily the same as that previously derived. Using Eq. (53), we deduce the general relationship between the Fourier transforms of the velocity components,

$$A = -\frac{(b_{12}b_{33} - b_{13}b_{32})}{(b_{12}b_{31} - b_{11}b_{32})} C \equiv T(k_x, k_y)C(k_x, k_y) \tag{55}$$

and

$$B = -\frac{(b_{13}b_{31} - b_{11}b_{33})}{(b_{12}b_{31} - b_{11}b_{32})} C \equiv U(k_x, k_y)C(k_x, k_y) \ . \tag{56}$$

Setting $\Omega = 0$ in the dispersion relationship Eq. (41) gives

$$\sigma k_z^2 + (ik_z)\,\sigma\gamma\beta + \sigma\left(k_x^2 + k_y^2\right) - u_o^2 k_x^2 + (1-\gamma)\sigma\beta^2 = 0 \ . \tag{57}$$

We now let

$$\lambda = -ik_z \ , \tag{58}$$

anticipating an exponential decay with altitude. This results (recalling that $\sigma = (G/\beta) >> u_o^2$) in the equation

$$\lambda^2 + \lambda\gamma\beta - k_x^2 - k_y^2 + (\gamma - 1)\beta^2 = 0 \ . \tag{59}$$

The roots of Eq. (59) are given by

$$\lambda = \frac{-\gamma\beta \pm \sqrt{(\gamma\beta)^2 + 4\left[k_x^2 + k_y^2 - \beta^2(\gamma - 1)\right]}}{2} \ . \tag{60}$$

When $k_x^2 + k_y^2 >> \beta^2$, the two roots of Eq. (60) are

$$\lambda = \pm \sqrt{k_x^2 + k_y^2} , \tag{61}$$

where only the positive root is acceptable on physical grounds since this quarantees that the perturbations will dampen at high altitudes. Using the plus root of Eq. (61) in Eqs. (55 and 56), and consistently neglecting Ω in the expressions for the b_{ik}'s, give

$$T(k_x, k_y) = \frac{-ik_x}{\sqrt{k_x^2 + k_y^2}} , \tag{62}$$

$$U(k_x, k_y) = \frac{-ik_y}{\sqrt{k_x^2 + k_y^2}} . \tag{63}$$

From Eqs. (61, 62, and 63), we deduce the following expressions for the perturbed velocity components:

$$\bar{w}(x, y, z) = \int_{-\infty}^{+\infty} \int_{-\infty}^{+\infty} C(k_x, k_y)\, e^{i(k_x x + k_y y)}\, e^{-\sqrt{k_x^2 + k_y^2}\, z}\, dk_x dk_y , \tag{64}$$

$$\bar{u}(x, y, z) = \int_{-\infty}^{+\infty} \int_{-\infty}^{+\infty} (-ik_x) \left(k_x^2 + k_y^2\right)^{-1/2} e^{i(k_x x + k_y y)} \tag{65}$$

$$C(k_x, k_y)\, e^{-\sqrt{k_x^2 + k_y^2}\, z}\, dk_x dk_y ,$$

$$\bar{v}(x, y, z) = \int_{-\infty}^{+\infty} \int_{-\infty}^{+\infty} (-ik_y) \left(k_x^2 + k_y^2\right)^{-1/2} e^{i(k_x x + k_y y)} \tag{66}$$

$$C(k_x, k_y)\, e^{-\sqrt{k_x^2 + k_y^2}\, z}\, dk_x dk_y .$$

The function $C(k_x, k_y)$ is determined by application of the perturbed boundary condition. Let

$$\phi(x, y, z) = 0 = z - f(x, y) \tag{67}$$

be the equation of the earth's surface. The normal to this surface is $\nabla\phi$:

$$\nabla\phi = -\vec{i}\,\frac{\partial f}{\partial x} - \vec{j}\,\frac{\partial f}{\partial y} + \vec{k}\ . \tag{68}$$

On physical grounds, we must necessarily demand that the wind velocity be parallel to the surface $z = f(x, y)$ at every point. Thus, the boundary conditions are mathematically stated as

$$\left[(\vec{v} \cdot \nabla\phi)\right] = 0 \quad \text{along } z = f(x, y)\ , \tag{69}$$

where

$$\vec{v} = \vec{i}\,u + \vec{j}\,v + \vec{k}\,w = \vec{i}\,u_o + (\vec{i}\,\bar{u} + \vec{j}\,\bar{v} + \vec{k}\,\bar{w})\ . \tag{70}$$

Inserting Eq. (70) into (69) gives

$$\bar{w}(x, y, z = f) = u_o\left(\frac{\partial f}{\partial x}\right) + \bar{u}(x, y, z = f)\left(\frac{\partial f}{\partial x}\right) + \bar{v}(x, y, z = f)\left(\frac{\partial f}{\partial y}\right)\ . \tag{71}$$

Using Eqs. (62 to 66) in Eq. (71) yields the integral equation for $C(k_x, k_y)$:

$$\int_{k_x}\int_{k_y}\left[1 - T(k_x, k_y)\left(\frac{\partial f}{\partial x}\right) - U(k_x, k_y)\left(\frac{\partial f}{\partial y}\right)\right] C(k_x, k_y)\, e^{ik_x x}\, e^{ik_y y}\, e^{\left[-\left(k_x^2 + k_y^2\right)^{1/2} f(x, y)\right]}\, dk_x dk_y$$

$$= u_o \int_{k_x}\int_{k_y} (ik_x)\, F(k_x, k_y)\, e^{ik_x x}\, e^{ik_y y}\, dk_x dk_y\ , \tag{72}$$

where

$$F(k_x, k_y) = \left(\frac{1}{2\pi}\right)^2 \iint f(x, y)\, e^{-ik_x x}\, e^{-ik_y y}\, dxdy ,$$

and

$$f(x, y) = \iint F(k_x, k_y)\, e^{ik_x x}\, e^{ik_y y}\, dk_x dk_y . \tag{73}$$

The solution for $C(k_x, k_y)$ is impossible to achieve by direct means because of the dependence of the integration of the left hand side of Eq. (72) on f(x, y) and on the derivatives of f(x, y). However, a systematic perturbation method for computing $C(k_x, k_y)$ can be deduced. The approximation to $C(k_x, k_y)$, achieved by setting $\exp -\left[\sqrt{k_x^2 + k_y^2}\, f(x, y)\right]$ equal to unity, is equivalent to assuming that the maximum elevation, f_{max}, is small compared to the wavelength of the horizontal oscillation; or in simpler terms, the slope of the terrain is small. On the other hand, the neglect of $\bar{u}(\partial f/\partial x)$ as compared to $u_o(\partial f/\partial x)$ is necessarily consistent with the initial premise of the perturbation method used in this analysis, namely that the change in the velocity field be small compared to the initial velocity. This obviously must apply when comparing $\bar{u}$ to u_o. The neglect of $\bar{v}(\partial f/\partial y)$ as compared to $u_o(\partial f/\partial x)$ is somewhat difficult to justify, under all cases. Although $\bar{v}$ is assumed small compared to u_o, we must also be sure that $(\partial f/\partial y)$ is not substantially greater than $(\partial f/\partial x)$.

The a priori assumption,

$$\bar{u}\left(\frac{\partial f}{\partial x}\right) + \bar{v}\left(\frac{\partial f}{\partial y}\right) < u_o\left(\frac{\partial f}{\partial x}\right) , \tag{74}$$

is equivalent to neglecting $-T(\partial f/\partial x) + U(\partial f/\partial y)$ as compared to unity in Eq. (72). The systematic method for computing $C(k_x, k_y)$ is based upon Eq. (74) coupled with the previously mentioned approximation,

$$\exp\left(-\sqrt{k_x^2 + k_y^2}\, f(x, y)\right) \equiv \Gamma \approx 1 . \tag{75}$$

Introduction of the functions

$$\xi = 1 - \Gamma = - \sum_{n=1}^{\infty} \frac{\phi^n}{n!} \ , \tag{76}$$

where

$$\phi = - \sqrt{k_x^2 + k_y^2}\, f(x, y) \ , \tag{77}$$

and

$$\tau = T(k_x, k_y)\left(\frac{\partial f}{\partial x}\right) + U(k_x, k_y)\left(\frac{\partial f}{\partial y}\right) , \tag{78}$$

permits Eq. (72) to be written as

$$\int C(\vec{k})\, e^{i\vec{k}\cdot\vec{r}}\, d\vec{k} = u_o \int H(\vec{k})\, e^{i\vec{k}\cdot\vec{r}}\, d\vec{k} + \int \Delta C(\vec{k})\, e^{i\vec{k}\cdot\vec{r}}\, d\vec{k} \ ; \tag{79}$$

$$\Delta = (\tau + \xi - \xi\,\tau) = \Delta(\vec{k}, x, y)$$

$$H(\vec{k}) = ik_x F(\vec{k}) \ ,$$

$$\vec{k} = \vec{i}\,k_x + \vec{j}\,k_y \ ,$$

$$d\vec{k} = dk_x dk_y \ .$$

Multiplying Eq. (79) by $\exp(-i\vec{k}'\cdot\vec{r})$ and then integrating over $\vec{r}$ give:

$$C(\vec{k}') = u_o H(\vec{k}') + \left(\frac{1}{2\pi}\right)^2 \int_{\vec{k}} \int_{\vec{r}} \Delta(\vec{k}, \vec{r})\, C(\vec{k})\, e^{i(\vec{k} - \vec{k}')\cdot\vec{r}}\, d\vec{k}\, d\vec{r}. \tag{80}$$

The perturbation scheme is developed by regarding the second term on the right hand side of Eq. (80) as small. The first approximation to $C(\vec{k})$, denoted by $C^{(1)}$, is deduced by completely disregarding the second term of the right hand side. Thus

$$C^{(1)}(\vec{k}') = u_o H(\vec{k}') = u_o(ik_x)\, F(k) \ . \tag{81}$$

Since F(k) is the sum of individual contributions to the topography, we see that the principle of linear superposition is also reflected in $C^{(1)}(k)$. The second approximation is obtained by using Eq. (81) for $C(\vec{k})$ in the integral expression.

$$C^{(2)}(\vec{k}') = u_o H(\vec{k}') + \left(\frac{1}{2\pi}\right)^2 \int_{\vec{k}} \int_{\vec{r}} \Delta(\vec{k}, \vec{r}) \left[u_o H(\vec{k})\right] e^{i(\vec{k} - \vec{k}') \cdot \vec{r}}\, d\vec{k}\, d\vec{r} \ . \tag{82}$$

It follows by inspection that the n^{th} approximation to $C(\vec{k})$ is given by

$$C^{(n)}(\vec{k}') = u_o H(\vec{k}') + \left(\frac{1}{2\pi}\right)^2 \int_{\vec{k}} \int_{\vec{r}} \Delta(\vec{k}, \vec{r})\, C(k)^{n-1}\, e^{i(\vec{k} - \vec{k}') \cdot \vec{r}}\, d\vec{k} d\vec{r} \ , \tag{83}$$

with

$$C^{(0)} = 0 \ .$$

The corresponding Fourier transforms of the perturbed x and y components of the wind field, $A(\vec{k})$ and $B(\vec{k})$ respectively, are found from Eqs. (55 and 56) to the same order of approximation. The ultimate validity of this perturbation method can be evaluated only posteriorly by comparing the calculated change in the magnitude of the wind field with u_o. Mathematically, the developed theory is valid so long as

$$\bar{u}^2 + \bar{v}^2 + \bar{w}^2 < u_o^2 \ .$$

The prescription for calculating the wind field due to orographic effects is summarized as follows. Equation (83) is used to compute the Fourier transform

of the vertical wind. The Fourier transform of the change in the horizontal components of the wind field is then determined by Eqs. (55 and 56). Finally, the inversion formula,

$$\begin{pmatrix} \bar{u} \\ \bar{v} \\ \bar{w} \end{pmatrix} = \iint \begin{pmatrix} A(k_x, k_y) \\ B(k_x, k_y) \\ C(k_x, k_y) \end{pmatrix} e^{ik_x x} e^{ik_y y} e^{-\sqrt{k_x^2 + k_y^2}\, z} \, dk_x dk_y , \qquad (84)$$

is employed to compute $\bar{u}(\vec{r})$, $\bar{v}(\vec{r})$, and $\bar{w}(\vec{r})$.

The value of computing $C(\vec{k})$ beyond the first approximation is worthwhile, even though the hydrodynamics model considers only the first correction to the flow, because the iteration scheme can more precisely establish the range of validity of the first approximation to $C(\vec{k})$ and the dependence of $C(\vec{k})$ on the characteristic features of the terrain. Most topography is complex and, as such, cannot always be represented by a simple periodic structure, but rather by a sum of frequencies. The higher corrections to $C(\vec{k})$ take into account the interaction between the Fourier components of the ground structure and, consequently, must be evaluated to more firmly establish the validity of the superposition principle implicit in the first approximation.

In the following section, we shall apply the first order theory to compute changes in the wind field caused by specific orographic effects. However, presently, we shall consider a simple two-dimension periodic structure to exhibit the method for computing higher-order corrections to $C(\vec{k})$.

Let

$$f(x) = h\, e^{ik_o x} , \qquad (85)$$

from which it follows that

$$F(k) = \frac{h}{2\pi} \int e^{ik_o x} e^{-ikx} \, dx = h\, \delta(k - k_o) \qquad (86)$$

and

$$H(k) = ikh\delta(k - k_o) = ik_o h\delta(k - k_o) , \tag{87}$$

where $\delta(k)$ is the Dirac delta function. The first correction to the Fourier transform of the vertical velocity field is

$$C^{(1)}(k) = iku_o h\delta(k - k_o) = iu_o(k_o h)\,\delta(k - k_o) , \tag{88}$$

which yields

$$\bar{w}(x, z) = \int iku_o h\delta(k - k_o)\, e^{ikx}\, e^{-|k|z}\, dk \tag{89}$$

$$= ik_o hu_o h e^{ik_o x}\, e^{-|k_o|z} . \tag{90}$$

Since $T(k_x, k_y = 0) = -ik/|k|$, it follows that

$$\bar{u}(x, z) = + u_o(|k_o|h)\, e^{ik_o x}\, e^{-|k_o|z} . \tag{91}$$

Within the confines of the first approximation, the inequality of Eq. (84) reduces to

$$\sqrt{2}(|k_o|h) << 1 , \tag{92}$$

which basically shows that the slope of the terrain must be less than unity. The second approximation to $C(\vec{k})$ is given by

$$C^{(2)}(\vec{k}') = iu_o(k_o h)\delta(k' - k_o) + \left(\frac{1}{2\pi}\right) \int_k \int_x \Delta(k, x) \left[iu_o(k_o h)\delta(k - k_o)\right] e^{i(k - k')x}\, dk dx , \tag{93}$$

where

$$\Delta(k, x) = T(k)\left(\frac{\partial f}{\partial x}\right) - \sum_{n=1}^{\infty} \frac{(-1)^n}{n!}(|k|f)^n + T(k)\left(\frac{\partial f}{\partial x}\right) \sum_{n=1}^{\infty} \frac{(-1)^n}{n!}(|k|f)^n . \tag{94}$$

Inserting Eq. (94) into Eq. (93) and performing the integration over k and x give the following expression for $C^{(2)}(\vec{k}')$.

$$C^{(2)}(\vec{k}') = iu_o(k_o h)\delta(k'-k_o) + iu_o(k_o h)^2 \delta(k'-2k_o)\,\mathrm{sgn}(k_o)$$

$$- iu_o(k_o h) \sum_{n=1}^{\infty} \frac{(-1)^n}{n!}\left(|k_o|h\right)^n \delta\left[k'-(n+1)k_o\right] \qquad (95)$$

$$+ iu_o(k_o h)^2 \,\mathrm{sgn}(k_o) \sum_{n=1}^{\infty} \frac{(-1)^n}{n!}\left(|k_o|h\right)^n \delta\left[k'-(n+2)k_o\right] ,$$

where

$$\mathrm{sgn}(k_o) \equiv \frac{|k_o|}{k_o} .$$

It is easy to show that the vertical component of velocity corresponding to $C^{(2)}(k')$ is given by

$$\bar{w}(x, z) = iu_o(k_o h)\, e^{\left(ik_o x - |k_o| z\right)} \left[2 - e^{-|k_o| h \exp\left(ik_o x - |k_o| z\right)}\right]$$

$$+ \mathrm{sgn}(k_o)\, iu_o(k_o h)^2\, e^{2\left(ik_o x - |k_o| z\right)} e^{-|k_o| h \exp\left(ik_o x - |k_o| z\right)} . \qquad (96)$$

Examination of the second term in Eq. (96) shows that the uncertainties introduced in the computation of $\bar{w}(x, z)$ by neglecting higher-order terms are of the order of $(k_o h)^2$ for a one-dimensional periodic structure. The degree of accuracy to which one may choose to compute the velocity field for fallout computations should be consistent with the uncertainties introduced in other aspects of the calculation.

APPLICATION OF THE THEORY TO SPECIFIC GEOMETRIES

In this section we shall apply the first-order theory to a two-dimensional mountain ridge in which the flow is perpendicular to the mountain; a three-dimensional mountain; and a three-dimensional mountain ridge which is not perpendicular to the flow. Within the context of the theory, valleys are considered as "inverted" mountains. For all cases considered, the perturbed components of velocity are computed.

TWO-DIMENSIONAL MOUNTAIN RIDGE

Queney[1] has shown that a one-dimensional mountain ridge can be represented by the equation,

$$z = f(x) = \frac{h}{1 + (x/a)^2} \; . \tag{97}$$

The Fourier transform of the mountain ridge function is

$$F(k) = \frac{(a^2 h)}{2\pi} \int_{-\infty}^{+\infty} \frac{e^{-ikx}}{a^2 + x^2} \, dx = \frac{(a^2 h)}{2\pi} \left[\left(\frac{\pi}{a} \right) e^{-|k|a} \right] = \frac{(ah)}{2} e^{-|k|a} \; . \tag{98}$$

Using the inversion formula (Eq. 84) gives

$$\bar{w}(x, z) = \frac{u_o(ah)}{2} \int_{-\infty}^{+\infty} (ik) \, e^{ikx} \, e^{-|k|a} \, e^{-|k|z} \, dk \tag{99}$$

$$= u_o(ah) \frac{\partial}{\partial x} \left[\frac{(z + a)}{(z + a)^2 + x^2} \right] ,$$

$$\bar{w}(x, z) = - u_o(ah)(z + a) \frac{(2x)}{\left[(z + a)^2 + x^2 \right]^2} \; ; \tag{100}$$

$$\bar{u}(x, z) = \frac{u_o(ah)}{2} \int_{-\infty}^{+\infty} -i \frac{k}{|k|} (ik)\, e^{ikx} e^{-|k|(z+a)}\, dk\,, \tag{101}$$

$$\begin{aligned} \bar{u}(x, z) &= u_o(ah) \int_0^{\infty} k \cos kx\, e^{-k(z+a)}\, dk \\ &= u_o(ah)(-1) \frac{\partial}{\partial z} \left[\frac{(z+a)}{(z+a)^2 + x^2} \right], \end{aligned} \tag{102}$$

$$\bar{u}(x, z) = -u_o(ah) \frac{\left[x^2 - (z+a)^2\right]}{\left[(z+a)^2 + x^2\right]^2}\,. \tag{103}$$

The total horizontal velocity is

$$u(x, z) = u_o \left\{ 1 - (ah) \frac{\left[x^2 - (z+a)^2\right]}{\left[(z+a)^2 + x^2\right]^2} \right\}. \tag{104}$$

Using Eqs. (100 and 104), we find that the magnitude of the perturbed component of velocity is

$$(\bar{u}^2 + \bar{w}^2)^{1/2} = \frac{u_o(ah)}{x^2 + (z+a)^2}\,; \tag{105}$$

the requirement that this be less than u_o is given by

$$\rho = \frac{ah}{x^2 + (z+a)^2} << 1\,. \tag{106}$$

According to the perturbation theory, $\rho(x, z)$ must be less than unity in the region $z \geq f(x) = h/(1 + (x/a)^2)$. For a given value of a, the precise point at which $\rho(x, z)$ maximizes, in the region $z \geq f(x)$, will depend on h, or equivalently (h/a). Application of Eq. (106) should then establish the conditions on h which will ensure us that the magnitude of the perturbed velocity is less than u_o. It is not necessary to perform a detailed analysis on $\rho(x, z)$ for the purpose of evaluating the perturbation scheme. Consider the value of ρ at the top of the mountain ridge (x=0, z=h).

$$\rho(x=0,\ z=h)=\rho_b = \frac{ah}{(a+h)^2} = \frac{(h/a)}{(1+h/a)^2} \quad . \tag{107}$$

Clearly, ρ_t is always less unity regardless of the ratio (h/a). Thus, post-examination of the velocity field shows that the first-order perturbation will work even for an infinitely steep mountain ridge. The results deduced from Eq. (107) are also borne out by the more extensive analysis of $\rho(x, z)$ previously mentioned. Apparently, higher-order corrections to the Fourier transform of the vertical wind, as computed by the iteration scheme of Eq. (83), are necessary to more firmly establish the range of validity of the first-order perturbation theory.

When the theory is applied to a valley, in which case h is replaced by $-|h|$, and the ratio of the perturbed velocity is then compared to u_o at the bottom of valley (x=0, z=-h), we obtain the following expression for ρ_b,

$$\rho_b = \frac{a|h|}{(a-|h|)^2} \quad . \tag{108}$$

The condition that

$$\rho_b << 1 \ , \tag{109}$$

for this case, is obviously satisfied for a small slope, $|h| << a$.

THREE-DIMENSIONAL MOUNTAIN

Investigations have shown that a suitable representation for a mountain is

$$z = f(x, y) = \frac{h(a^3)}{(a^2 + r^2)^{3/2}} = \frac{A}{(a^2 + r^2)^{3/2}} \tag{110}$$

with

$$r^2 = x^2 + y^2 .$$

Although one can construct several mountain functions which are similar to f(x, y), this particular function was selected because it ultimately yields analytic expressions for the perturbed components of the wind field. The Fourier transform of f(x, y) is

$$F(k_x, k_y) = \frac{A}{(2\pi)^2} \int_{-\infty}^{+\infty} \int_{-\infty}^{+\infty} e^{-i\vec{k}\cdot\vec{r}} \frac{1}{(a^2 + r^2)^{3/2}} \, dxdy$$

$$= \frac{A}{(2\pi)^2} \int_{0}^{2\pi} \int_{0}^{\infty} e^{-ikr\cos\phi} \frac{1}{(a^2 + r^2)^{3/2}} \, d\phi r dr ,$$

$$F(k_x, k_y) = F(k) = \frac{A}{(2\pi)k^{1/2}} \int_{0}^{\infty} \frac{r^{1/2}}{(a^2 + r^2)^{3/2}} J_0(kr)(kr)^{1/2} \, dr \tag{111}$$

with

$$k = \sqrt{k_x^2 + k_y^2} .$$

The integral in Eq. (111) is recognized[2] as the Hankel transform of $r^{1/2}(r^2 + a^2)^{-3/2}$, so that F(k) becomes

$$F(k) = \frac{A}{2\pi a} e^{-ak} . \tag{112}$$

If u_o is the unperturbed velocity, it follows that the first-order correction to the vertical component of the wind is given by

$$\bar{w}(x, y, z) = u_o \int\int (ik_x)\, F(k)\, e^{i(k_x x + k_y y)}\, e^{-kz}\, dk_x dk_y$$

$$= u_o \frac{\partial}{\partial x} \int_0^{2\pi} \int_0^{\infty} F(k)\, e^{-kz}\, e^{ikr\cos\phi}\, k\,dk\,d\phi$$

$$= 2\pi u_o \frac{\partial}{\partial x} \int_0^{\infty} F(k)\, e^{-kz}\, J_o(kr)\,dk\,,$$

$$\bar{w}(x, y, z) = \frac{u_o A}{a} \frac{\partial}{\partial x} \int_0^{\infty} e^{-(a+z)k}\, J_o(kr)\,dk\,. \tag{113}$$

Again from Ref. 2, we find that

$$\bar{w}(x, y, z) = \frac{u_o A}{a} \frac{\partial}{\partial x} \left[\frac{\lambda}{(r^2 + \lambda^2)^{3/2}} \right]$$

$$= \frac{-3\lambda A u_o}{a} \frac{x}{(x^2 + y^2 + \lambda^2)^{5/2}} = \frac{-3\lambda a^2 h x u_o}{(r^2 + \lambda^2)^{5/2}}\,, \tag{114}$$

where

$$\lambda = (z + a)\,. \tag{115}$$

The changes in the x and y components of velocity are determined from Eqs. (65 and 66). Thus, we have

$$\bar{u}(x, y, z) = - u_o \int\int \frac{(ik_x)(ik_x)}{k} F(k)\, e^{i(k_x x + k_y y)}\, e^{-kz}\, dk_x dky$$

$$= - u_o \frac{\partial}{\partial x^2} \int_0^{2\pi} \int_0^{\infty} F(k)\, e^{ikr \cos \phi}\, e^{-kz}\, dk d\phi \ , \tag{116}$$

and

$$\bar{v}(x, y, z) = - u_o \int\int \frac{(ik_y)(ik_x)}{k} F(k)\, e^{i(k_x x + k_y y)}\, e^{-kz}\, dk_x dk_y$$

$$= - u_o \frac{\partial^2}{\partial x \partial y} \int_0^{2\pi} \int_0^{\infty} F(k)\, e^{ikr \cos \phi}\, e^{-kz}\, dk d\phi \ . \tag{117}$$

Using Eq. (112), the integral in Eqs. (116 and 117) becomes

$$\int_0^{2\pi} \int_0^{\infty} F(k)\, e^{ikr \cos \phi}\, e^{-kz}\, dk d\phi = \frac{A}{a} \int_0^{\infty} e^{-(z+a)k} J_o(kr) dk$$

$$= \frac{(a^2 h)}{\sqrt{r^2 + \lambda^2}} \tag{118}$$

with

$$\lambda = (z + a) \ .$$

Inserting Eq. (118) into Eqs. (116 and 117) gives the following expressions for $\bar{u}(x, y, z)$ and $\bar{v}(x, y, z)$:

$$\bar{u}(x, y, z) = - u_o (a^2 h) \frac{\partial^2}{\partial x^2} (r^2 + \lambda^2)^{-1/2} = u_o (a^2 h) \frac{(y^2 + \lambda^2 - 2x^2)}{(r^2 + \lambda^2)^{5/2}} \ ; \tag{119}$$

$$\bar{v}(x, y, z) = - u_o(a^2h) \frac{\partial^2}{\partial x \partial y} (r^2 + \lambda^2)^{-1/2} = \frac{3u_o(a^2h)xy}{(r^2 + \lambda^2)^{5/2}} . \qquad (120)$$

The magnitude of the perturbed velocity is given by

$$(\bar{u}^2 + \bar{v}^2 + \bar{w}^2)^{1/2} = \frac{(a^2h)u_o}{(r^2 + \lambda^2)^{5/2}} \left[9\lambda^2x^2 + (y^2 + \lambda^2 - 2x^2)^2 + 9x^2y^2\right]^{1/2} \qquad (121)$$

$$= \frac{(a^2h)u_o}{(r^2 + \lambda^2)^2} (r^2 + \lambda^2 + 3x^2)^{1/2} ,$$

which reduces to $\left[(a^2h)u_o\right]/(h + a)^3$ at the top of the mountain.

THREE-DIMENSIONAL MOUNTAIN RIDGE NOT PERPENDICULAR TO THE FLOW

In this case, the perpendicular to the line depicting the crest of the mountain is at an angle γ with respect to the direction of flow, as shown in Figure C-2.

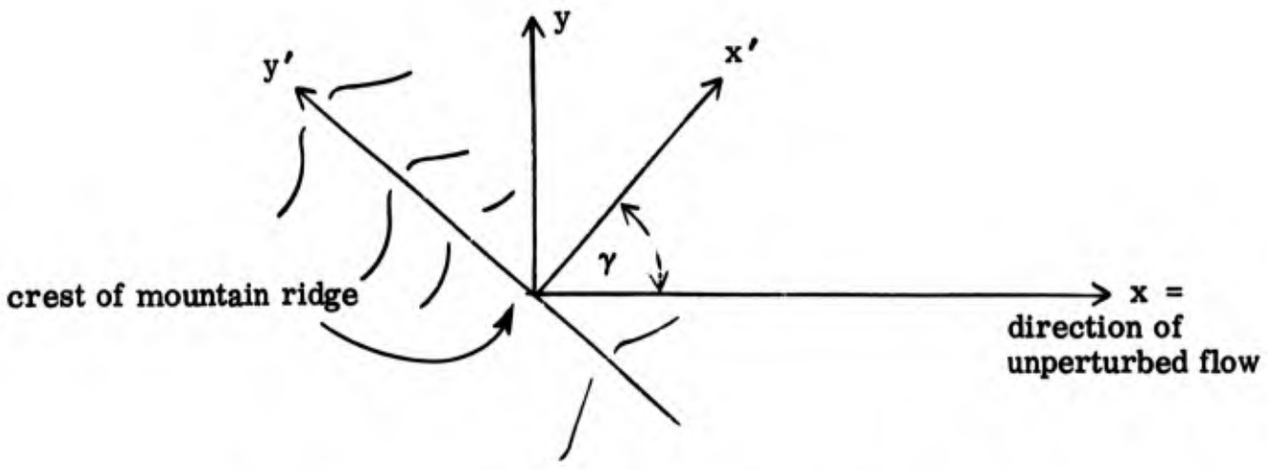

Figure C-2. Mountain Ridge Not Perpendicular to Flow

The Fourier transform of the mountain ridge function is

$$F(k_x, k_y) = \left(\frac{1}{2\pi}\right)^2 \int\int f(x, y)\, e^{-ik_x x - ik_y y}\, dxdy \ . \tag{122}$$

Since $\vec{k} \cdot \vec{r}$ is invariant under an orthogonal transformation, Eq. (122) becomes

$$F(k_x', k_y') = \left(\frac{1}{2\pi}\right)^2 \int\int f(x', y')\, e^{-ik_x' x' - ik_y' y'}\, dx'dy' \ , \tag{123}$$

where

$$x = x' \cos\gamma - y' \sin\gamma \ ,$$

$$k_x = k_x' \cos\gamma - k_y' \sin\gamma \ ,$$

$$y = x' \sin\gamma + y' \cos\gamma \ ,$$

$$k_y = k_x' \sin\gamma + k_y' \cos\gamma \ .$$

In terms of the new coordinate system, the equation for the mountain ridge is

$$z = \frac{h}{1 + (x'/a)^2} \ , \tag{124}$$

which when inserted into Eq. (124) gives

$$F(k_x', k_y') = \left(\frac{ah}{2}\right) e^{-|k_x'|a}\, \delta(k_y') \ . \tag{125}$$

Using the inversion formula (Eq. 84) with $C(k_x, k_y) = ik_x u_o F(k_x, k_y)$ yields the following expression for $\bar{w}(x, y, z)$:

$$\begin{aligned} \bar{w}(x, y, z) &= u_o \int\int (ik_x)\, e^{ik_x x}\, e^{ik_y y}\, F(k_x, k_y)\, e^{-\sqrt{k_x^2 + k_y^2}\, z}\, dk_x dk_y \\ &= u_o \frac{\partial}{\partial x} \int\int e^{i(k_x' x' + k_y' y')}\, F(k_x', k_y')\, e^{-\sqrt{k_x'^2 + k_y'^2}\, z}\, dk_x' dk_y' \ , \end{aligned} \tag{126}$$

where

$$F(k'_x, k'_y) = F\left[k_x(k'_x, k'_y), k_y(k'_x, k'_y)\right] .$$

Inserting Eq. (125) into Eq. (126) reduces this expression to

$$\bar{w}(x, y, z) = u_o \frac{\partial}{\partial x} \int e^{ik'_x x'} \left(\frac{ah}{2}\right) e^{-|k'_x|a} e^{-|k'_x|z} dk'_x$$

$$= u_o(ah) \cos\gamma \frac{\partial}{\partial x'} \left(\frac{\lambda}{\lambda^2 + x'^2}\right) = \frac{-u_o(ah)\lambda 2 \cos\gamma x'}{(\lambda^2 + x'^2)^2} ,$$

$$\bar{w}(x, y, z) = \frac{-2u_o(ah)\lambda \cos\gamma (x\cos\gamma + y \sin\gamma)}{\left[(x \cos\gamma + y \sin\gamma)^2 + \lambda^2\right]^2} , \tag{127}$$

where

$$\lambda = (z + a) . \tag{128}$$

Since in reality a mountain ridge is never infinite, the origin of the system could be located at the center of the crest-line. It is also easy to show that the perturbed x and y components of wind velocity are given by

$$\bar{u}(x, y, z) = \frac{-u_o(ah) \cos^2\gamma \left(\left[x \cos\gamma + y \sin\gamma\right]^2 - \lambda^2\right)}{\left(\left[x \cos\gamma + y \sin\gamma\right]^2 + \lambda^2\right)^2} , \tag{129}$$

and

$$\bar{v}(x, y, z) = \frac{-u_o(ah) \cos\gamma \sin\gamma \left(\left[x \cos\gamma + y \sin\gamma\right]^2 - \lambda^2\right)}{\left(\left[x \cos\gamma + y \sin\gamma\right]^2 + \lambda^2\right)^2} . \tag{130}$$

It should be noted that u, v, and w really depend on $x' = x \cos \gamma + y \sin \gamma$, so that the origin of the (x, y) system can be located anywhere along the crest-line. For convenience it will be located at the center of the crest-line in the actual computations.

FALLOUT PARTICLE STREAMLINES AND WIND STREAMLINES IN TWO DIMENSIONS

It is of interest to obtain analytic expressions and pictorial representations for the trajectories of fallout particles for the purpose of assessing the importance of the orographic effects. If u_p and w_p denote the horizontal and vertical components of the fallout particle velocity in a two-dimensional system, it follows (see Appendix A) that these quantities are related to the wind velocity through the equations

$$u_p = u_o + \bar{u} \ , \tag{131}$$

and

$$w_p = - V_F + \bar{w} \ , \tag{132}$$

where V_F is the so-called fall velocity. Strictly speaking, V_F is a function both of particle size and of altitude,[3] but below 10,000 ft its variation with z can be neglected. Figure C-3 shows the average fall velocity, between 0 and 10,000 ft, plotted as a function of particle size for spherical particles with an assumed density of 2.5 g cm^{-3} (data taken from Ref. 3).

The flow lines, or trajectories, of fallout particles can be determined from a quantity called the stream function,[4] $\Phi(x, z)$, defined by the partial differential equations

$$w_p = - V_F + \bar{w} \equiv - \frac{\partial \Phi}{\partial x} (x, z) \ , \tag{133}$$

and

$$u_p = u_o + \bar{u} \equiv \frac{\partial \Phi}{\partial z} (x, z) \ . \tag{134}$$

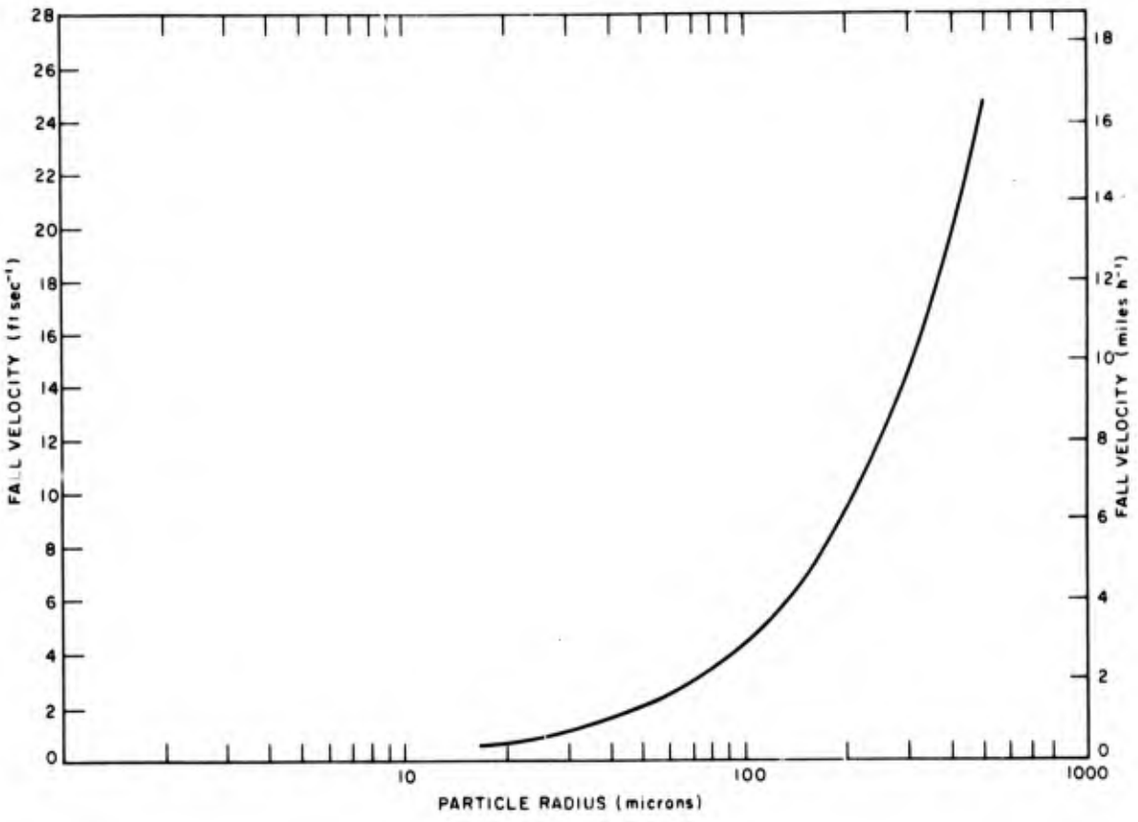

Figure C-3. Fall Velocity Vs Particle Size

On the other hand, the equation for the flow lines is

$$\frac{dx}{u_p} = \frac{dz}{w_p} \text{ or } - w_p dx + u_p dz = 0 \ , \tag{135}$$

which, when used with Eqs. (133 and 134),

$$\frac{\partial \Phi}{\partial x} dx + \frac{\partial \Phi}{\partial z} dz = 0 \text{ or } d\Phi = 0 \ . \tag{136}$$

We thus see that the curves for which

$$\Phi = \text{constant} \tag{137}$$

are the streamlines. In the case of the mountain ridge, it was shown that the perturbed components of the wind field, $\bar{u}$ and $\bar{w}$, are given by (see Eqs. 99 and 102)

$$\bar{u} = -u_o(ah)\frac{\partial}{\partial z}\left[\frac{(z+a)}{(z+a)^2+x^2}\right] = \frac{\partial}{\partial z}\Psi(x, z) \tag{138}$$

and

$$\bar{w} = u_o(ah)\frac{\partial}{\partial x}\left[\frac{(z+a)}{(z+a)^2+x^2}\right] = \frac{-\partial}{\partial x}\Psi(x, z)\ , \tag{139}$$

where the perturbed stream function $\Psi(x, z)$ is, by inspection,

$$\Psi = \frac{-u_o(ah)(z+a)}{(z+a)^2+x^2}\ . \tag{140}$$

Using Eqs. (138 and 139), and recalling that u_o and V_F are both independent of position, enable us to construct the entire stream function, $\Phi(x, z)$. The function $\Phi(x, z)$, which has as its partial derivates w_p and u_p, is

$$\Phi = u_o z + \Psi + V_F x\ ; \tag{141}$$

and the curves of constant Φ, which are the flow lines, are determined from the equation

$$\text{constant} = C = u_o z - \frac{u_o(ah)(z+a)}{(z+a)^2+x^2} + V_F x\ . \tag{142}$$

Each value of C describes a different flow line, while a specific value of C is determined by requiring that the flow lines pass through a particular point (x, z). For computational purposes, it is desirable to cast Eq. (142) in dimensionless

form; this is accomplished by dividing both sides of Eq. (142) by $(u_o a)$. There results

$$\text{constant} = C' = \bar{z} + \gamma \bar{x} - \alpha \frac{(1 + \bar{z})}{(1 + \bar{z})^2 + \bar{x}^2} , \tag{143}$$

where

$\alpha = \frac{h}{a}$ = ratio of height to half-width of mountain ridge,

$\gamma = \frac{V_F}{u_o}$ = ratio of the magnitude of fall velocity to the unperturbed wind velocity, u_o,

$\bar{x} = (x/a)$ = horizontal dimension in units of a,

$\bar{z} = (z/a)$ = vertical position in units of a.

In the absence of a mountain ridge, $\alpha = 0.$ and Eq. (143) reduces to

$$\bar{z} = C' - \gamma \bar{x} , \tag{144}$$

which is the equation of the straight-line descent of a fallout particle with slope $-V_F/u_o$. On the other hand, the streamlines deduced from Eq. (143) when $\gamma = 0$ depict the flow of the wind field over the mountain ridge. The solid lines in Figures C-4, C-5, and C-6 show the wind streamlines at various initial altitudes for values of $\alpha = 0.25$, 0.50, and 0.75. The dashed line on each figure is the mountain ridge function

$$\left(\frac{z}{a}\right) = \left(\frac{h}{a}\right) \frac{1}{1 + (x/a)^2} = \frac{\alpha}{1 + (x/a)^2} .$$

We can readily observe in all cases that the higher altitude streamlines are less affected by the mountains than the lower ones. This is to be expected. It is also interesting to note that the wind flow corresponding to the surface streamline actually hits the mountain ridge in all cases. This is not unexpected in view of the

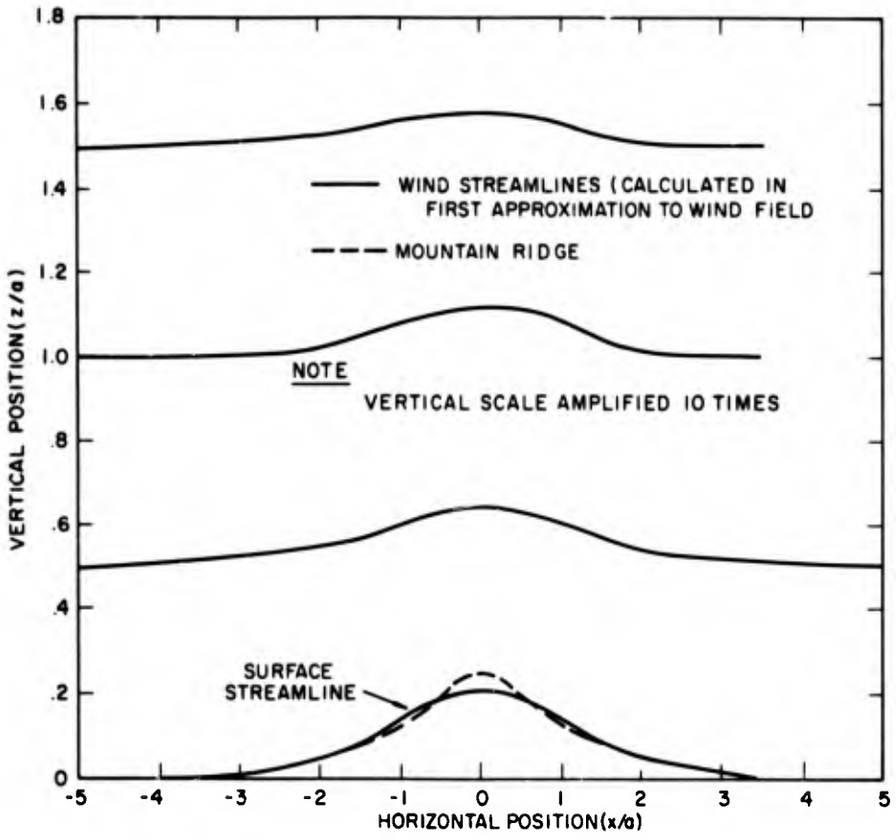

Figure C-4. Wind Streamlines for $\alpha = 0.25$

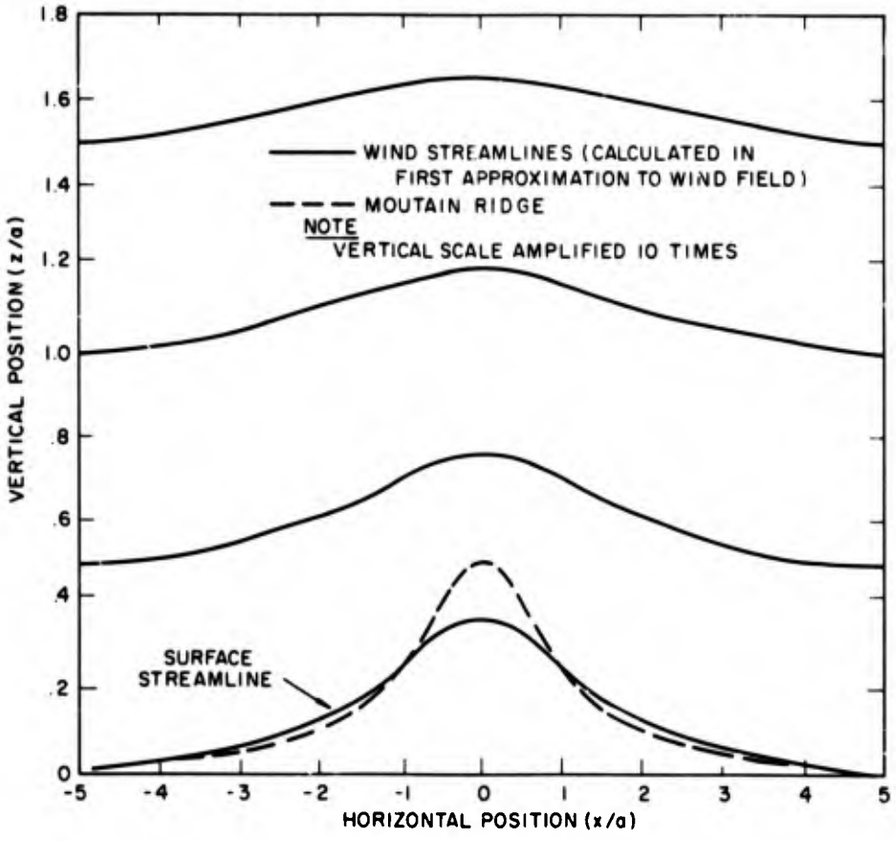

Figure C-5. Wind Streamlines for $\alpha = 0.50$

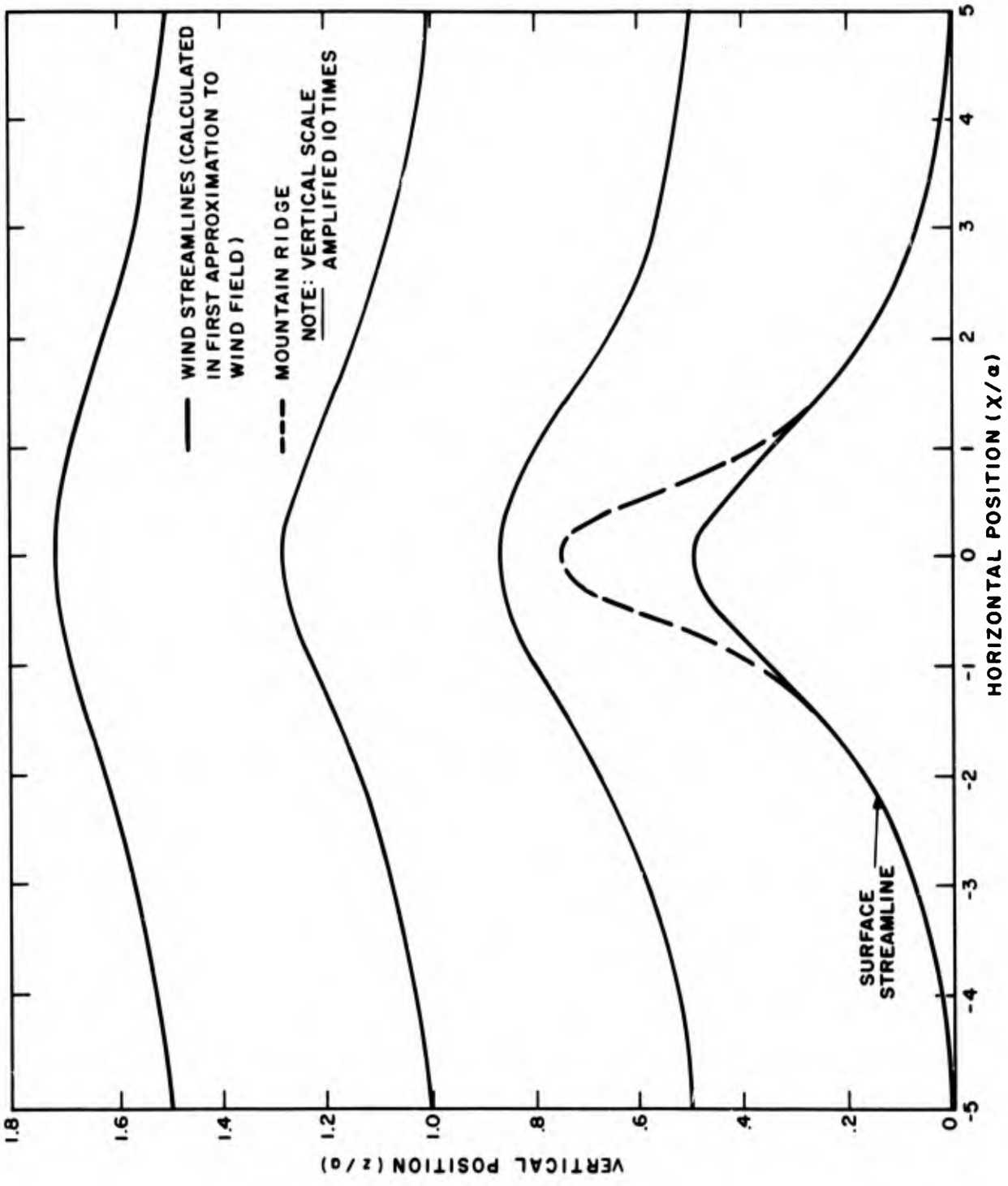

Figure C-6. Wind Streamlines for $\alpha = 0.75$

approximate nature of the first-order calculation of the Fourier transform of the vertical component, C(k), of the wind. It will be recalled that the perturbed boundary conditions were applied exactly (see Eq. 69 in which we required that the wind velocity be parallel to the earth's surface). However, in the process of determining the wind field, an iteration scheme was developed to compute C(k), and the results shown in this section correspond to the first approximation

$$C^{(1)}(k) = \frac{u_o(ah)}{2} \, (ik) \, e^{-|k|a} \, .$$

The uncertainties in the calculation (as noted earlier) should increase in proportion to the slope, which in the case of a mountain ridge is typified by the ratio (h/a). This is especially well borne out by the results which show that the relative difference, Δ, between the height of the mountain ridge and the maximum elevation increases with a corresponding increase in (h/a). We define Δ by the equation

$$\Delta = \frac{(h/a) - \bar{Z}_{om}}{(h/a)} \times 100 = \frac{\alpha - \bar{Z}_{om}}{\alpha} \times 100 \, , \qquad (145)$$

where $\bar{Z}_{om}$ is the maximum elevation of the surface trajectory in units of a. Figure C-7(a) shows a plot of Δ vs $(h/a) = \alpha$. As observed, the relative difference of trajectories increases as (h/a), the average slope of the mountain ridge increases, thereby reflecting the uncertainties in the calculation attributable to the first-order approximation.

The results also show that the first approximation to the wind field underestimates the air lift due to the mountain ridge. This is perhaps better illustrated by a comparison of $\bar{Z}_{om}$ vs α, which like Figure C-7(a) shows that the discrepancies between the actual maximum "lift" and the ideal lift increase with α. (Mathematically, this discrepancy is the difference between the 45^{o} ideal lift line and the actual curve of $\bar{Z}_{om}$ vs α. Figure C-7(b) illustrates the necessity of executing the iteration scheme for C(k) in order to ensure the proper evaluation of the wind field. However, since this may be a complicated process, we can use the results of Figure C-7(b) to establish an empirical relationship between calculated trajectories

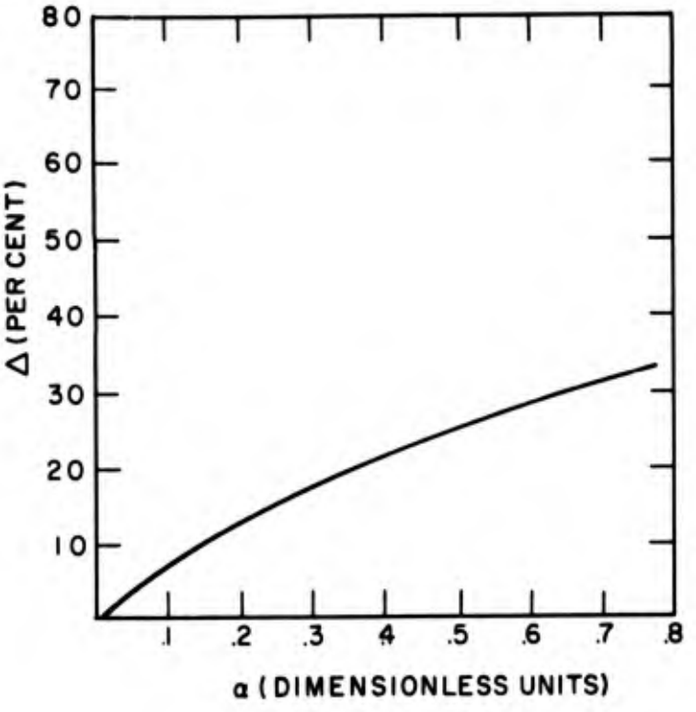

(a)

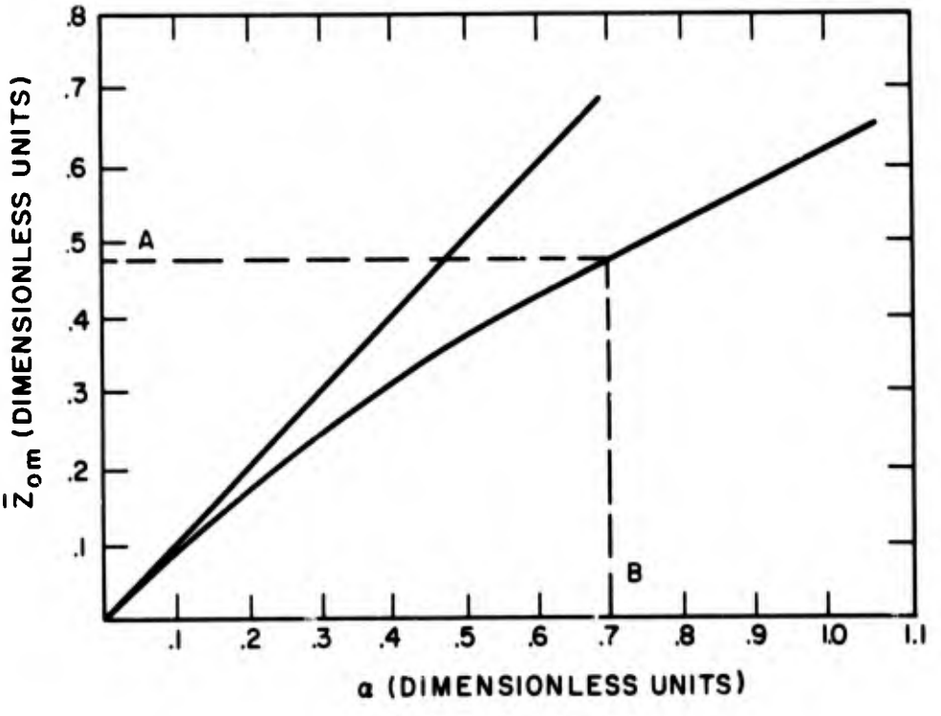

(b)

Figure C-7. Differences Between Surface Trajectory and Mountain Ridge

and the true mountain profile. Thus, suppose we have a mountain ridge whose maximum elevation, also measured in units of its half-width, is .48 (point A in Figure C-7b). The curve shows that to ensure that the calculated surface trajectory would actually rise to a maximum elevation of .48, it is necessary to perform the calculations for an α equal to .7 (point B in Figure C-7b).

The curves of the fallout particle trajectories shown in Figures C-8, C-9, and C-10 depict a mountain ridge corresponding to the maximum elevation $\bar{Z}_{om}$,

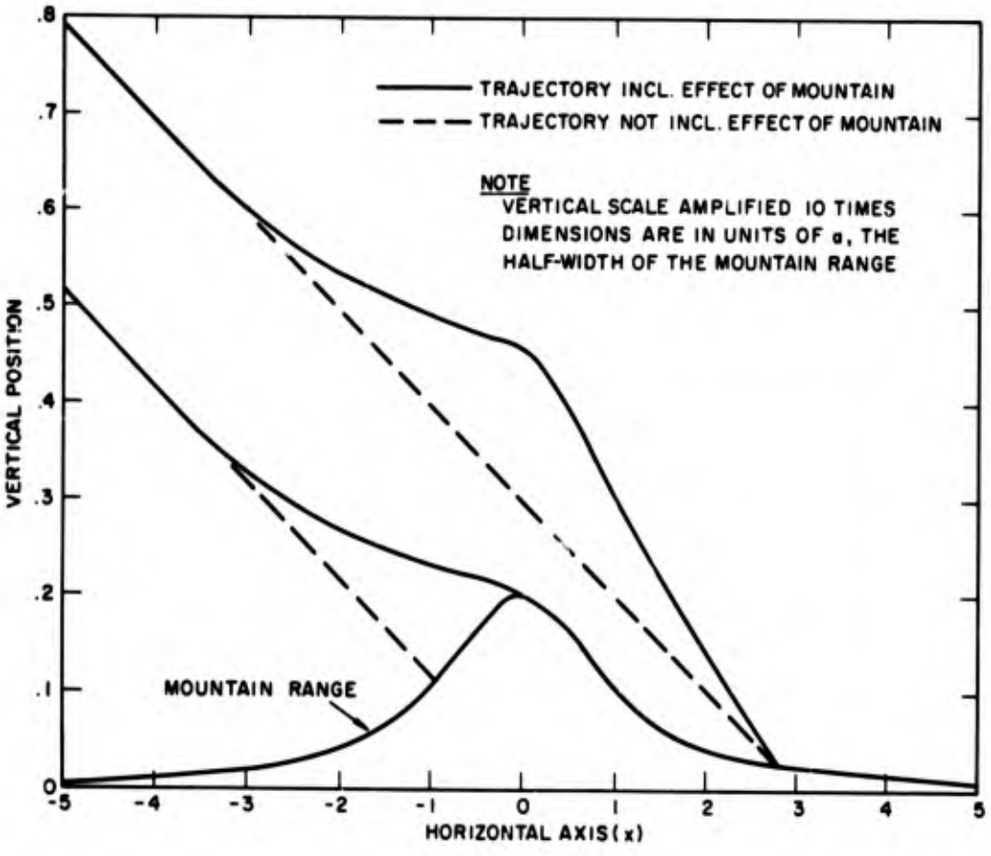

Figure C-8. Fallout Particle Trajectories ($V_F/u_o = 0.1$; $\alpha = 0.25$; $\bar{Z}_{om} = 0.2$ = adjusted mountain height)

although, as in the case for the wind streamlines, the calculations were performed for the corresponding values of α. Since it is beyond the scope of this report to perform a parametric analysis of the stream function (Eq. 13), we present the results for a fall-to-wind velocity ratio, V_F/u_o, equal to 0.1; the curves differ only in the choice of α, or equivalently, $\bar{Z}_{om}$. All the curves originate at the

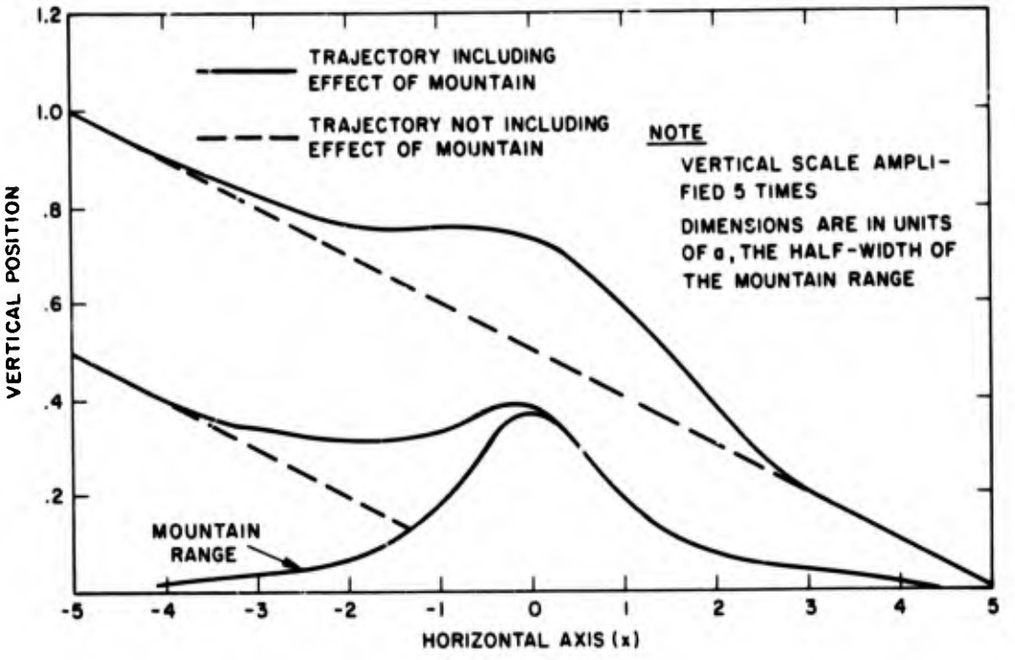

Figure C-9. Fallout Particle Trajectories ($V_F/u_o = 0.1$; $\alpha = 0.50$; $\bar{Z}_{om} = 0.37$ = adjusted mountain height)

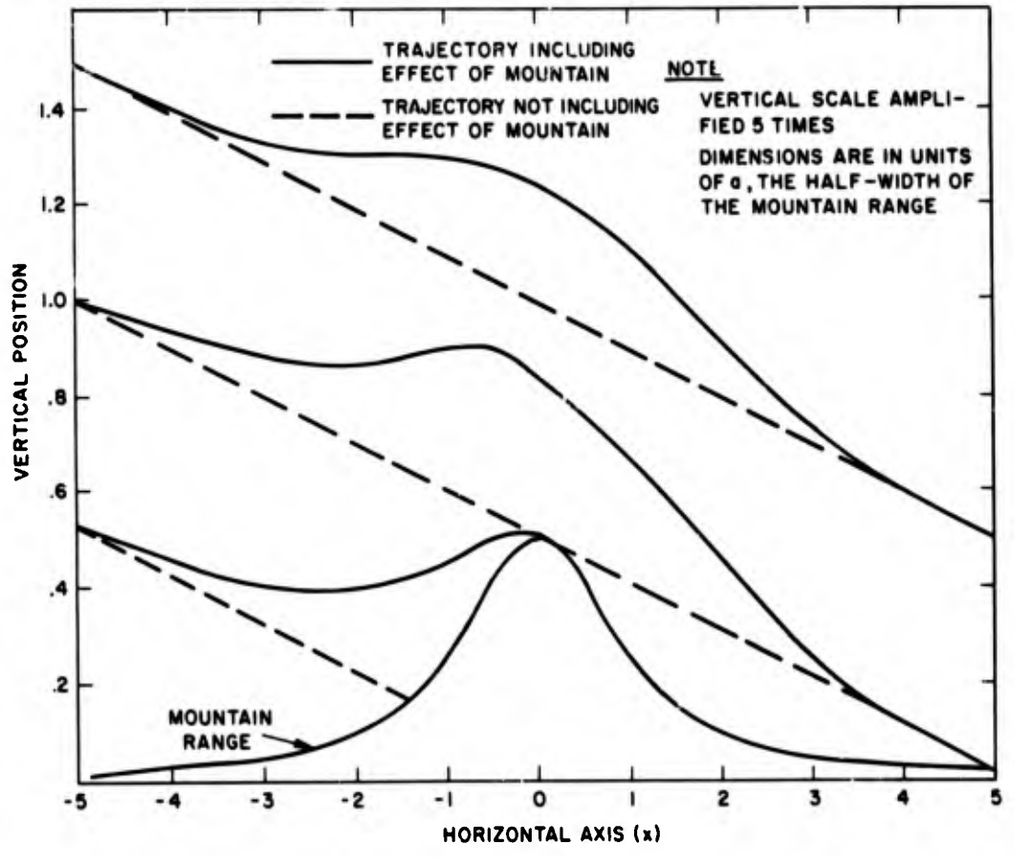

Figure C-10. Fallout Particle Trajectories ($V_F/u_o = 0.1$; $\alpha = 0.75$; $\bar{Z}_{om} = 0.5$ = adjusted mountain height)

dimensionless horizontal displacement, (x/a) = -5, sufficiently removed from the center of the mountain ridge so that orographic effects would not be felt. Examination of all three curves for the same initial vertical position of the streamlines shows that increases in the mountain ridge height lead to an enhanced downstream drift of the fallout particles. For those streamlines, whose unperturbed trajectories pass over the crest of the mountain ridge (e.g., the middle unperturbed trajectory of Figure C-10), the mountain ridge causes no permanent displacement of the streamlines. We have also constructed a digital program to compute the transport times for fallout particles traversing a two-dimensional mountain ridge for arbitrary γ and α, and applied the code for the cases $\gamma = 0.1$; $\alpha = 0.25$, 0.50, and 0.75 (between the limits $-5 \leq x \leq 5$). The results show no additional time delay due to the effect of the mountain ridge. On the contrary, we found a relative speed-up of between 1 to 2%. Apparently, the increase in path length is slightly more than counterbalanced by the increase in velocity.

The fact that the perturbed trajectories will fail to intercept the mountain ridge always end up on the same unperturbed streamline is a general result, as can be seen by examination of the stream function (Eq. 143),

$$C' = \bar{z} + \gamma \bar{x} - \left[\frac{\alpha(1+\bar{z})}{(1+\bar{z})^2 + \bar{x}^2} \right] .$$

The function in brackets is the contribution to the stream function attributable to the mountain ridge; for either large negative or positive values of $\bar{x}$, this goes to zero.

The middle set of curves in Figure C-10 can be used to obtain some estimate of the enhanced fallout range caused by the mountain ridge for $(V_F/u_o) = 0.1$ with $(\bar{Z}_{om}/a) = 0.5$. From Figure C-3, we see that this would correspond to a 100-μ particle with $u_o = 30$ mph, 150-μ particle with $u_o = 50$ mph, or a 230-μ particle with $u_o = 70$ mph, all of which are quite possible situations. If the actual mountain ridge peak were 1 mile, the intercept of the alluded-to trajectory would hit the horizontal axis at $\bar{x} = 5$, or x = 10 miles.

For heavy fallout particles, orographic effects are less important since the vertical lift decreases. At the other extreme, extremely light fallout particles will follow the wind streamlines.

REFERENCES

1. P. Queney, "The Problem of Air Flow Over Mountains: A Summary of Theoretical Studies," Bull. Am. Meteorol. Soc. 29, 16 (1948).

2. A. Erdélyl, et al., Tables of Integral Transforms, Volume 2 (New York, N. Y.: McGraw-Hill Book Company, Inc., 1954).

3. W. W. Kellogg, R. R. Rapp, and S. M. Greenfield, "Close-in Fallout," J. Meteorol. 14, 1 (1957).

4. P. Morse and H. Feshback, Methods of Theoretical Physics (New York, N. Y.: McGraw-Hill Book Company, Inc., 1953).

BLANK PAGE

APPENDIX D

THE INCORPORATION OF THE SEA BREEZE IN THE CALCULATION OF FALLOUT

INTRODUCTION

The effects of the sea breeze will be considered in our calculations of fallout. It is appreciated that this local circulation phenomenon can have an important affect on the lighter fallout particles, particularly on a clear day, when the temperature-induced circulating winds are larger than the so-called fall velocity, V_F.

The sea breeze is characterized by relatively large changes in the wind direction over short distances, and, as such, its internal features cannot be satisfactorily analyzed with existing installations due to the unavailability of sufficiently dense meteorological observation points in the vicinity of the coastline. We have developed, therefore, a suitable sea-breeze model which can be applied in a digital computer program leading to the determination of fallout distribution. As in the overall DOD fallout model, space is divided into cells, with each compartment characterized by a distinct wind field. In the general case, the wind parameters for these cells are deduced (by suitable mathematical techniques) from sounding stations which are in close proximity to the geometric center of the cell. The construction of the cell's wind field by this method is appropriate throughout most of space, where changes in the wind velocity occur over dimensions which are large compared to the distance between observation points. The sea breeze, and other local circulation systems such as mountain and valley winds, however, cannot be treated by this method. Consequently, the geometric region enclosing the sea breeze is divided into a special cell which is treated separately. The nature of the problem dictates that analytic mathematical functions be used to generate the wind field in this cell. These functions, moreover, should be applicable for most situations. The specific parameters which describe the cell are discussed on pp. D-4 through D-18.

REVIEW OF THE SEA-BREEZE THEORIES

The sea breeze is perhaps one of the best examples of an atmospheric process which can be treated analytically with a degree of success. Jeffreys[1] was the first to treat the problem in an exact way, although his results were not in full agreement with observations. As pointed out by Schmidt,[2] the former's model led to a solution in which the daily wind variation was in phase with the daily temperature curve. This was not always consistent with the measured results. In Jeffreys' model, the only forces that are taken into account are the two due to friction and to the pressure gradient resulting from the unequal heating. Haurwitz[3] classifies such a model as an equilibrium theory of the sea breeze; a theory which neglects the inertia of the wind and, consequently, the temporal changes of the wind that are of the order of $\Omega = 2\pi/(\text{sidereal day}) = 7.3 \times 10^{-5}$ sec. In retrospect, the main flaw in Jeffreys' treatment was not so much his neglect of the inertia of the wind (as will be shown later, this can be justified in some cases) but rather his deletion of the Coriolis terms which account for the veering of the wind in the course of time. This effect was included in the subsequent papers.

Both Schmidt's and Haurwitz's works were less concerned with rendering a complete theory of the sea breeze than with clarifying the characteristic phenomena of the land and sea breezes, such as the phase shift between wind and temperature or the influence of the earth's rotation. These investigations did much to improve our understanding of the sea breeze, but they cannot be considered as complete in the usual sense. (A more thorough critique of their work is given by Defant,[4] who also discusses research performed by other investigators.)

In analytical treatments of the sea breeze, it is necessary to make simplifying assumptions in order to obtain mathematically tractable equations. We can categorically say that all the analytical treatments are based upon linearization of the equations of motion which describe the sea-breeze circulation. The more complete analytical treatments of the sea breeze have been successful in accounting for the large-scale characteristics of the sea-breeze circulation. Notable among this group are the investigations of Defant[4,5] and Haurwitz,[6] which form the basis of the sea-breeze model used in our fallout computation. (A more extensive discussion of their work is given in the following section of this appendix.) Generally, the terms in

the dynamical equations which deal with the horizontal advection of temperature are omitted, although in the Defant-Haurwitz models, vertical advection of temperature is retained, and the diffusion of heat upward by turbulent processes is included. Despite the approximations resulting from linearization, the linear models yield a satisfactory reproduction of the fundamental field of motion of the sea breeze.

The development of high-speed numerical methods has made possible a more refined treatment of the sea breeze which can account for not only horizontal advection but also the spatial variation of the viscosity and turbulent diffusion constants. Pierce[7] was perhaps the first who succeeded in integrating by numerical methods a set of non-linear sea-breeze equations. The main drawback in Pierce's model was his introduction of a somewhat artificial mechanism to transfer the heat absorbed by the earth to the atmosphere. The physical consequences of this are more fully discussed by Fisher.[8] As pointed out by Fisher, the most important feature of the numerical method lies in the fact that the non-linear advective terms in the equations may be retained, thus allowing the feedback effect of the wind field itself on the sea breeze to be studied. Fisher's model is conceptually identical to the linear model of Haurwitz, and may be considered the most definitive work in the field inasmuch as it includes not only the non-linear horizontal advection but also the spatial variation of the transport parameters. This solution shows the sea breeze in the stages of development and decay and succeeds in reproducing the gross features of the wind system and many of its small details as well.

The main drawback in applying Fisher's model to the fallout problem is its sheer complexity, particularly in view of the fact that, as pointed out by Fisher himself, its principal contribution is its ability to describe the fine structure in the sea-breeze development. Although we can justify the incorporation of the sea breeze in fallout models, we are hard-pressed to justify the inclusion of its subtleties. Other effects such as the irregularity of the coastline, the presence of a prevailing wind, and uncertainties in the transport coefficients would completely overshadow any improvement attributed to incorporation of the sea-breeze fine structure. (Recently, an attempt was made by Travelers Insurance Research Laboratory[9] to employ Fisher's observed data for calculation of fallout in a sea breeze. In view

of the extensive amount of "function-fitting" employed, it becomes difficult to appraise their model.)

SEA-BREEZE MODEL

WIND FIELD PARAMETERS

In this section, we shall present the expressions for the components of the wind field, used in our sea-breeze calculations, which are identical to those deduced by Defant.[5] The derivation of our final results, however, closely resembles Haurwitz's treatment of the sea-breeze circulation, because it shows more clearly the assumptions which are made concerning the pressure variation.

Defant's approach to the sea breeze problem is based on Lord Rayleigh's convection theory.[10] The dynamics of Defant's model are governed by the continuity equation, the three equations of motion, the equation of state, and the heat-diffusion equation. By neglecting variations in density, except in so far as they modify the action of gravity, it becomes possible to construct a stream function which is used to describe the motion in a plane perpendicular to the coast. The mathematical equations are based on the assumption of an infinitely long coastline which we designate as the y axis. Variations of the meteorological equations in this direction are ignored. The x axis is perpendicular to the coast, and positive inland, while the z axis denotes the vertical. The equations which describe the system are:

$$\frac{\partial u}{\partial x} + \frac{\partial w}{\partial z} = 0 \,, \tag{1}$$

$$\frac{\partial u}{\partial t} + u\frac{\partial u}{\partial x} + w\frac{\partial u}{\partial z} - fv = -\frac{1}{\rho}\frac{\partial p}{\partial x} - \sigma u \,, \tag{2}$$

$$\frac{\partial v}{\partial t} + u\frac{\partial v}{\partial x} + w\frac{\partial v}{\partial z} + fu = -\sigma v \,, \tag{3}$$

$$\frac{\partial w}{\partial t} + u\frac{\partial w}{\partial x} + w\frac{\partial w}{\partial z} = -\frac{1}{\rho}\frac{\partial p}{\partial z} - g - \sigma w \,, \tag{4}$$

$$p = \rho RT \,, \tag{5}$$

$$\frac{\partial T}{\partial t} + u\frac{\partial T}{\partial x} + w\frac{\partial T}{\partial z} = K\frac{\partial^2 T}{\partial z^2} \,, \tag{6}$$

where u, v, and w are the velocity components along the x, y, and z axes, respectively; p denotes the pressure; T is the temperature; ρ is the mass density; g is the gravitational constant; K is the thermal diffusion constant; and R is the gas constant. The quantity $f = 2\Omega \sin \phi$ is the Coriolis parameter, while the effect of friction is taken in account through the Guldberg-Mohn friction parameter, σ. To be sure, this is the simplest way to incorporate the effect of viscosity into the theory. (Haurwitz offers an alternative approach to turbulent dissipation, but, as we shall discuss later, this has its drawbacks.) With the exception of Eq. (1) (the continuity equation derived by setting $(d\rho/dt) = 0$, see Ref. 8), all the others are non-linear, in the sense that there are terms which involve multiplication of the dependent meteorological variables. Application of the following boundary conditions suffices to determine the problem in all cases.

$$w(z = 0) = 0 \ ,$$

$$w(z \to \infty) = 0 \ , \tag{7}$$

$$T(z = 0) = T_o + T(x,t) \ .$$

The function T(x,t) is the surface temperature differential, defined as the difference between the actual temperature above the water or land and a suitable reference temperature, T_o, which we take to be the temperature along the coastline. In the theory of the sea breeze, T(x,t) performs the role of the "driving-force" in that it, alone, is responsible for the circulation.

Equations (1 to 6) can be simplified by introducing two new variables, the stream function ψ and vorticity η, which are related to the x and z component of the velocity by

$$u = -\frac{\partial \psi}{\partial z}, \qquad w = \frac{\partial \psi}{\partial x} \ ; \tag{8}$$

$$\eta = \frac{\partial u}{\partial z} - \frac{\partial w}{\partial x} = -\nabla^2 \psi \ . \tag{9}$$

By operating on Eq. (2) with $(\partial/\partial z)$, and on Eq. (4) with $(\partial/\partial x)$, and then subtracting the resulting second expression from the resulting first expression gives us the following equation for η:

$$\frac{\partial \eta}{\partial t} + \left(u \frac{\partial}{\partial x} + w \frac{\partial}{\partial z}\right)\eta - f \frac{\partial v}{\partial z} = -\frac{1}{\rho^2}\left(\frac{\partial \rho}{\partial z}\frac{\partial p}{\partial x} - \frac{\partial \rho}{\partial x}\frac{\partial p}{\partial z}\right) - \sigma\eta \,. \tag{10}$$

The first term on the right hand side is what Haurwitz calls the solenoidal term, S, which can be simplified by use of the ideal gas law $p = \rho RT$.

$$S = -\frac{1}{\rho^2}\left(\frac{\partial \rho}{\partial z}\frac{\partial p}{\partial x} - \frac{\partial \rho}{\partial x}\frac{\partial p}{\partial z}\right) = \frac{R}{p}\left(\frac{\partial T}{\partial x}\frac{\partial p}{\partial z} - \frac{\partial T}{\partial z}\frac{\partial p}{\partial x}\right) . \tag{11}$$

Since the first part of S is much larger than the second (see Ref. 6), then

$$S = \frac{R}{p}\left(\frac{\partial T}{\partial x}\frac{\partial p}{\partial z}\right) = -\frac{g}{T}\left(\frac{\partial T}{\partial x}\right) . \tag{12}$$

As is commonly done in dynamic meteorology, we now replace $(1/T)(\partial T/\partial x)$ in Eq. (12) by $(1/\tilde{\theta})(\partial\tilde{\theta}/\partial x)$, where $\tilde{\theta}$ is the so-called potential temperature. In Eq. (6) we replace T by $\tilde{\theta}$; thus,

$$\frac{\partial \tilde{\theta}}{\partial t} + u\frac{\partial \tilde{\theta}}{\partial x} + w\frac{\partial \tilde{\theta}}{\partial z} = K\frac{\partial^2 \tilde{\theta}}{\partial z^2} . \tag{13}$$

Note in Eqs. (6 and 13) that only the vertical heat conduction has been taken into account, since the vertical temperature gradient is generally much larger than the horizontal gradient.

At this point, the system of equations is linearized. That is, the meteorological variables are assumed to consist of an unperturbed part, that contribution which exists in the absence of the temperature differential T(x, t); and a smaller perturbed part, attributed to the driving force. Since in the system we consider

all the initial velocities equal to zero, u, v, and w are themselves the perturbed velocities. For the potential temperature, we write

$$\vartheta = \theta_o(z) + \theta(x, z, t) \ , \tag{14}$$

where θ_o and θ are the perturbed and unperturbed parts, respectively. We then arrive at a set of linearized equations:

$$-\frac{\partial}{\partial t}(\nabla^2\psi) - f\frac{\partial v}{\partial z} = -\frac{g}{\theta_o}\frac{\partial \theta}{\partial x} + \sigma\nabla^2\psi \ , \tag{15}$$

$$\frac{\partial v}{\partial t} - f\frac{\partial \psi}{\partial z} = -\sigma v \ , \tag{16}$$

$$\frac{\partial \theta}{\partial t} + \Gamma\frac{\partial \psi}{\partial x} = K\frac{\partial^2 \theta}{\partial z^2} \ , \tag{17}$$

where

$$\Gamma = \frac{\partial \theta_o}{\partial z} \ .$$

Specifically, the convection terms, such as $u(\partial u/\partial x)$, $u(\partial w/\partial x)$, and $w(\partial u/\partial z)$, have been neglected in the derivation of Eqs. (15 to 17). The justification for this can be examined by a comparison of their importance with the corresponding friction term. For example, let us compare the anticipated "numerical value" of the convection operator $D_u = u(\partial/\partial x) + w(\partial/\partial z)$ with σ, the Guldberg-Mohn parameter in Eq. (2). Roughly speaking, D_u can be assigned a value approximately equal to:

$$D_u \approx \frac{\bar{u}}{L_x} + \frac{\bar{w}}{L_z} \ , \tag{18}$$

where $\bar{u}$ and $\bar{w}$ are suitable average values of the respective velocity components, and L_x and L_z are characteristic dimensions of the horizontal and vertical extent

of the sea breeze. L_x is a given quantity in that it is known a priori, while L_z is determined from the theory. The landward range of the sea breeze is estimated by many observers to lie in the range 15 to 50 km in the temperate zones, while in the tropical regions it can extend from 50 to 65 km and even as high as 124 to 145 km in the interior.[4] Representative values for different locations are included in Table D-1. The vertical extent of the sea breeze, L_z, varies with

TABLE D-1

TYPICAL SEA-BREEZE VALUES

Range (km)	Location
16-32	New England
15	Flemisn Coast
20-30	Baltic Sea
30-40	Holland
40-50	Sweden
up to 50	Jutland
40	Albania
>50	Northern Coast of Java

location, but it is substantially smaller than the horizontal dimension. Its altitude varies from 150 m over medium-sized lakes to 200 to 500 m over large lakes and the coastal regions, and rises to more than 1000 m in warm climates. It is also a characteristic feature of the sea breeze that the horizontal velocity greatly exceeds the vertical component. Under a set of conditions which gave results consistent with observation, Defant found an average horizontal velocity component of $\bar{u} = 2$ msec^{-1} for every centigrade degree of temperature difference as opposed to a corresponding value of $\bar{w} = 2$ cm sec^{-1} ^{o}C^{-1}. If these results are used in Eq. (18) with $L_x = 20$ km, $L_z = 500$ m, and a maximum temperature differential of 5^{o}C, we obtain for D_u the value,

$$D_u \approx \frac{10}{20 \times 10^3} + \frac{0.1}{500} = 7 \times 10^{-4} \text{ sec}^{-1} . \qquad (19)$$

Unfortunately, this is greater than a realistically high value of $\sigma = 2.5 \times 10^{-4}$, so that we cannot unequivocally disregard the non-linear terms based upon the rough estimate of D_u. It is possible that phase differences between the constituents of the operator $D_u(u, \partial/\partial x, w, \partial/\partial z)$ can lead to cancellations, thereby precluding the use of a meaningful average. Despite this seeming contradiction, the remarkable feature of Defant's model is that it works. Apparently, the non-linear terms do not significantly alter the main features of the sea breeze.

Within the altitude range for which the sea breeze is important, the potential temperature θ_o can be considered constant in Eq. (15), and its derivative at equilibrium, Γ, a constant in Eq. (17). This procedure renders Eqs. (15 to 17) linear with constant coefficients, and thus amenable to a solution by separation of variables.

Since the temperature varies as $\exp(i\Omega t)$, it will drive the other meteorological variables at the same frequency in the equilibrium situation. Thus, the partial derivative operator $(\partial/\partial t)$ can be replaced by $i\Omega$ in Eqs. (15 to 17). Next, we assume that the spatial behavior of the variables is

$$\theta = A(z) \sin \lambda x, \tag{20}$$

$$\psi = B(z) \cos \lambda x \begin{cases} u = -\partial\psi/\partial z = -\cos \lambda x \, B'(z) \\ w = \partial\psi/\partial x = -\lambda \sin \lambda x \, B(z) , \end{cases} \tag{21}$$

$$v = C(z) \cos \lambda x, \tag{22}$$

in which λ is the separation constant for the x direction and is given by

$$\lambda = \frac{\pi}{L_x} , \tag{23}$$

where L_x is the size of the circulation cell. This cell extends equally in the positive and negative directions up to a maximum value $L_x/2$. When Eqs. (20 to 22) are inserted into Eqs. (15 to 17), the resulting set of coupled equations is

$$(\sigma + i\Omega)(B'' - \lambda^2 B) + f C' = + \alpha\lambda A , \tag{24}$$

$$(\sigma + i\Omega) C = f B' , \tag{25}$$

$$i\Omega A - \lambda\Gamma B = KA'' \ , \tag{26}$$

where

$$\alpha = \frac{g}{\theta_o} \ .$$

Eliminating C from Eq. (25) gives

$$B'' = \frac{q^2\lambda^2}{(q^2 + f^2)} B + \frac{q\alpha\lambda}{(q^2 + f^2)} A \tag{27}$$

and

$$A'' = \left(\frac{i\Omega}{K}\right) A - \frac{\Gamma\lambda}{K} B \ , \tag{28}$$

where

$$q = i\Omega + \sigma \ . \tag{29}$$

For computational purposes it is more convenient to deal with a function W(z) defined by

$$W(z) = -\lambda B(z) \ , \tag{30}$$

in terms of which the velocity components become:

$$w(x, z) = W(z) \sin \lambda x \ , \tag{31}$$

$$u(x, z) = \frac{1}{\lambda} \left(\frac{dW(z)}{dz}\right) \cos \lambda x \ , \tag{32}$$

$$v(x, z) = -\frac{f}{q} u \ . \tag{33}$$

Inserting Eq. (30) into Eqs. (27 and 28) gives

$$W'' = \frac{q^2\lambda^2}{(q^2+f^2)} W - \frac{q\alpha\lambda^2}{(q^2+f^2)} A = r_1 W - r_2 A \tag{34}$$

and

$$A'' = \left(\frac{i\Omega}{K}\right) A + \frac{\Gamma}{K} W = r_3 A + r_4 W \ . \tag{35}$$

If we now let

$$A = A_o e^{az} \tag{36}$$

and

$$W = W_o e^{az} \ , \tag{37}$$

and then substitute these expressions into Eqs. (34 and 35), we derive the following matrix equation which must be satisfied in order to obtain a non-trivial solution.

$$\begin{pmatrix} r_2 & (a^2 - r_1) \\ (a^2 - r_3) & -r_4 \end{pmatrix} \begin{pmatrix} A_o \\ W_o \end{pmatrix} = 0 \ . \tag{38}$$

As is well known from matrix theory, the only non-trivial solutions which exist are those for which the determinant of Eq. (38) vanishes. This condition sets the "allowed" values of

$$\mu = a^2 \ , \tag{39}$$

which are determined from the solution of the quadratic equation

$$\mu^2 - (r_1 + r_3) + (r_1 r_3 + r_2 r_4) = 0 \ . \tag{40}$$

The two roots of μ are denoted by μ_1 and μ_2, and are given by

$$\mu_1 = \frac{(r_1 + r_3) + \sqrt{(r_1 + r_3)^2 - 4(r_1 r_3 + r_2 r_4)}}{2} \tag{41}$$

and

$$\mu_2 = \frac{(r_1 + r_3) - \sqrt{(r_1 + r_3)^2 - 4(r_1 r_3 + r_2 r_4)}}{2} \; . \tag{42}$$

Before delving into the numerics of Eqs. (41 and 42), it is important to discuss their features with regard to a^2. Each equation has two roots, both of which will, in general, be complex. Thus,

$$\mu_1 = \mu_{1R} + i\mu_{1I} = \left(\mu_{1R}^2 + \mu_{1I}^2\right)^{1/2} e^{i\phi_1} \; , \quad \phi_1 = \tan^{-1}(\mu_{1I}/\mu_{1R}) \; ;$$

$$\mu_2 = \mu_{2R} + i\mu_{2I} = \left(\mu_{2R}^2 + \mu_{2I}^2\right)^{1/2} e^{i\phi_2} \; , \quad \phi_2 = \tan^{-1}(\mu_{2I}/\mu_{1R}) \; .$$

The subscripts I and R distinguish between the real and imaginary parts. From Eq. (39) we observe that there are four roots.

$$a = \pm\sqrt{\mu_1} \text{ and } a = \pm\sqrt{\mu_2} \; , \tag{43}$$

with

$$\sqrt{\mu_1} = \left(\mu_{1R}^2 + \mu_{1I}^2\right)^{1/4} \left[\cos(\phi_1/2) + i \sin(\phi_1/2)\right]$$

and

$$\sqrt{\mu_2} = \left(\mu_{2R}^2 + \mu_{2I}^2\right)^{1/4} \left[\cos(\phi_2/2) + i \sin(\phi_2/2)\right] \; .$$

Only those roots which have a negative real part, however, are acceptable, since they lead to an exponential decay with altitude. There will be two such roots, $\sqrt{\mu_1}$ or $-\sqrt{\mu_1}$ and $\sqrt{\mu_2}$ or $-\sqrt{\mu_2}$, which we shall henceforth call a_1 and a_2. The spatial parts of the vertical velocity and temperature become

$$\theta(x, z) = \sin \lambda x \left(A_1 e^{a_1 z} + A_2 e^{a_2 z} \right) , \tag{44}$$

$$w(x, z) = \sin \lambda x \left(S_1 A_1 e^{a_1 z} + S_2 A_2 e^{a_2 z} \right) , \tag{45}$$

where

$$S_1 = \frac{-r_2}{a_1^2 - r_1} \tag{46}$$

and

$$S_2 = \frac{-r_2}{a_2^2 - r_1} . \tag{47}$$

Now we apply the boundary conditions at $z = 0$.

$$w(x, z=0) = 0 \tag{48}$$

and

$$\theta(x, z=0) = \Delta T \sin \lambda x , \tag{49}$$

where ΔT is a specified temperature differential; in reference to the previous discussion, the surface temperature is given by*

$$\tilde{\theta}(z=0) = T_o + \Delta T \, e^{i\Omega t} \sin \lambda x .$$

*At the earth's surface the potential temperature equals the kinetic (usual) temperature.

Using Eqs. (48 and 49), we obtain

$$A_1 = \left(\frac{S_2}{S_2 - S_1}\right)\Delta T = \frac{-S_2}{S_1 - S_2}\,\Delta T = \left(\frac{a_1^2 - r_1}{a_1^2 - a_2^2}\right)\Delta T \tag{50}$$

and

$$A_2 = \frac{S_1}{S_1 - S_2}\,\Delta T = -\frac{\left(a_2^2 - r_1\right)}{\left(a_1^2 - a_2^2\right)}\,\Delta T\ . \tag{51}$$

In principle, the sea-breeze problem is solved at this point. However, the actual, physical solution is obtained by taking the real or imaginary parts of the derived expressions (see following section).

Before proceeding with our discussion of the final computations of the wind field, it is appropriate to review a variation of the sea-breeze model as rendered by Haurwitz.[6]

The difference between Haurwitz's model and Defant's lies in the method of treating turbulent friction. Instead of using the Guldberg-Mohn friction parameter, σ, to describe turbulent dissipation, Haurwitz employs kinematic viscosity. Thus, in lieu of the terms, $-\sigma u$ and $-\sigma v$, which appear in our Eqs. (2 and 3), his corresponding friction terms are $K\partial^2 u/\partial z^2$ and $K\partial^2 v/\partial z^2$, where the kinematic viscosity K is assumed to be independent of position. Haurwitz also neglects the viscous effects on the vertical wind component; we do not. When viscosity is introduced by the expressions $K\partial^2 u/\partial z^2$ and $K\partial^2 v/\partial z^2$, which are then used with the boundary conditions $u(z=0) = v(z=0) = 0$, we arrive at a sea-breeze model in which a boundary layer (in the sense of Schlicting and Prandtl) is built into the theory. In such a situation, the horizontal components of velocity increase with altitude from a minimum value of zero at the land-and-water surface. According to Haurwitz's model, the distance over which this buildup occurs is of the order of the characteristic height of the sea breeze. This seems to be somewhat inconsistent with the everyday experiences at the ocean front, where strong horizontal

winds are evident a few feet from the ground. Strictly speaking, when boundary layer theory is used, the temperature of the moving fluid at the boundary is the same as the surface temperature. Thus, if the theory of the boundary layer were rigorously applied on a clear sunny day in the summertime, we would necessarily have to use a land temperature of about 90° to 100°F and a water temperature between 60° to 70°F. This corresponds to a temperature differential of about 20°C, which would produce wind velocities greater than those measured. In addition, according to the usual boundary layer theory, this is also the surface air temperature differential. Again, this is inconsistent with observations.

Haurwitz's treatment of friction seems to lead to inconsistencies, at least in the lower regions of the sea breeze. It is also more complicated, in so far as it introduces a much more cumbersome expression for the vertical attenuation constant. Consequently, the fundamental equations which describe our system are based on the Defant sea-breeze model.

FINAL WIND-FIELD EQUATIONS

The purpose of this section is to present the final mathematical formulas of the sea-breeze wind field, which will be used in the computer program.

The expressions deduced for w, u, v, and θ (still in complex form) are:

$$w(x, z, t) = \left(\frac{r_2}{a_2^2 - a_1^2}\right) \Delta T \sin \lambda x \left[e^{a_1 z} - e^{a_2 z}\right] e^{i\Omega t} , \tag{52}$$

$$u(x, z, t) = \frac{\Delta T}{\lambda} \cos \lambda x \frac{r_2}{\left(a_2^2 - a_1^2\right)} \left[a_1 e^{a_1 z} - a_2 e^{a_2 z}\right] e^{i\Omega t} , \tag{53}$$

$$v(x, z, t) = -\frac{f}{q} u(x, z, t) , \tag{54}$$

$$\theta(x, z, t) = \Delta T \sin \lambda x \left[e^{a_2 z} + \frac{a_2^2 - r_3}{a_2^2 - a_1^2} \left(e^{a_1 z} - e^{a_2 z}\right)\right] e^{i\Omega t} . \tag{55}$$

The terms in Eqs. (52 to 55) are defined as follows:

$$f = 2\Omega \sin \phi = \text{Coriolis parameter},$$

$$q = (i\Omega + \sigma),$$

$$a_1^2 = \frac{r_1 + r_3}{2} + R,$$

$$a_2^2 = \frac{r_1 + r_3}{2} - R,$$

$$R = \frac{\sqrt{(r_1 + r_3)^2 - 4(r_1 r_3 + r_2 r_4)}}{2},$$

$$r_1 = \frac{q^2 \lambda^2}{(q^2 + f^2)},$$

$$r_2 = \frac{\gamma \alpha \lambda^2}{(q^2 + f^2)},$$

$$r_3 = \frac{i\Omega}{K},$$

$$r_4 = \frac{\Gamma}{K},$$

$$\lambda = \frac{\pi}{L_x},$$

L_x = extent of the sea breeze,

$$\alpha = \frac{g}{\theta_o},$$

$$\Gamma = \frac{d\theta_o}{dz} = \text{unperturbed vertical temperature gradient},$$

K = thermal eddy diffusivity,

σ = Guldberg-Mohn parameter,

ΔT = temperature differential ,

$$a_1 = + \left(a_1^2\right)^{1/2} \text{ or } - \left(a_1^2\right)^{1/2} ,$$

$$a_2 = + \left(a_2^2\right)^{1/2} \text{ or } - \left(a_2^2\right)^{1/2} .$$

(As previously mentioned, the choice of the plus-or-minus signs for a_1 and a_2 is determined by requiring that their real parts be negative so as to ensure a decrease in temperature and velocity with altitude.)

Since the velocity field and potential are in complex form (Eqs. 52 to 55), the remaining task is the resolution of these equations on the real axis. Although we are at liberty to take either the real or imaginary parts of w, u, v, and θ, it is more convenient to take the real part, with time t measured from 12 noon (this is approximately the time when the surface temperature differential reaches its maximum). Thus, the equations representing the actual velocity field and temperature are

$$\theta = \Delta T \sin \lambda x \left[e^{-g_2 z} \cos(\Omega t + h_2 z) + e^{-g_1 z} \mathcal{A} \cos(\Omega t + h_1 z + \theta) - e^{-g_2 z} \mathcal{A} \cos(\Omega t + h_2 z + \theta) \right] , \tag{56}$$

$$u = - \frac{\Delta T \cos \lambda x}{\lambda} \mathcal{B} \left[P_1 e^{-g_1 z} \cos(\Omega t + h_1 z + \psi - S_1) - P_2 e^{-g_2 z} \cos(\Omega t + h_2 z + \psi - S_2) \right] , \tag{57}$$

$$v = \frac{\Delta T \cos \lambda x}{\lambda} \mathcal{B} Q \left[P_1 e^{-g_1 z} \cos(\Omega t + h_1 z + \psi + \rho - s_1) - P_2 e^{-g_2 z} \cos(\Omega t + h_2 z + \psi + \rho - s_2) \right] , \tag{58}$$

$$w = \Delta T \sin \lambda x \; \mathcal{B} \left[e^{-g_1 z} \cos(\Omega t + h_1 z + \psi) - e^{-g_2 z} \cos(\Omega t + h_2 z + \psi) \right] . \qquad (59)$$

The constants shown in these equations are determined from the relationships:

$$a_1 = - g_1 + i h_1 ,$$

$$a_2 = - g_2 + i h_2 ,$$

$$\frac{r_2}{a_2^2 - a_1^2} = \mathcal{B} e^{i\psi} ,$$

$$\frac{a_2^2 - r_3}{a_2^2 - a_1^2} = \mathcal{A} e^{i\phi} ,$$

$$\frac{f}{q} = \mathcal{Q} e^{i\rho} , \qquad (60)$$

$$\tan s_1 = h_1 / g_1 ,$$

$$\tan s_2 = h_2 / g_2 ,$$

$$P_1 = \sqrt{h_1^2 + g_1^2} ,$$

$$P_2 = \sqrt{h_2^2 + g_2^2} .$$

REFERENCES

1. H. Jeffreys, "On the Dynamics of Wind," Quart. J. Roy. Mateorol. Soc. 48, 29 (1922).

2. F. H. Schmidt, "An Elementary Theory of the Land and Sea-Breeze Circulation," J. Meteorol. 4, 9 (1947).

3. B. Haurwitz, "Comments on the Sea-Breeze Circulation," J. Meteorol. 4, 1 (1947).

4. F. Defant, "Local Winds," in Compendium of Meteorology (Boston, Mass.: Am. Meteorol. Soc., 1951) pp. 655-671.

5. F. Defant, "Theorie der Land-und Seewinde," Arch. Meteorol. Geophys. Bioklimatol. 2, 404 (1950).

6. B. Haurwitz, "A Linear Sea Breeze Model," New York University, College of Engineering Research and Development, Quarterly Progress Report No. 3, Project Nr. 3-36-05-401, 1959.

7. R. P. Pierce, "The Calculation of the Sea Breeze Circulation in Terms of the Differential Heating Across the Coast Line," Quart. J. Roy. Meteorol. Soc. 81, 351 (1955).

8. E. L. Fisher, "A Theoretical Study of the Sea Breeze," J. Meteorol. 18, 216 (1960).

9. Travelers Research Center, Inc., "The Influence of Local Winds on Fallout," Contract No. DA 36-039 AMC-03283(E), July, 1964.

10. Lord Rayleigh, "On Convection Currents in a Horizontal Layer of Fluid When the Higher Temperature is on the Under Side," Phil. Mag. 32, 529 (1916).

BLANK PAGE

APPENDIX E

CARD INPUTS FOR THE OUTPUT PROCESSOR

The Output Processor, like each of the other major subdivisions of the DOD Fallout Prediction System, requires a deck of input cards to identify and control its operation. In brief, these inputs consist of: (1) a single set of identification and overall control data which will be referred to as initialization data; and (2) a series of local data sets each of which indicates the geographic limits of a map to be produced by the program. Within each local data set there may be any number of individual map requests of the form

NREQ T1 T2 ,

where NREQ is a code integer denoting the kind of computation to be performed and T1 and T2 are arguments to be used in deposited mass, dose rate, and accumulated dose computations.

Each map request results in the preparation and printing of a separate map showing the output indicated by the request code NREQ. The end of a local data set is indicated to the Output Processor by a map request card having a zero in the NREQ code field (a blank card will suffice). Table E-1 gives details of the card formats, program variable names, and the meanings and uses of variables for initialization data and local data sets. Note that a final blank card is required to indicate the end of the data deck and cause the program to terminate correctly.

DISCUSSION OF CARD INPUTS

CARD 1. OUTPUT PROCESSOR RUN IDENTIFICATION

This card can be used to uniquely identify the current run of the Output Processor. The content of the card (except Columr. 1) is made part of the hard copy output produced by the run.

TABLE E-1

DETAILS OF THE OUTPUT PROCESSOR DATA DECK

Card Set and Number		Content	Name of Program Variable	Format
Initialization Data	1	71 character identifier for the Output Processor run	FORMAT 8	(1X, 71H)
	2	List of logical tape numbers of those tape units available for use in sorting	I0T(J)	(18I4)
	3	Overall control variables	IC(J)	(18I4)
	4	Printer description	IH, IV	(2I4)
First Local Data Set	5	Map parameters, limiting coordinates, and grid intervals	XMAX, XMIN, YMAX, YMIN, DGX, DGY	(6F10.3)
	6	Local control variables	JC(J)	(18I4)
	7	First processing request on current map	NREQ, T1, T2	(I4, 2F10.3)
	8	Second request		
	.	.		
	.	.		
	.	.		
		Request termination card (blank)		blank
Next Local Data Set		Next map specification (see Card No. 5) Next local control variables (see Card No. 6) Next deck if processing requests (see Card No. 7) Request termination card (blank)		
Final Data Card		Data deck termination card (blank)		blank

CARD 2. AVAILABLE TAPE IDENTIFICATIONS

When required, extensive use is made of secondary tape memory so that the Output Processor can be reasonably efficient in producing large output maps or tabulations. This card should contain the "logical" identification numbers of all tapes which are available for use by the Output Processor. The program checks the input values to exclude FMS system tapes and the grounded particles tape; use of the remaining available tapes is made only when required for sorting particle data. As many as 18 tape numbers may be listed, but at least one is required by the program.

CARD 3. OVERALL CONTROL VARIABLES

Provision has been made for the specification of 18 unique overall control variables whose values are stored in the program in the array (IC(J), J=1, 18). At present, only two of these variables have been given functions within the program, and the others remain for use in control and interprogram communication. The functioning variables are as follows:

IC(18) Controls the option to print the content of the grounded particles tape.

IC(18) > 0 causes the grounded particles tape to be printed.

IC(18) = 0 bypasses the printing of the grounded particle tape.

IC(17) Controls the entrance to the Output Processor.

IC(17) > 0 causes the program to stop without really entering the Output Processor proper. (This setting is used if only a printing of the grounded particles tape is desired.)

IC(17) = 0 causes a normal entrance to the main body of the Output Processor regardless of whether or not the grounded particles tape has been printed.

CARD 4. PRINTER DESCRIPTION

To simplify the production of undistorted maps, the Output Processor needs two constants which describe the character spacing of the off-line printer that is to be used. These constants IH and IV give, respectively, the horizontal and vertical character spacings of the printer in characters per inch.

CARD 5. MAP PARAMETERS

The desired output map is characterized as an input to the Output Processor by its limiting coordinates and its grid intervals (grid point spacing). All maps are rectangular and North-South and East-West in orientation, with North always at the top. The variables XMAX and XMIN indicate the maximum and minimum values of the East-West coordinates of the map. YMAX and YMIN similarly indicate maximum and minimum values of the North-South map coordinates. To allow flexibility, the scaled spacing between grid points on the output map has been arranged to be set by the user. The variables DGX and DGY indicate the inter-grid-point distances in the East-West and North-South directions, respectively. It should be noted that on the printed map the actual physical spacing of the data points (decimal points are a handy reference) is fixed by the printer's character and line spacing. Map printing formats have been arranged to achieve the greatest reasonable data point density on the printed page; on IBM printers, this amounts to three lines per grid interval in the vertical direction, and six characters per grid interval in the horizontal direction. If the user wishes to have a map of some particular scale produced by the Output Processor, he must set the parameters DGX and DGY to account for both the character spacing of the printer as well as the inter-data-point character counts used by the program (3 lines per interval in the vertical direction and six characters per interval in the horizontal direction). Obviously, zero values should never be assigned to DGX or DGY.

An option exists within the Output Processor to cause it to adjust the grid intervals put in by the user so as to yield an undistorted map, i.e., a map on which the same scale factor applies in all directions . If the user has specified (by parameter JC(16)) the automatic undistorted map option, the program makes use of either DGX or DGY as the scale factor basis, depending upon which of these two parameters will yield the largest undistorted map (smallest scale factor).

CARD 6. LOCAL CONTROL VARIABLES

Provision has been made for the specification of 18 unique local control variables whose values are stored in the program in the array (JC(J), J = 1, 18). At present, only three of these variables have been given functions within the program,

and the others remain for use in control and interprogram communication at the local level. The functioning variables are as follows:

JC(1) Output format control variable JC(1) = 1 results in the printing of the output map in a two-line "E" format which has the power of ten printed on one line and the associated multiplier printed immediately below it.

JC(1) = 2 results in the printing of a two-line F11.3 format which has the six highest order characters printed on the the first line, and the five lowest order characters on the second line.

JC(16) Automatic undistorted map parameter JC(16) = 0 results in the automatic adjustment of the grid interval DGX or DGY to yield an undistorted output map.

JC(16) $\neq$ 0 results in no adjustment to the grid intervals.

JC(18) Grid interval adjustment control parameter

JC(18) = 0 indicates the user's permission for the program to make a small adjustment to the grid intervals to achieve greater program efficiency. This adjustment may result in increased map resolution but cannot result in decreased resolution.

JC(18) > 0 indicates the user's wish to have no adjustment made to the grid intervals. JC(18) > 0 overrides JC(16) = 0, i.e., for an automatic undistorted map JC(18) and JC(16) must both equal zero.

CARDS 7, 8.... PROCESSING REQUESTS

Table E-2 presents the meanings of the computation codes (NREQ) and arguments (T1 and T2) for currently available computation options.

TABLE E-2

AVAILABLE COMPUTATION CODES

Computation Code NREQ	Computation Type Description
1	Count of wafers covering output point
2	Dose rate normalized to time H + 1 hour
3	Dose rate at time H + T1
4	Integrated dose H + T1 to ∞
5	Integrated dose H + T1 to H + T2
6	Total mass deposited
7	Total mass deposited from time H + T1 to H + T2
0	Termination of the set of requests

UNCLASSIFIED
Security Classification

DOCUMENT CONTROL DATA - R&D

(Security classification of title, body of abstract and indexing annotation must be entered when the overall report is classified)

1. ORIGINATING ACTIVITY *(Corporate author)*
Technical Operations Research
Burlington, Massachusetts

2a. REPORT SECURITY CLASSIFICATION
UNCLASSIFIED

2b. GROUP
NA

3. REPORT TITLE
Development of an Improved Land-Surface Fallout Model

4. DESCRIPTIVE NOTES *(Type of report and inclusive dates)*
Interim Report No. 1, 1 April 1965 to 31 October 1965

5. AUTHOR(S) *(Last name, first name, initial)*
Norment, H. G.
Schwenke, T. W.
Kohlberg, I.

6. REPORT DATE
January 1966

7a. TOTAL NO. OF PAGES
181

7b. NO. OF REFS
39

8a. CONTRACT OR GRANT NO.
DA 28-043 AMC-1309(E)

b. PROJECT NO.
1VO-14501-B-53A-01

c. TASK
DASA MIPR 204-64(NDL)
Subtask NWER 10.058

d.

9a. ORIGINATOR'S REPORT NUMBER(S)
TO-B 65-99

9b. OTHER REPORT NO(S) *(Any other numbers that may be assigned this report)*

10. AVAILABILITY/LIMITATION NOTICES
Distribution of this document is unlimited.

11. SUPPLEMENTARY NOTES

12. SPONSORING MILITARY ACTIVITY
U. S. Army Electronics Command
Fort Monmouth, New Jersey AMSEL-BL-MA

13. ABSTRACT

A new concept in fallout models, the DOD Fallout Prediction System, is being designed and constructed to serve as a basis for the next generation of fallout prediction models. The model considers in detail the dynamics of cloud rise and growth and provides for fallout particle transport through a three-dimensional time variant atmosphere that includes analytical wind models of local circulation systems such as mountain winds and sea breezes. The model is being programmed for machine computation in a highly modular and flexible fashion to facilitate research usage of the program. Coding is being done exclusively in FORTRAN language. ( )

DD FORM 1 JAN 64 1473

UNCLASSIFIED
Security Classification

14. KEY WORDS	LINK A		LINK B		LINK C	
	ROLE	WT	ROLE	WT	ROLE	WT
Fallout Precipitation Circulation systems Cloud dynamics						

INSTRUCTIONS

1. ORIGINATING ACTIVITY: Enter the name and address of the contractor, subcontractor, grantee, Department of Defense activity or other organization *(corporate author)* issuing the report.

2*a*. REPORT SECURITY CLASSIFICATION: Enter the overall security classification of the report. Indicate whether "Restricted Data" is included. Marking is to be in accordance with appropriate security regulations.

2*b*. GROUP: Automatic downgrading is specified in DoD Directive 5200.10 and Armed Forces Industrial Manual. Enter the group number. Also, when applicable, show that optional markings have been used for Group 3 and Group 4 as authorized.

3. REPORT TITLE: Enter the complete report title in all capital letters. Titles in all cases should be unclassified. If a meaningful title cannot be selected without classification, show title classification in all capitals in parenthesis immediately following the title.

4. DESCRIPTIVE NOTES: If appropriate, enter the type of report, e.g., interim, progress, summary, annual, or final. Give the inclusive dates when a specific reporting period is covered.

5. AUTHOR(S): Enter the name(s) of author(s) as shown on or in the report. Enter last name, first name, middle initial. If military, show rank and branch of service. The name of the principal author is an absolute minimum requirement.

6. REPORT DATE: Enter the date of the report as day, month, year, or month, year. If more than one date appears on the report, use date of publication.

7*a*. TOTAL NUMBER OF PAGES: The total page count should follow normal pagination procedures, i.e., enter the number of pages containing information.

7*b*. NUMBER OF REFERENCES: Enter the total number of references cited in the report.

8*a*. CONTRACT OR GRANT NUMBER: If appropriate, enter the applicable number of the contract or grant under which the report was written.

8*b*, 8*c*, & 8*d*. PROJECT NUMBER: Enter the appropriate military department identification, such as project number, subproject number, system numbers, task number, etc.

9*a*. ORIGINATOR'S REPORT NUMBER(S): Enter the official report number by which the document will be identified and controlled by the originating activity. This number must be unique to this report.

9*b*. OTHER REPORT NUMBER(S): If the report has been assigned any other report numbers *(either by the originator or by the sponsor)*, also enter this number(s).

10. AVAILABILITY/LIMITATION NOTICES: Enter any limitations on further dissemination of the report, other than those imposed by security classification, using standard statements such as:

(1) "Qualified requesters may obtain copies of this report from DDC."

(2) "Foreign announcement and dissemination of this report by DDC is not authorized."

(3) "U. S. Government agencies may obtain copies of this report directly from DDC. Other qualified DDC users shall request through

_____."

(4) "U. S. military agencies may obtain copies of this report directly from DDC. Other qualified users shall request through

_____."

(5) "All distribution of this report is controlled. Qualified DDC users shall request through

_____."

If the report has been furnished to the Office of Technical Services, Department of Commerce, for sale to the public, indicate this fact and enter the price, if known.

11. SUPPLEMENTARY NOTES: Use for additional explanatory notes.

12. SPONSORING MILITARY ACTIVITY: Enter the name of the departmental project office or laboratory sponsoring *(paying for)* the research and development. Include address.

13. ABSTRACT: Enter an abstract giving a brief and factual summary of the document indicative of the report, even though it may also appear elsewhere in the body of the technical report. If additional space is required, a continuation sheet shall be attached.

It is highly desirable that the abstract of classified reports be unclassified. Each paragraph of the abstract shall end with an indication of the military security classification of the information in the paragraph, represented as *(TS), (S), (C), or (U).*

There is no limitation on the length of the abstract. However, the suggested length is from 150 to 225 words.

14. KEY WORDS: Key words are technically meaningful terms or short phrases that characterize a report and may be used as index entries for cataloging the report. Key words must be selected so that no security classification is required. Identifiers, such as equipment model designation, trade name, military project code name, geographic location, may be used as key words but will be followed by an indication of technical context. The assignment of links, rules, and weights is optional.